Summer 2007

Annual and Interannual Variability in the Wind Field and the Hydrography Along the Seward Line in the Northern Gulf of Alaska

Isaac Schroeder
Old Dominion University

ANNUAL AND INTERANNUAL VARIABILITY IN THE WIND FIELD AND THE HYDROGRAPHY ALONG THE SEWARD LINE IN THE NORTHERN GULF OF ALASKA

by

Isaac Schroeder
M.S. in Physics - University of Missouri

A Dissertation Submitted to the Faculty of
Old Dominion University in Partial Fulfillment of the
Requirement for the Degree of

DOCTOR OF PHILOSOPHY

OCEANOGRAPHY

OLD DOMINION UNIVERSITY
August 2007

Approved by:

Thomas C. Royer (Director)

Chester E. Grosch

Nicholas A. Bond

Larry P. Atkinson

ABSTRACT

ANNUAL AND INTERANNUAL VARIABILITY IN THE WIND FIELD AND THE HYDROGRAPHY ALONG THE SEWARD LINE IN THE NORTHERN GULF OF ALASKA

Isaac Schroeder
Old Dominion University, 2007
Director: Dr. Thomas C. Royer

The Northeast Pacific GLOBEC (GLOBal ocean ECosystems dynamics) program (October 1997 to December 2004) collected hydrographic data along the Seward Line that stretches from the inner shelf (GAK1 59.8°N, 149.5°W) and extends over 200 km beyond the continental slope (GAK13 58.1°N, 147.8°W). The complexity of the interannual hydrographic variability in this area stems from the interacting influences of local forcing such as winds, coastal freshwater discharge, eddies, fronts and remote forcing like El Niño-Southern Oscillation. Until now, the influence of winds on the system has been calculated using coarse resolution upwelling index data or spatially sparse buoy data. The coarse resolution wind measurements cannot describe the cross shelf spatial variations of the winds which are expected to be significant due to the influence of the high coastal mountain chain on atmospheric motion. A new source of high resolution wind velocity data is from satellite scatterometers. Scatterometer wind data have spatial resolutions fine enough to calculate velocity shears across the shelf. On average the wind shears produce positive wind stress curls which promote upwelling due to Ekman pumping. Calculations show that the transport due to this upwelling is 25% - 50% of the transport due to Ekman transport. On average Ekman transport produces downwelling while the transport due to Ekman pumping produces upwelling. The effect of the downwelling due to Ekman transport is apparent near the coast (0 - 20 km from the coast) at depths between 50 - 250 m. In this area there is a significant positive correlation between the anomalies of salinity with the anomalies of Ekman transport. The effect of the upwelling due to Ekman pumping is seen in the mid-shelf area (40 - 80 km from the coast) at depths between 100 - 200 m. Here the anomalies of salinity are positively correlated with the anomalies of vertical velocities. The covariance between the temperature and salinity

across the Seward Line suggests that offshore surface spreading of the Alaska Coastal Current and entrainment generates a deep onshore flow of high saline, warm water onto the shelf. The onshore flow of water is expected to be high in nutrients which can then be brought up to the euphotic zone by the upwelling produced by Ekman pumping. The upwelling could be an important mechanism to supply nutrients to the surface layer.

To Nandita.

ACKNOWLEDGMENTS

I want to thank Dr. Royer and Dr. Grosch for their guidance and patience. They both allowed me succeed at my own pace and when results were lacking they both directed me toward more promising directions without a heavy hand. I would also like to thank Nandita's parents who with much sacrifice have made the completion of this dissertation possible – without their help I would have never been able to finish. I want to thank all of the people who collected and analyzed the NEP GLOBEC data, especially the crew of the Alpha Helix. And also to Ian for no particular reason.

TABLE OF CONTENTS

LIST OF TABLES

LIST OF FIGURES

CHAPTER 1

INTRODUCTION

The primary dynamical meteorological drivers in the Gulf of Alaska (GOA) are three atmospheric pressure systems – the Aleutian Low, the Siberian High and the East Pacific High [*Wilson and Overland* 1986]. Of the three, the primary one affecting ocean dynamics of the region is the Aleutian Low that is the dominant pressure system during the winter. High mountains along the coastline force storm systems to stay within the gulf.

Presently there is not much knowledge of the small scale and meso scale winds in the Gulf of Alaska. There are a few direct oceanic wind observations from National Data Buoy Center (NDBC) buoys, with the longest series at buoy 46001 (56.3°N - 148.17°W) (Figure 1). There are also few coastal meteorological stations but some are sheltered by mountains leading to winds that are altered by orographic effects [*Livingstone and Royer* 1980]. Most frequently, when wind measurements are used they are geostrophic component of winds calculated from pressure gradients. Geostrophic winds are used to compile the upwelling indices [*Bakun* 1973]. The pressure grids used in the climate models are problematic due to sparse data coverage of synoptic pressure measurements. One source of new wind data is wind velocity derived from satellite scatterometers. Scatterometers allow twice daily measurements on a fine resolution (25 km for QuikSCAT). Knowledge of the spatial structure of the wind field is important since there are different ocean responses to different wind field variables. For example, turbulent mixing, which is a function of the cube of the wind speed, affects the SST; Ekman transport is a function of the square of the wind vector; and geostrophic transport is a function of the curl of the wind field [*Pond and Pickard* 1995].

The low level of the tropopause at these high latitudes and the high mountains promote high rates of orographic rainfall. Precipitation rates exceed 2 m yr^{-1} with extremes of 8 m yr^{-1} in both southeast and south Alaska [*Royer* 1982]. Since the mountains are adjacent to the coast there are very narrow drainage basins. However, there are numerous small rivers/glaciers discharging freshwater all along the coastline. As a result the drainage into the gulf can be thought to be a line source [*Royer* 1982].

The journal model for this dissertation is *Journal of Geophysical Research.*

Because of the nonlinear nature of the equation of state of sea-water, in regions of cold water and high ranges of salinity, the significance of temperature as a controller of density decreases (and the role of salinity consequently increases) [*Pickard and Emery* 1990]. As mentioned before, this is a region of high rainfall. Thus any atmospheric variables that can be used to determine how the rainfall and runoff is deposited into the gulf, will greatly help in describing the shelf circulation. The runoff drives the Alaska Coastal Current (ACC) [*Royer* 1981]. The changes of the atmospheric pressure have been frequently studied [*Royer et al.* 2001], but the effects of wind changes have not. The wind in this region is responsible for the large circulation of the subarctic gyre by the process of Ekman pumping. Also the wind is responsible for Ekman transport onto the shelf which results in downwelling at the coast. This downwelling has mostly been studied by looking at downwelling indices which are calculated by using geostrophic wind calculations [*Bakun* 1973, *Schwing et al.* 1996].

Alongshore wind stress at coastal boundaries results in cross-shore Ekman transport and coastal downwelling or upwelling, depending on wind direction. Ekman transport, as measured by the upwelling index (UI), has been widely used to relate upwelling processes with biological production [*Narváez et al.* 2006, *Cooney et al.* 2001]. Recent studies have suggested, however, that the curl of the wind stress might be just as important in driving coastal downwelling and upwelling. Through the process of Ekman pumping, wind stress curl causes ocean surface layer convergences (divergences) that result in downward (upward) vertical water velocities. *Murphree et al.* [2003] found that the area-averaged temperatures below the seasonal thermocline in a 5-degree area box off the northern California coast are the coolest for periods of positive wind stress curl. These observations were made by looking at climatological wind stress curl derived from course resolution (2.5° × 2.5°) National Center for Environmental Prediction (NCEP) and National Center for Atmospheric Research (NCAR) reanalysis surface winds. On a much smaller scale, Pickett and Paduan (2003) used high-resolution (9 × 9 km grid) winds from the Coupled Ocean/Atmospheric Mesoscale Prediction System (COAMPS) to study small scale non-geostrophic winds around coastal promontories. Their calculations of the vertical transport due to Ekman pumping, caused by the curvature of the winds around the promontories, show that it is of the same magnitude as the upwelling due to the alongshore wind stress. In the Gulf of Alaska, coastal barrier jets form when oceanic storms press up against the coastal mountains and combine with cold interior Arctic

air. These barrier jets are highly variable spatially and have large velocity gradients [*Winstead et al.* 2005]; they can act in a way to enhance the alongshore wind (within 50 - 100 km off shore), resulting in positive wind stress curls which should produce upwelling mid-shelf [*Stabeno et al.* 2004].

The Seward Line consists of 22 hydrographic stations that were sampled extensively as part of the NEP GLOBEC (Northeast Pacific GLOBal ocean ECosystems dynamics) project. The Seward Line stretches from the inner shelf and extends over 200 km beyond the continental slope. The horizontal structure of the Seward Line can be thought of consisting of 4 parts: (a) the inner shelf which includes the Alaska Coastal Current (ACC); (b) the mid-shelf; (c) the outer shelf or the shelf break and (d) the continental slope [*Childers et al.* 2005]. There is much mesoscale variability around the shelf-break. Those that have been identified include Alaska Current meandering [*Niebauer et al.* 1981] and the passage of eddies that moved in from the southeast coast [*Okkonen et al.* 2003]. Semi-permanent mesoscale variability has been identified by D. Musgrave (University of Alaska Fairbanks, personal communication). Using satellite images he has identified a cyclonic eddy he named the 'Seward Eddy'; it has a diameter ranging from 50 to 100 km, and is visible for the majority of the year. He proposes topographic effects to explain its existence. This eddy seems to bifurcate into another anticyclonic eddy at the shelf break.

Results from GAK1 (59°50.7'N, 149°28.0'W; the innermost hydrographic station along the Seward Line, at the mouth of Resurrection Bay) (Figure 1) suggest a two layer system [*Royer* 2005]. The two layer system has temperature and salinity in the top layer of the water column out of phase seasonally with those at the bottom. *Royer* [2005] proposed several mechanisms to explain the phase shift: (1) intrusion of high salinity offshore water due to weakening Ekman transport during the summer; (2) an estuarine-type flow due to large horizontal pressure gradients due to maximum runoff in the fall (October) resulting in high salinities in the lower layer; and, (3) downwelling winds which force surface waters into the second layer; depending on the time of year the surface waters will either be warmer or colder than the lower layers.

Royer [2005] identified three local forcing functions at GAK1: heat flux, wind stress and freshwater discharge. Upwelling indices were used as a proxy for the wind stress, because of the limited long term direct wind measurements. Of the three,

the wind stress is hypothesized to be the most important in understanding the inter-annual variability of the hydrographic data across the Seward line. Upwelling indices might not be a sufficient replacement for actual wind measurements. The main objective of this study is to assess the various time scales and spatial variability of the wind forcing, as measured by the scatterometer on the QuikSCAT satellite, during the NEP GLOBEC time period. And then to correlate the timescales and spatial variability of the wind forcing to changes in the hydrographic structure of the Seward Line. My results can then be used by the NEP GLOBEC community in the study of biological processes, such as the responses of plankton to storm events.

1.1 RESEARCH OBJECTIVES

The research objectives of this study are to:

1. Understand the temporal and spatial response of the hydrography across the Seward Line to wind forcing. To achieve this objective a high spatial resolution wind product is constructed for the northern Gulf of Alaska.

2. Understand the mechanisms by which the hydrography is affected by the winds. Especially how regional and local winds along with freshwater discharge affect shelf-slope exchange.

1.2 DATA

During the NEP GLOBEC study data were collected along the Seward Line from October 1997 to December 2004. The Seward line starts at the inner shelf (GAK 1) and extends a distance of over 200 km to beyond the edge of the continental slope (GAK 13) (Figure 1). The shelf break is located approximately 150 km (GAK 9) from the coast. For most years data were collected in March, April, May, August, October, and December. Also cruises in July were conducted in 1998, 2001, and 2002. Cruises were not conducted in December 1997 and August 1998.

Validation of the satellite scatterometer data was done with comparisons with NDBC buoys. The NDBC data has continuous wind measurements (6 per hour) for 4 buoys located within the Gulf of Alaska. The buoys are numbered 46001, 46080, 46082, and 46083 (Figure 1). Buoy 46001 is moored in deep water (4206 meters) and the others are located on the shelf(approximately 200 meters water depth). Buoys 46082 and 46083 are the nearest to shore, within 100 km of land. Only Buoy 46001

has data throughout the GLOBEC time period. Buoy 46083 began measurements in 2001, while Buoys 46080 and 46082 began in 2002. The time series for these three buoys are not continuous, with up to several months missing for some years.

Satellite wind data are available during the NEP GLOBEC time period from the QuikSCAT scatterometers. The QuikSCAT coverage is from July 1999 to the present. The satellite measures the surface wind twice daily over ascending and descending swathes of fixed width. The spatial resolution is 25 km for Quikscat. The quality of the wind data has an accuracy of $\pm 20°$ in direction and ± 2 m s^{-1} in speed.

Monthly mean discharge data will be from the *Royer* [1982] discharge model. Upwelling indices are estimates of the across shelf component of Ekman transport. The indices are calculated at various locations around the gulf and are found at http://www.pfeg.noaa.gov/.

1.3 DISSERTATION STRUCTURE

This dissertation is divided into four primary topics: *QuikSCAT Validation*, *Wind Vector Climatology*, *Ekman Transport and Pumping* and *Singular Value Decomposition (SVD) between Temperature and Salinity.* The *QuikSCAT Validation* chapter assesses the quality of the satellite data in the Gulf of Alaska. Because the QuikSCAT data are relatively unused in the NEP GLOBEC community, basic seasonal cycles of the wind vector are presented in the *Wind Vector Climatology* chapter. Once a basic description of the winds has been established, the QuikSCAT data are then used to construct time series of Ekman transport and Ekman pumping. The resulting time series are correlated with hydrographic data in the *Ekman Transport and Validation* chapter. The *SVD between Temperature and Salinity* chapter explores how the salinity and temperature across the shelf covary temporally and spatially. The SVD results are analyzed to find dynamical mechanisms that might allow the transport of nutrients onto the shelf. The *Conclusions* chapter discusses the implications of this study in context of the GLOBEC scientific goals in the area and outlines possible topics of future study.

CHAPTER 2

QUIKSCAT VALIDATION

2.1 INTRODUCTION

Although wind measurements derived from satellite measurements have been available previously, since the ERS1 satellite began operation in August 1991, there have been limited applications in the oceanographic community. The reasons include the limitations of the data such as poor quality near land, rain contamination, and short temporal coverage. The benefits of the QuikSCAT data are both relatively high spatial resolution and daily temporal resolution.

In the Gulf of Alaska the only long term wind time series on the shelf has been from Middleton Island (59°26' N, 146°18' W). Middleton Island wind data have been continuously collected by the FAA (Federal Aviation Administration) from 1974 to the present. The data were recorded hourly. Unfortunately the wind direction and magnitude are recorded to the nearest 10 degrees and nearest knot [*Weingartner et al.* 2005]. *Livingstone and Royer* [1980] and *Weingartner et al.* [2005] note that Middleton Island is far enough offshore to not experience katabatic winds and local gap winds. Near-shore barrier jets with length scales of one Rossby radius, 50 to 100 km, might be experienced at Middleton Island [*Stabeno et al.* 2004]. The Middleton Island winds have been used as a proxy for large scale forcing but very little is known about along-shore and across-shelf variations in the wind. The QuikSCAT winds are the only data with the spatial resolution to begin a description of wind variability on the shelf. Of special interest is the across-shelf shear produced by barrier jets and the effects of the coastal mountain ranges on the winds. The close proximity of the mountains to the shore-line causes the winds to increase in magnitude within the Rossby radius [*Wilson and Overland* 1986]. The winds increase because geostrophic balance is destroyed when isobars intersect the mountain ridges perpendicularly and the resultant flow will be an ageostrophic wind, blowing from regions of high to low pressure.

The quality of the QuikSCAT data are assessed by comparisons with winds collected from the few buoys moored on the shelf and in deep water. Scatter plots of buoy meridional and zonal wind components versus QuikSCAT meridional and zonal wind components are constructed. Correlation coefficient r values of the fitted linear

regressions are calculated. The complex correlations are also calculated between the buoy and QuikSCAT wind vector time series. The complex correlations provide an estimate of the correlation of the wind vector magnitudes and indicate an average degree of rotation of the buoy wind vectors relative to the QuikSCAT wind vectors.

2.2 BUOY DATA

Validations of QuikSCAT winds were done by comparisons with data from 6 NDBC buoys. The NDBC buoy data were obtained from web site http://www.ndbc.noaa.gov and they provide wind magnitudes and directions measured at 10 minute intervals (NBDC continuous data) or at hourly intervals (NBDC historical data). The buoys are labeled 46001, 46078, 46080, 46082, 46083 and 4084 (Figure 1). Three buoys are located in the western part of the Gulf (46001, 46078 and 46080) and are relatively close to the Seward Line. C-MAN stations, such as the one maintained at Pilot Rock (PILA2) are not considered in the comparison because of the near-shore location; a basic data processing procedure for the QuikSCAT data is the removal of any data that lays over land [*Tang et al.* 2004]. Thus there is at least a 25 km gap between land and the nearest QuikSCAT measurement. The location, mooring depth, anemometer height and temporal coverage for the six buoys are listed in Table 1. Buoys 46001, 46078, 46080 and 46084 are moored in the deepest water with 46001 being the farthest offshore. Buoys 46080, 46082, 46083 and 46084 are located near shore. All of the nearshore moorings except 46084 are moored on the shelf; buoy 46084 mooring depth is 1307 m.

The anemometer height for all six buoys is 5 meters. The QuikSCAT winds are set to 10 m neutral equivalent winds using a Geophysical Model Function (GMF) [*Ebuchi et al.* 2002]. Winds at 5 meters are projected to 10 m using the *Large and Pond* [1981] algorithm. The difference of the wind speeds at 5 m as compared to 10 meters is approximately 0.5 m s^{-1}. The effects of this algorithm are demonstrated on buoy 46001 daily winds (Figure 2). The magnitude of the wind vectors at 10 m are just a fraction higher than at 5 m, with the mean of the difference being 0.42 m s^{-1}. The algorithm increases the variance from 8.75 m^2 s^{-2} at 5 m to 9.92 m^2 s^{-2} at 10 m.

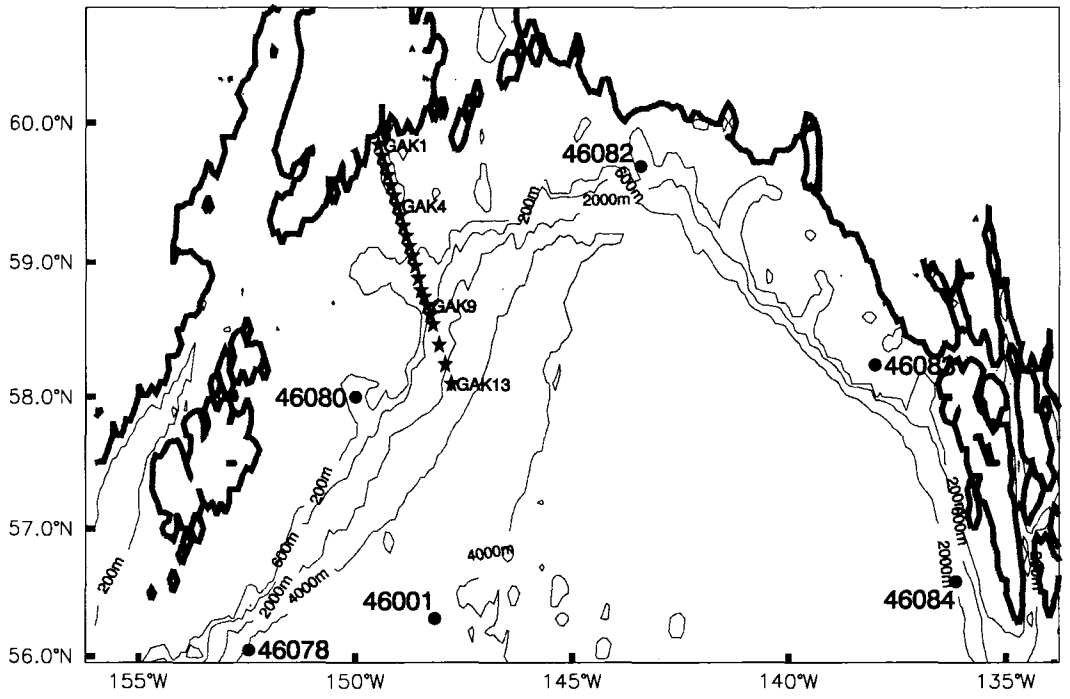

Figure 1. Map of the Gulf of Alaska. The locations of the 6 buoys where continuous wind measurements were measured are labeled along with the location of the QuikSCAT grid location used in the comparison. The 200, 600, 2000 and 4000 meter bathymetric contours are labeled. The Seward Line stations are marked with stars.

Table 1. Description of the 6 buoys used for the QuikSCAT validation.

Buoy	Lat (°N)	Lon (°W)	Water Depth (m)	Anemometer Height (m)	Temporal Coverage
46001	56.3	148.17	4206	5	1/00 - 12/03, 6/04 - 12/04
46078	56.05	152.45	4206	5	5/04 - 11/04
46080	58.00	150.00	374.3	5	5/03 - 11/03
46082	59.69	143.42	134.7	5	9/02 - 7/03, 12/03 - 10/04
46083	58.24	138.01	142.6	5	8/02 - 9/04
46084	56.59	136.16	1307.2	5	1/02 - 1/04 6/02 - 12/04

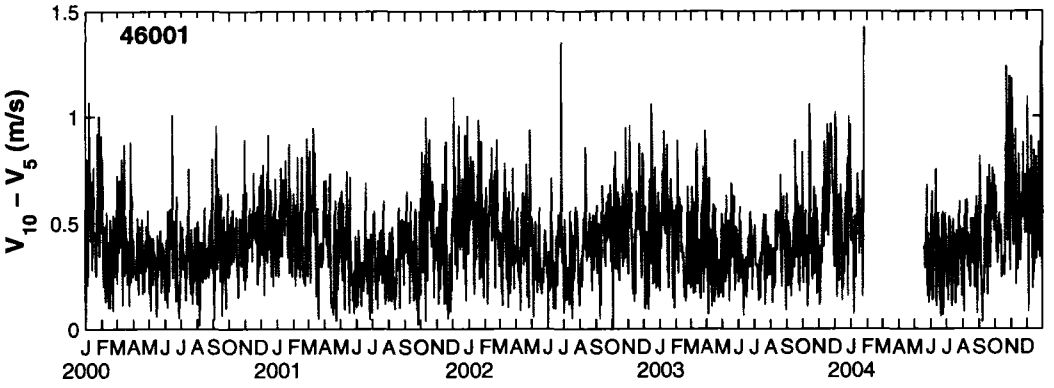

Figure 2. Difference between daily wind magnitude calculations at 10 m and observations at 5 m. The 10 m wind magnitudes were obtained by applying the *Large and Pond* [1981] algorithm on buoy 46001 daily winds. V_{10} is the magnitude of the wind vector at 10 m and V_5 is the magnitude at 5 m.

2.3 QUIKSCAT DATA

The QuikSCAT wind time series that are used in the comparisons are level 3 gridded data processed by the Jet Propulsion Laboratory (JPL) (http://podaac.jpl.nasa.gov/ovw/). The QuikSCAT data consist of 2 measurements per day – an ascending and descending satellite orbital pass. The instrument makes measurements in a continuous, 1800 km wide band with a wind vector resolution of 25 km. Thus the data can be thought as a snap shot of the winds over a patch of ocean for a particular time. Daily means of the wind are an average of the ascending and descending passes. The data are processed with special algorithms to remove ambiguities in wind direction and rain-impact detection. Data accuracy decreases for low wind speeds and near swath edges, e. g. coast-lines. The $0.25° \times 0.25°$ JPL level 3 data consist of meridional and zonal components of the wind velocity for the ascending and descending orbital passes. Rain flag data have been removed and the resulting gaps have been replaced by linear interpolation of data using surrounding grid points.

2.4 METHODS

The buoy wind vector time series are constructed from the daily means of the continuous wind vectors. An example of the data involved in the comparison (Figure 3) for the month of August 2001 at buoy 46001. Figure 3 illustrates the similarities

between the hourly and daily means of the continuous buoy data and the mean of the ascending and descending orbital QuikSCAT data. The agreement between the three is very good. Nevertheless, there are a few obvious instances when the agreement between them is poor. For example, on the 10^{th} of August the u QuikSCAT data shows a negative value while the daily u magnitude from the buoy is positive. Also, on the 29^{th} of August the difference between the u component for the buoy and QuikSCAT is off by about 5 m s^{-1}. The reason for the poor agreement can be seen by looking at the hourly buoy data. During these two days abrupt shifts in the direction and magnitude of the winds occur. In both cases the u hourly data at the beginning of the day are positive. However, by mid-day the winds reverse direction and become strongly negative (approximately -9 m s^{-1}). Neither the ascending nor the descending pass of the QuikSCAT satellite takes place at this time and it misses the strong negative event. On August 20 the daily v between the buoy and QuikSCAT do not agree. The QuikSCAT data are zero thus suggesting that the the ascending and descending data have been rain contaminated.

To determine the quality of the QuikSCAT data scatter plots are constructed by plotting all of the daily QuikSCAT u or v components versus the corresponding daily buoy u and v components. Pearson correlation coefficients r values are then calculated [*Wilks* 1995]. This is done for all 6 buoys.

Another method to determine the quality of the QuikSCAT data is by calculated the complex correlation [*Ladd and Bond* 2002, *Kundu* 1976] between the QuikSCAT data and the buoy data. The complex correlation is calculated for monthly time series, e.g. the 31 values of October 2004 buoy wind vectors are correlated with the 31 daily QuikSCAT wind vectors. The reason that this is done is that a time series of monthly correlations can be constructed which will give an indication of a seasonal cycle. The complex correlation is calculated by writing the wind components as a complex number:

$$w(t_i) = u(t_i) + iv(t_i) \tag{1}$$

where t_i is the time, $u(t_i)$ is the zonal wind time series and $v(t_i)$ is the meridional time series. The complex correlation between two time series $w_1(t_i)$ and $w_2(t_i)$ is defined by *Kundu* [1976] as:

$$\rho = \sum_{i=1}^{n} \frac{w_1(t_i)^* w_2(t_i)}{\sqrt{w_1(t_i)^* w_1(t_i)}\sqrt{w_2(t_i)^* w_2(t_i)}} \tag{2}$$

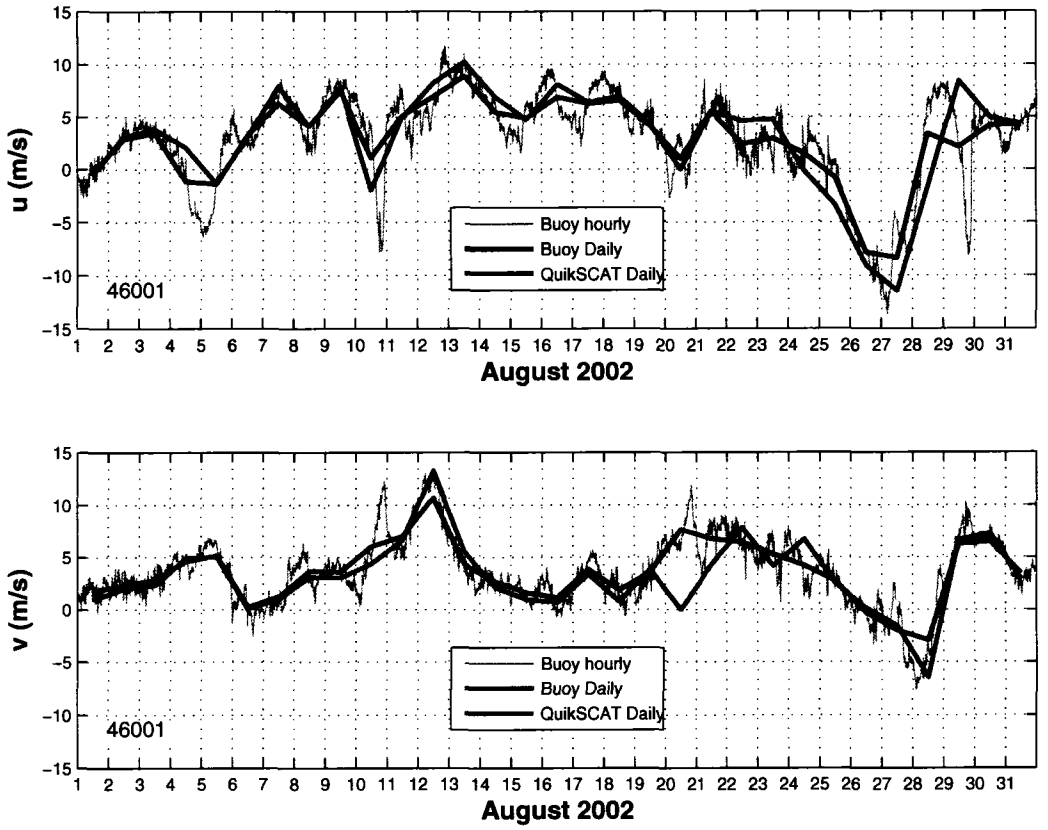

Figure 3. August 2002 buoy and QuikSCAT data at buoy location 46001. These are hourly and daily means of the continuous buoy measurements and the mean of the ascending and descending pass of the QuikSCAT data.

$$\rho = \sum_{i=1}^{n} \frac{[u_1(t_i)u_2(t_i) + v_1(t_i)v_2(t_i)] + i[u_1(t_i)v_2(t_i) - u_2(t_i)v_1(t_i)]}{\sqrt{u_1^2(t_i) + v_1^2(t_i)}\sqrt{u_2^2(t_i) + v_2^2(t_i)}} \tag{3}$$

where n is the number of elements in the $w_1(t_i)$ and $w_2(t_i)$ time series and the asterisk (*) denotes the complex conjugate. Equation 3 is complex and can be written in polar representation as:

$$\rho = re^{i\theta} \tag{4}$$

where r is the magnitude of the correlation and written in terms of u and v as:

$$r = \sum_{i=1}^{n} \frac{\sqrt{[u_1(t_i)u_2(t_i) + v_1(t_i)v_2(t_i)]^2 + [u_1(t_i)v_2(t_i) - u_2(t_i)v_1(t_i)]^2}}{[u_1^2(t_i) + v_1^2(t_i)][u_2^2(t_i) + v_2^2(t_i)]} \tag{5}$$

and θ is the phase angle and written in terms of u and v as:

$$\theta = \sum_{i=1}^{n} tan^{-1} \frac{u_1(t_i)v_2(t_i) - u_2(t_i)v_1(t_i)}{u_1(t_i)u_2(t_i) + v_1(t_i)v_2(t_i)}. \tag{6}$$

The magnitude of the correlation r will be between 0 and 1 with larger values signifying greater correlation. The phase angle θ lies in the range $-\pi \leq \theta \leq +\pi$. Negative values of θ indicate that w_1 is rotated counter-clockwise from w_2 and positive values indicate that w_1 is rotated clockwise from w_2.

2.5 RESULTS

The first comparison of the data sets is the scatter plot of all of the QuikSCAT and buoy velocities covering the same time period and the resulting linear regression fit using least squares (Figures 4 and 5). The Pearson correlation coefficient r values for the u (east/west) velocities for the buoys in the western gulf (46001, 46078 and 46080) are the highest of the six buoys and have values of 0.93 and higher. The r values for the u velocities for the buoys in the eastern gulf (46082, 46083 and 46084) are the lowest with values between 0.74 and 0.82. Similar to the u velocity comparisons, the v (north/south) velocities for buoys 46001, 46078 and 46080 have better r values than the other three buoys. The r values for the v component at 46001, 46078 and 46080 are 0.90 and higher; r values for 46082, 46083 and 46084 are no lower than 0.81. For all the buoys except 46084 the u velocities have a better fit than the v velocities. Buoy 46084 is probably different because it is located on the southeast coast of the Gulf of Alaska and the winds here are predominately south to north in direction and are steered by the coastal topography.

The complex correlation monthly time series for the six buoys (Figures 6 and 7) illustrate that the correlations, r, are the highest for the western buoys 46001, 46078 and 46080; the phase angle, θ, between the two imply that the buoy wind vectors are rotated clockwise with respect to the QuikSCAT wind vectors between 0° to 20° (Figure 6). The correlations, r, for eastern buoys 46082, 46083 and 46084 are not as high as the other 3 buoys; the θ values are about the same but with a few values greater than 20° (Figure 7). Buoy 46084 is the only buoy with negative θ values. The negative values mean that the buoy vectors are rotated counter-clockwise from the QuikSCAT vectors. Once again, this could be the influence of the coastal topography. For all of the buoys there is no noticible seasonal cycle in the complex correlations.

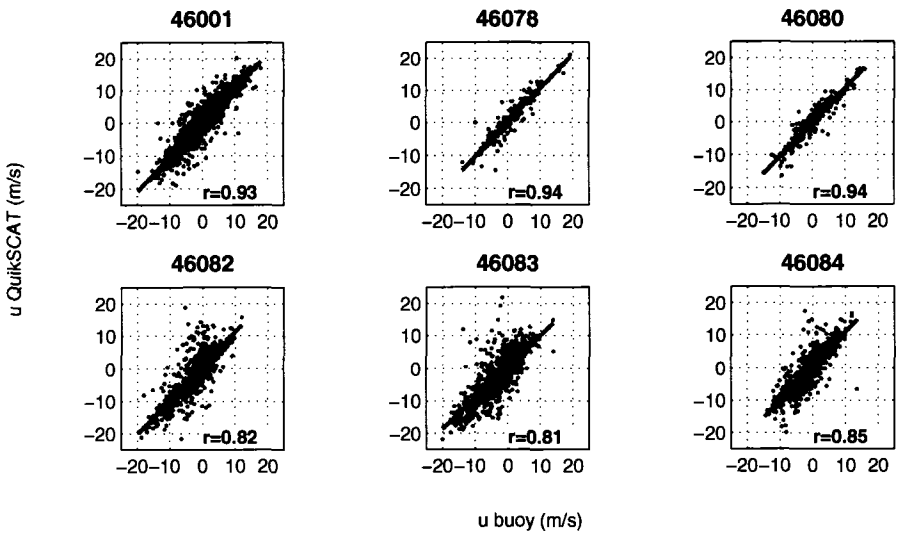

Figure 4. Scatter plots of daily QuikSCAT u velocities versus daily buoy u velocities. Correlations for all the buoys are significant (P>0.95).

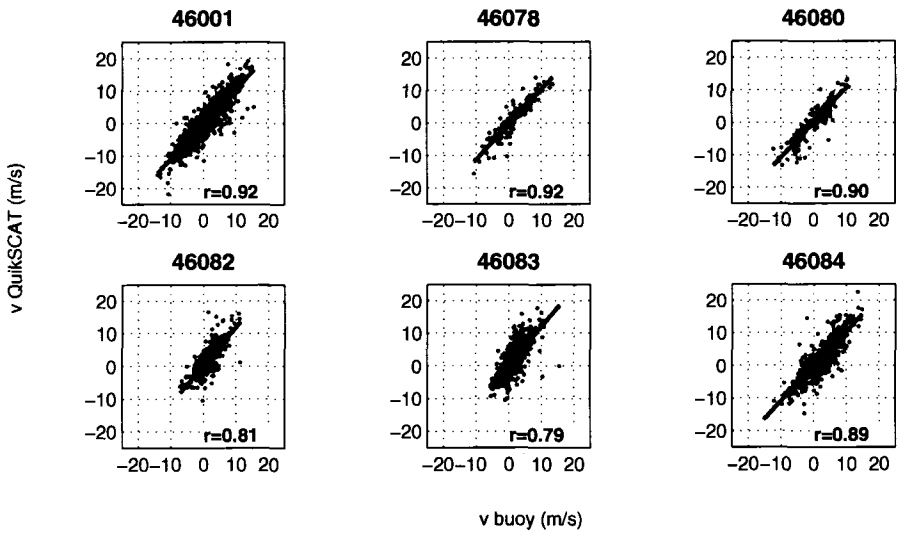

Figure 5. Scatter plots of daily QuikSCAT v velocities versus daily buoy v velocities. Correlations for all the buoys are significant (P>0.95).

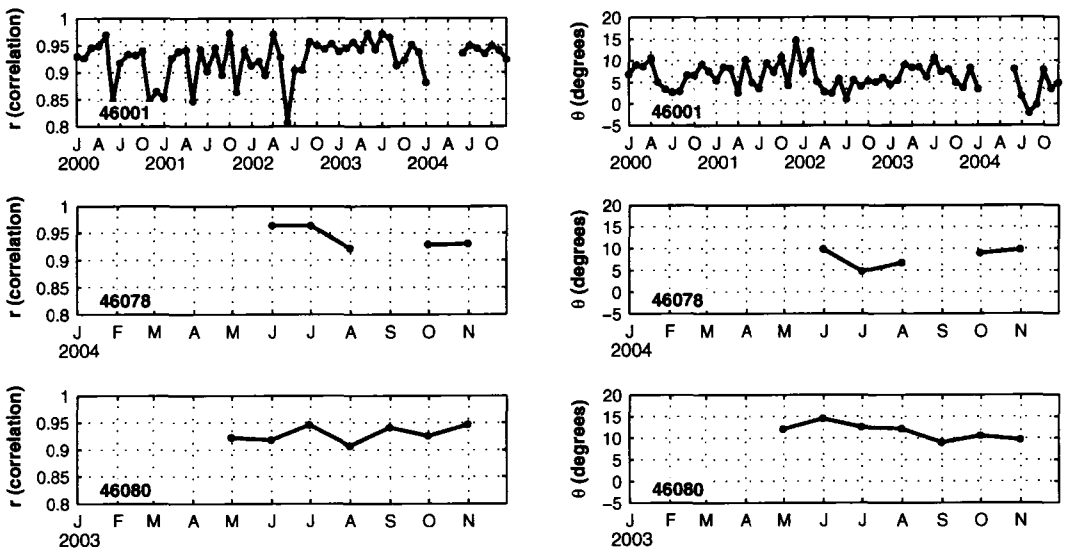

Figure 6. Monthly complex correlation values for buoys 46001, 46078 and 46080.

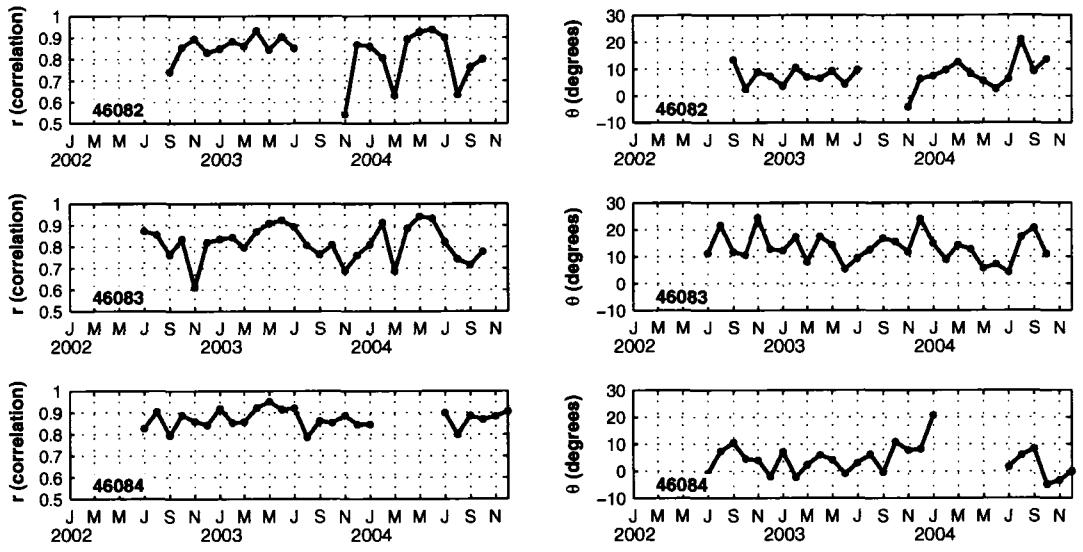

Figure 7. Monthly complex correlation values for buoys 46082, 46083 and 46084.

2.6 CONCLUSIONS

The QuikSCAT wind vectors are a "new" data set and has had very little application in the study of interannual variability on atmosphere/ocean forcing in the Gulf of Alaska. The QuikSCAT winds have been correlated with buoy measurements to see if they do a good job representing the winds at various locations in the gulf. The results show that the winds are best correlated with buoy wind measurements for locations farthest from the shore. When the QuikSCAT locations are closer to the shore the correlations are poorer than those farther offshore. On average the complex correlations of all the buoys are between 0.8 to 0.95 with the buoy vectors are rotated clockwise from the QuikSCAT vectors between 0° to 20°. Both the scatter plots and the complex correlations indicate that the daily QuikSCAT data can be used with confidence. This is really remarkable that twice a day measurements of the winds from the QuikSCAT satellite can be used to represent daily averages of continuous winds.

CHAPTER 3

WIND VECTOR CLIMATOLOGY

3.1 INTRODUCTION

A climatology of the wind vectors was calculated from the daily QuikSCAT wind vectors. Seven QuikSCAT grid points were chosen that lay along the Seward Line and seasonal cycles of the u and v components of the wind vector were constructed for these locations (Figure 8). These 7 locations along the Seward Line will describe "local" wind forcing and in later chapters (Chapters 4 and 5) changes in the Seward Line hydrography have been correlated with time series derived from these winds. Besides the "local" wind forcing, changes in the upstream wind stress are an important factor on the dynamics of the Alaska Coastal Current [*Weingartner et al.* 2005, *Royer* 2005]. Thus, a "regional" climatology was constructed for a domain in the Gulf of Alaska with the following boundaries 55°N – 60°N, 150°W – 140°W. The boundary on the east (140°W) is approximately 600 km from the Seward Line. This distance was chosen because the Alaska Coastal Current is assumed to have an average along shore coastal velocity of about 20 cm s^{-1} or approximately 20 km day^{-1}. So water from over 600 km upstream will reach the Seward Line in one month. The persistence of along-shore wind events is also analyzed in this section. Ekman theory [*Ekman* 1905] states that coastal sea-surface slopes (due to along-shore wind stress) need very little time (order of days) to setup. Thus the duration of upwelling and downwelling events for the "local" winds was analyzed to investigate whether there is ample time for the setup.

3.2 METHODS

The wind climatologies were calculated by averaging all of the daily wind vector components for a particular month for a particular QuikSCAT grid location. The 7 QuikSCAT grid locations along the Seward Line are shown in Figure 8. Each QuikSCAT station is labeled with a capital "Q" and numbered after the closest GAK station, e.g. the QuikSCAT grid location nearest to GAK7 is called Q7. The 7 QuikSCAT stations are very close to the Seward Line and none are farther away than 6.58 km (Table 2). The QuikSCAT data starts on July 19, 1999 and ends on

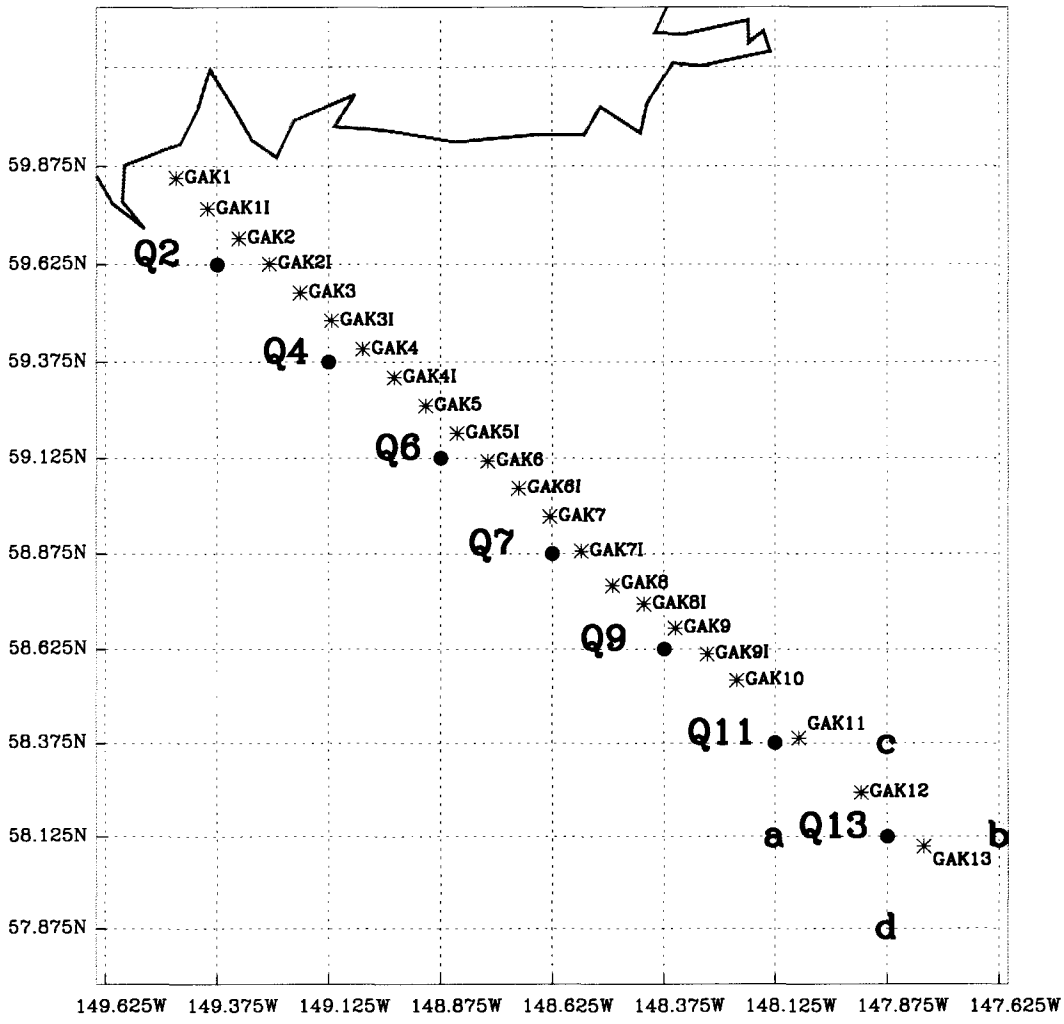

Figure 8. Seward Line and the QuikSCAT grid. QuikSCAT data are located at the intersections of the horizontal and vertical dashed lines. Seven QuikSCAT grid locations, numbered and marked by a dot, are located near the Seward Line. The 22 Seward Line (GAK) stations are marked by asterisks and labeled GAK1 to GAK13.

December 31, 2004. In total there are 1993 daily values and the total number of data points for a particular month are given in Table 3. There are at least 142 days of observations with the number increasing for August through December. Since the satellite was only operational starting mid-July of 1999, the months of January through June will have one month worth of data less; July has 18 days less. The data that are contaminated by rain events are flagged and treated as missing data. Gaps in the wind time series are ignored in the calculation of the climatologies.

The regional climatology was constructed for the domain 55°N – 60°N, 150°W–140°W. This configuration has 48 meridional grid points and 21 zonal grid points.

Table 2. Coordinates of the seven QuikSCAT locations that are nearest to the Seward Line. Also given is the nearest GAK station and the distance between the QuikSCAT location and GAK station.

QuikSCAT Location	QuikSCAT Lat (°N)	QuikSCAT Lon (°W)	Nearest GAK Station	Distance Between GAK and QuikSCAT (km)
Q2	59.625	149.375	2I	6.5811
Q4	59.375	149.125	4	5.7198
Q6	59.125	148.875	6	6.0628
Q7	58.875	148.625	7I	3.8092
Q9	58.625	148.375	9I	5.8081
Q11	58.375	148.125	11	3.4253
Q13	58.125	147.875	13	5.6582

Of these, 92 are on land and therefore not used in these calculations. This leaves 916 QuikSCAT grid points for use in constructing the climatology.

The climatology of three different measures of wind events is calculated for selected QuikSCAT grid points along the Seward Line. The three different measures are: (1) longest period of days with consecutive positive or negative zonal ($\pm u$) winds, (2) the mean length of the $\pm u$ in a month, and (3) the number of $\pm u$ events experienced during a given month. A wind event is defined as more than one day of winds blowing in the same direction. These three measures were calculated from the u time series at Q2 and Q13 for the time time period 7/1999 - 12/2004 (containing 1993 daily values). So, the climatology is for 5 years for January through June and 6 years for July through December.

3.3 RESULTS

There are two major points to be made about the zonal (u) climatology (Figure 9): the shear and the reversal. The zonal winds decrease in magnitude from coast to offshore, i.e. from QuikSCAT station Q2 to Q13. For all seven stations February has the highest westward winds and the largest offshore shear between Q2 and Q13. June has the least offshore wind shear all across the Seward Line. The June values are an abrupt departure from the values of the preceding and following months. June is a transitional month. In May, the Aleutian Low moves away from the gulf to the Bering Sea and in June the dominate pressure feature in the gulf is the East

Table 3. The number of days in each month that have QuikSCAT data. These data are used to calculate the seasonal cycle.

Month	Number of Days
1	155
2	142
3	155
4	150
5	155
6	150
7	168
8	186
9	180
10	186
11	180
12	186

Pacific High [*Wilson and Overland* 1986]. Mean sea-level pressure maps show that June should have stronger eastward winds than May and July [*Wilson and Overland* 1986]. The months of January through June have only eastward winds. Starting in July there are reversals of the winds from westward to eastward for the stations farthest from the shore, Q7 through Q13. QuikSCAT grid point Q13 has the most number of months with eastward winds (July through December).

The majority of the months have northward winds in the meridional wind climatology (Figure 10). In general the largest magnitude northward winds are at the grid points farthest offshore (Q11 and Q13). The magnitude of the northward winds decrease closer to shore. This is due to the influence of the coastal mountain chain on atmospheric motion (Chapter 2.1). For four of the months there is a switch from northward winds to southward winds at the grid points closest to the shore (Q2 - Q6). Eight of the months for the Q2 climatology have southward winds, this is presumably due to katabatic winds blowing out of Resurrection Bay [*Wilson and Overland* 1986]. February is the month where all seven QuikSCAT stations have northward winds; also, February has the largest wind magnitudes at almost 4 m s^{-1} at Q11.

The regional zonal wind climatology (Figure 11) is dominated by westward winds ($u < 0$). In all months except June, the general pattern is maximum westward winds along the coast and maximum eastward winds along 55°N. The westward winds

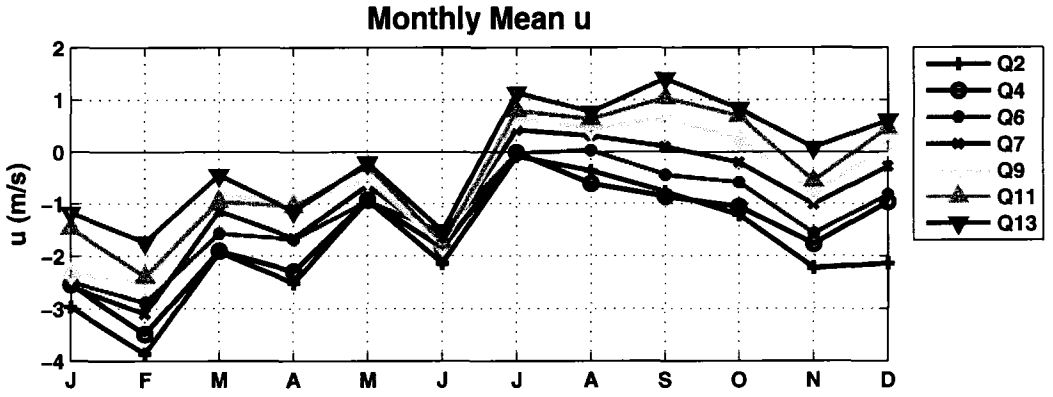

Figure 9. Seasonal cycle of the zonal wind (u) magnitudes at the 7 QuikSCAT locations which are near the Seward Line. Negative velocities denote winds that are downwelling inducing.

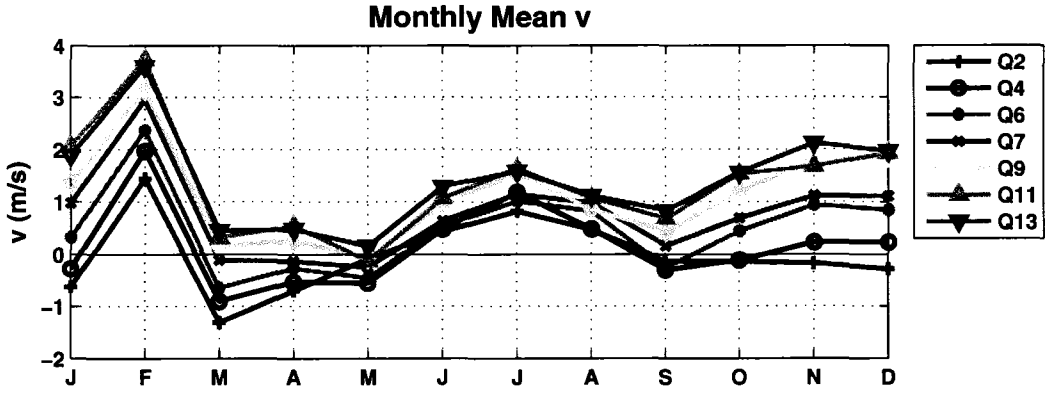

Figure 10. Seasonal cycle of the meridional wind (v) magnitudes at the 7 QuikSCAT locations which are near the Seward Line. Positive values are for northward winds.

decrease offshore until they approach zero and then reverse direction to eastward winds, which continue to increase farther offshore. The westward winds are strongest in January and February, and weakest in July and August. In January the maximum westward wind has a value of -5.6 m s^{-1} and occurs to the east of the Seward Line just south of Prince William Sound. The maximum westward wind in February is -4.62 m s^{-1} and occurs in the same location as that in January. Also in February the magnitude of the westward winds is largest for all the months along the Seward Line with values close to -4 m s^{-1}. The July westward winds are very weak with a maximum of -0.78 m s^{-1} just south of Prince William Sound. In general the westward winds are strongest near the coast and weaken off-shore, eventually reaching a line

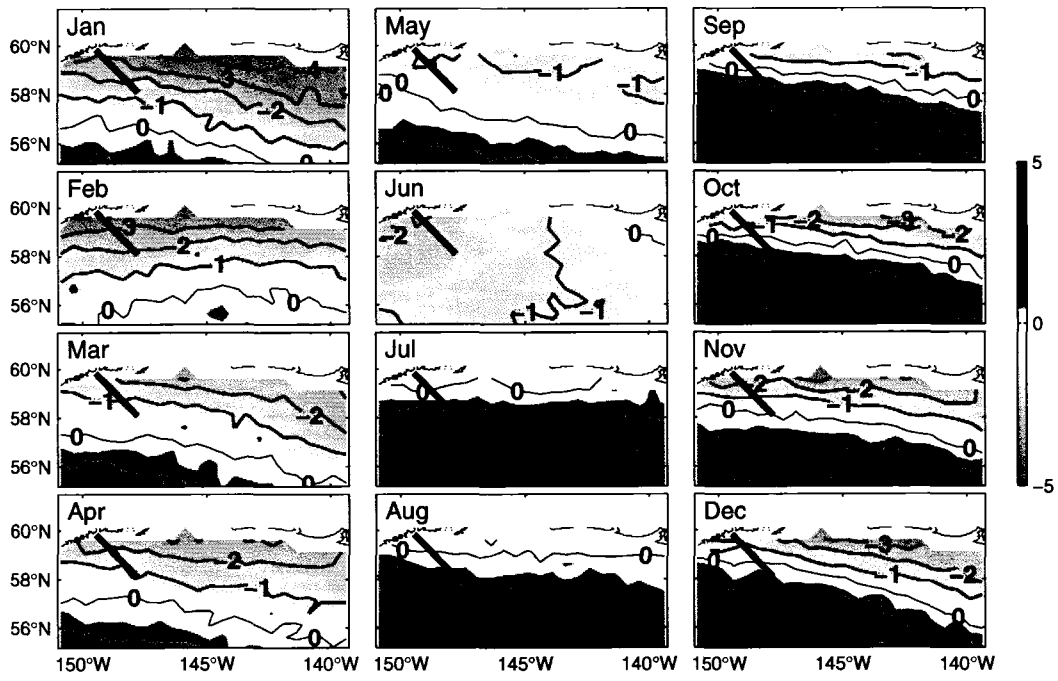

Figure 11. Seasonal cycle of the regional zonal wind (u) magnitudes. The units are in m s^{-1}. Positive (negative) velocities denote eastward (westward) winds that induce coastal upwelling (downwelling). The black solid line marks the Seward Line.

of zero velocity. The position of this line of zero velocity varies seasonally. The zero line is in the southern half of the domain in the months January through May and moves towards the north of the domain in the months July through December. The zero line does not appear in June, meaning that in June all the zonal winds are westward. For all months except June there are eastward winds in the southern part of the domain. The spatial coverage of the eastward winds are smallest for January through May and greatest from July through December. The maximum eastward wind is +3.68 m s^{-1} and occurs in October in the southwest corner of the domain. For all months, except May and June, the meridional shears are larger between 58°N and 60°N than elsewhere. This can be observed by inspection of the distances between contour levels. The months September through January especially have large westward wind shears; the westward winds decrease approximately 1 m s^{-1} in a distance on the order of 100 km.

The regional meridional wind climatology (Figure 12) is composed primarily of northward winds ($v > 0$). The strongest northward winds occur in the eastern part of the domain and have velocity greater than +3 m s^{-1}. The northward winds

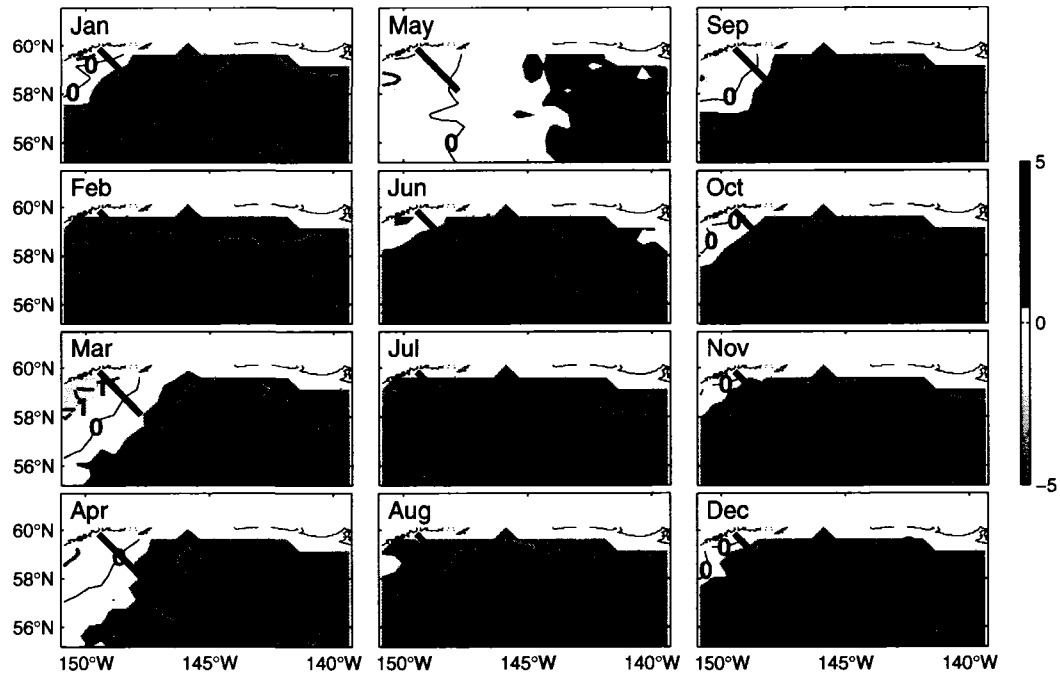

Figure 12. Seasonal cycle of the regional meridional wind (v) magnitudes. The units are in m s^{-1}. Positive values are for winds that blow from the south to the north. The black solid line marks the Seward Line.

decrease in magnitude going from east to west across the domain. In the majority of the months there is a reversal of the winds from northward to southward in the northwest corner of the domain around the Seward Line. These southward winds do not appear in February, June, July and August. February has the largest magnitude northward winds with speeds reaching 4.8 m s^{-1}; and is located in the southwest corner of the domain. In March, just west of GAK4, are the largest magnitude southward winds with speeds over -2 m s^{-1}.

The u and v regional climatologies (Figures 11 and 12) indicate that the Seward Line is located in a region where there are reversals of both the zonal (u) and meridional (v) winds. These reversals will tend to produce mesoscale wind features that are cyclonic. To better visualize these structures it is more advantageous to view the vector climatology (Figure 13). The mesoscale features are most apparent in September with the center of the cyclonic gyre located in the middle of the Seward Line. From October through December the center is located to the west of the Seward Line. The mesoscale structures are absent in February, June, July and August. Positive curl patterns on the shelf have also been calculated by *Chelton et al.* [2004];

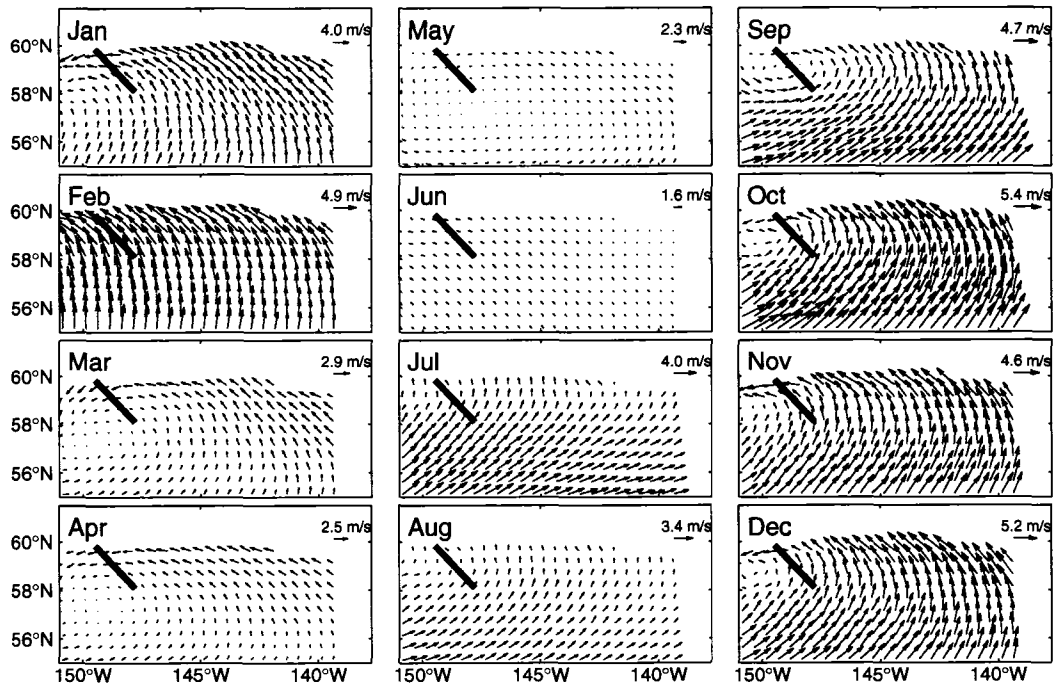

Figure 13. The seasonal cycle of regional vector field. For better visualization only every other grid point is plotted. For a particular month the maximum vector magnitude of the vector field is labeled in the upper right hand corner.

though, the calculation was in the context of a global curl calculation and was not reported as significant.

The complex correlation (Equation 2) of the QuikSCAT winds along the Seward Line with winds upstream and downstream of the Seward Line is used to test the spatial coherency. This is done to determine if the hydrographic response (hydgrographic response is defined to be significant correlation between hydrographic time series anomalies and wind forcing time series anomalies) along the Seward Line to certain wind derived time series (e.g. Ekman transport and pumping) can be done for winds at the Seward Line or at some distance upstream. The correlations of the wind time series (Figure 14) at one of the seven QuikSCAT grid points along the Seward Line was done with the wind time series upstream and downstream along the same line of latitude. For example the time series at QuikSCAT grid point Q2, that is located at 59.625°N, 149°W, is correlated with all the time series upstream and downstream located on the same line of latitude (59.625°N). The magnitude of the correlation (Figure 14a) quickly drops to 0.9 at a short distance upstream and downstream of the Seward Line. The correlation is around 0.8 at 152°W and 145°W.

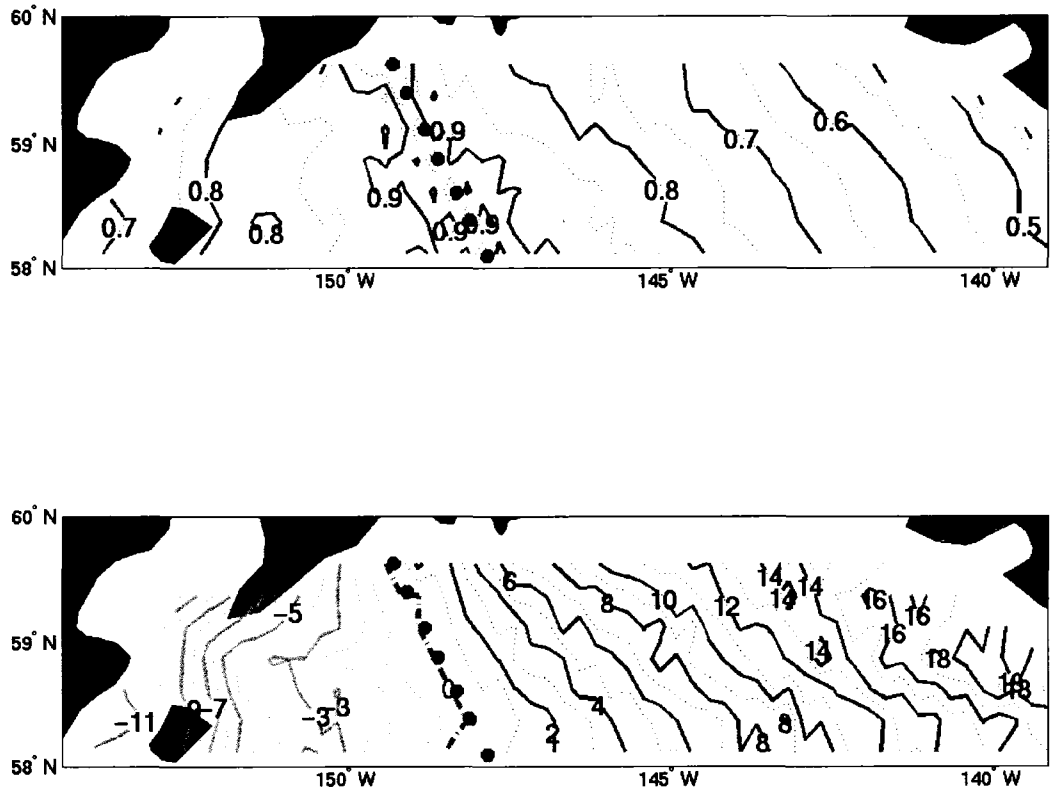

Figure 14. The complex correlation of the wind vector time series along the Seward Line to the wind vectors upstream and downstream. The circles denote the location of Seward Line wind vector time series. The correlations are between the time series located at the circles and times series along the same line of latitude. (a) is the magnitude of the correlation and (b) is the phase angle in degrees.

At 140°W the correlation is around 0.55 to 0.5. The phase angle (Figure 14b) is given in degrees and shows that the winds upstream from the Seward Line are rotated up to 18° clockwise. The winds downstream are rotated up to -11° counter-clockwise.

The complex correlations are high upstream of the Seward Line up to longitude 145°W. The alongshore winds between the Seward Line and 145°W are very spatially uniform. The Empirical Orthogonal Function (EOF) was calculated to determine the spatial variability of the alongshore winds. Standard EOF techniques were used and the eigenfunctions were calculated from the covariance matrix [*Wilks* 1995]. The EOF was calculated on the daily wind time series located in the domain of 58.1°N – 59.6°N, 149.9°W – 145.4°W (Figure 15). The first mode explains 84.5% of the total variance. The spatial variability of the first mode is uniformly positive, with the highest positive values in the southwest and smaller positive values in the northeast.

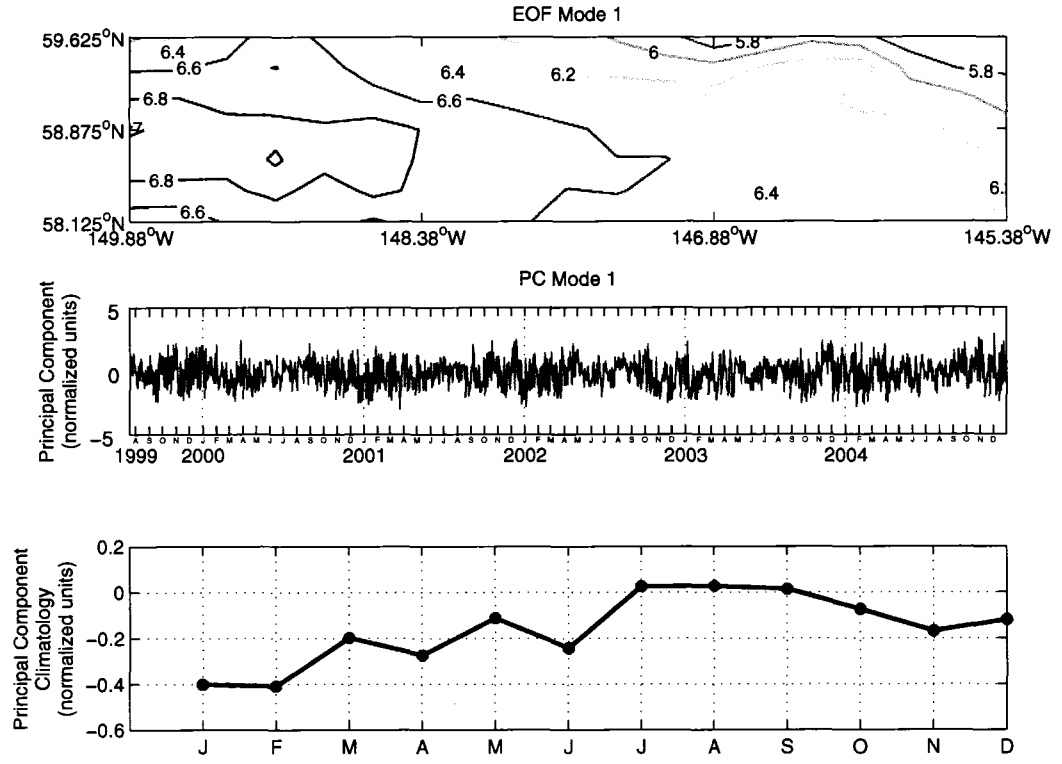

Figure 15. Mode 1 of the EOF of the daily alongshore winds for the region upstream the Seward Line. Positive values of the PC will result in eastward winds and negative values will result in westward winds. This mode is used to describe the relaxation of the regional downwelling winds upstream the Seward Line (Chapter 5 and 6).

The principal component (PC) describes the change of the EOF over time. When the PC is positive (negative) the alongshore winds blow eastward (westward). Because mode 1 describes most of the total variance it can be used as an index of the strength of the regional winds. When there are time periods of sustained positive PC values, such as August 2002 and November 2003, these are periods of relaxation of the expected coastal downwelling winds. In Chapters 4 and 5 the mean of the PC is used as an index for the relaxation of the downwelling winds for the region upstream the Seward Line.

3.4 EVENTS

Events of constant coastal upwelling (eastward) and downwelling (westward) days are analyzed to determine the duration of possible sea surface setups. A wind event is defined as 2 or more days of constant eastward or westward winds. The majority

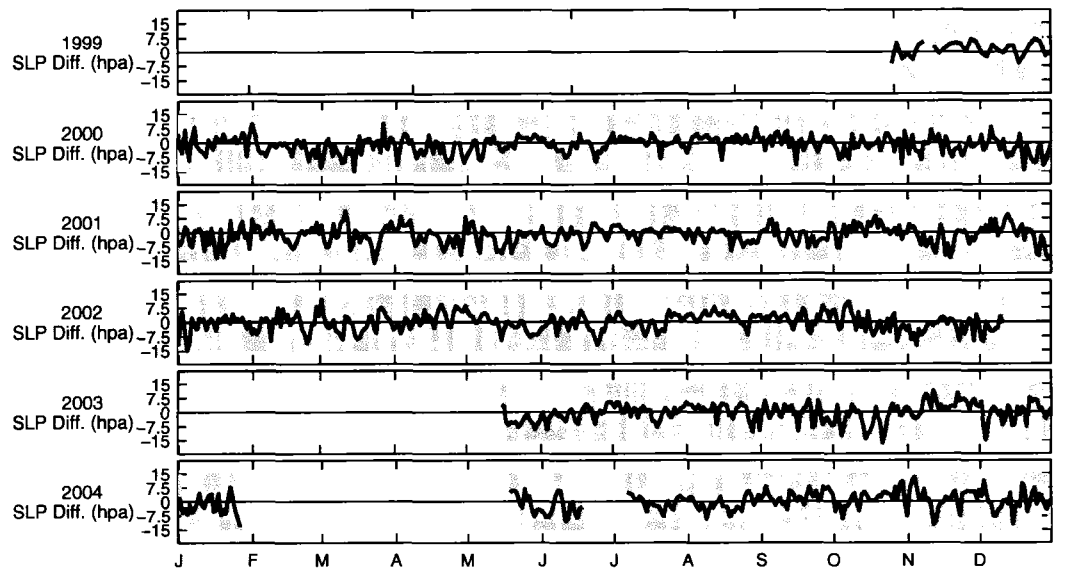

Figure 16. Distribution of wind events at Q2I. The shaded areas mark wind events 2 days or longer. The negative shaded areas are for westward events and positive shaded areas are for eastward events. Also on the figure is the time series of SLP difference between 46001 and PILA2 (46001 - PILA2).

of the wind events are due to large scale changes in the barometric sea level pressure (SLP). As a measure of these changes a time series is constructed by taking the difference of the SLP at buoy 46001 (56.30°N, 148.17°W) and the C-MAN station at PILA2 (Pilot Rock, 59.74°N, 149.47°W). PILA2 is approximately due north of buoy 46001 and the distance between the two buoys is approximately 390 km. Figures 16 and 17 show the distribution of zonal ($\pm u$) events at Q2 and Q13. Marked on these figures are the consecutive $\pm u$ events 2 days and longer. The eastward events are marked by positive shaded areas and the westward events are marked by negative shaded areas. Also on the figures is the time series of the SLP difference between the offshore buoy and Pilot Rock. The SLP difference is calculated by subtracting the SLP at PILA2 from the SLP at 46001 (46001 - PILA2). Negative SLP differences correspond to westward (downwelling) wind events and positive SLP differences correspond to eastward (upwelling) wind events. For all six years the winds rarely switch back and forth between eastward and westward on a daily basis. The longest stretch of the switching between eastward and westward winds is 8 days for both Q2 and Q13. This occurs at the end of February 2001. Events, especially those 5 days and longer, occur at Q2 and Q13 at the same time. For example, there are long eastward

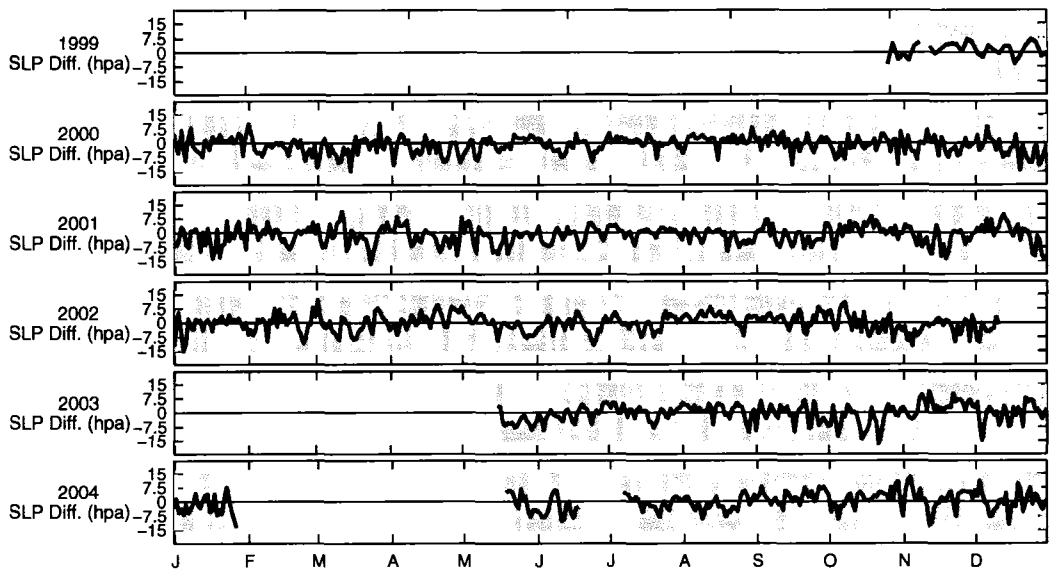

Figure 17. Distribution of wind events at Q13. The shaded areas mark wind events 2 days or longer. The negative shaded areas are for westward events and positive shaded areas are for eastward events. Also on the figure is the time series of SLP difference between 46001 and PILA2 (46001 - PILA2).

events at Q2 and Q13 in the following months: August 2000, October 2001, August 2002, November 2003 and October 2004. The long eastward events usually happen between August and December. From the UI at 60°N, 149°W *Royer* [2005] it is surprising to see such long eastward events in October through December. There are also common occurrences of westward events between the two locations (Q2 and Q13). Examples of these are in the following months: March and December 2000, August and September 2001, November 2002, May and June 2003. As expected there are more westward events that eastward events. Long westward events occur in all twelve months.

The seasonal cycle of the wind events at Q2 is summarized in Table 4. Since 1999 the longest duration of eastward ($+u$) winds is 12 days during August; the longest duration of westward ($-u$) winds is 16 days in March. The average length of the eastward wind events last between 2.4 days to 3.8 days. For the twelve months the mean number of eastward events are between 1.4 to 4.0. The average length of westward winds last between 3.2 days to 5.4 days. The mean number of these events for the twelve months are 2.8 to 4.4. So in general, for all twelve months, there are around 3 $\pm u$ events per month, each lasting approximately 3 days. As expected, from

Table 4. The climatology of $\pm u$ wind events at QuikSCAT location Q2. The three different measures of wind events are: longest event, average length of the events, and average number of events per month.

Month	Longest +u event (days)	Length of +u events (days)	Average number of +u events	Longest -u event (days)	Length of -u events (days)	Average number of -u events
Jan	7	2.4	6.2	11	3.6	6.6
Feb	4	2.4	5.6	9	4.1	5.8
Mar	9	3.8	4.6	16	4.8	4.2
Apr	7	3.5	4.4	12	4.5	4.2
May	10	3.5	4.4	8	3.9	5
Jun	8	2.7	4.2	12	5.4	4.4
Jul	7	3.1	4.9	11	3.8	5.1
Aug	12	3.5	5.3	9	3.2	5.2
Sep	5	2.7	5.8	10	3.2	5.7
Oct	7	3.4	6.3	10	3.5	6.5
Nov	9	2.8	4.8	15	4.4	5
Dec	9	3.1	5.7	13	3.8	5.5

the UI, the westward events have a longer duration than the eastward events. This is also reflected in the longest event; the longest period event is longer for westward events for all months except May and August. An unexpected result is the average length of the westward events in June; it is the longest for the entire time series. This is contrary to the UI, from which one expects mostly upwelling in June. The seasonal cycle of the wind events at Q13 is summarized in Table 5. Since 1999 the longest duration of eastward winds is 19 days during November; the longest duration of westward winds is 14 days for May. The average length of the eastward wind events in a month last from 2.4 days to 4.3 days. The mean number of eastward events are between 2.2 to 4.7 for the twelve months. The average length of westward winds in a month last from 3.1 days to 4.5 days. There are 2.7 to 4.0 mean number of these events for the twelve months. So in general, for all twelve months, there are around 3 $\pm u$ events, each lasting approximately 3 days, similar to the winds at Q2.

The eastward wind events correspond with time periods where the SLP is lower at PILA2 than at 46001. Conversely, the westward wind events occur when the SLP is higher at PILA2 than at 46001. These wind events are geostrophic. To determine the extent of the geostrophic winds across the Seward Line the daily SLP differences were correlated (Figure 18) to the daily u winds at all 7 QuikSCAT stations along

Table 5. The climatology of $\pm u$ wind events at QuikSCAT location Q13. The three different measures of wind events are: longest event, average length of the events, and average number of events per month.

Month	Longest +u event (days)	Length of +u events (days)	Average number of +u events	Longest -u event (days)	Length of -u events (days)	Average number of -u events
Jan	6	2.9	6.8	9	3.4	7
Feb	4	2.4	6	10	3.9	5.8
Mar	17	3.1	5.2	12	3.9	5.2
Apr	8	4.2	4.6	8	3.6	4.6
May	10	3.6	4.8	14	3.5	5
Jun	8	2.9	4.6	9	4.5	4.6
Jul	12	4.1	4.9	10	3.4	4.4
Aug	14	4.3	4.5	10	4.3	4
Sep	8	3.3	6	10	3.1	5.3
Oct	13	3.6	6	9	3.6	5.7
Nov	19	2.7	5.2	12	3.6	5.2
Dec	9	3.9	5.5	11	3.8	4.8

the Seward Line. Spearman's rank correlation method at lag 0 was the correlation method used [*Kendall and Gibbons* 1990]. The SLP data for both of 46001 and PILA2 have gaps and correlations are only done only for months which have at least 15 days of SLP difference data. The seasonal signal in the correlations indicate higher correlations during March through June and lower correlations during the other months. All correlations are statistically significant at a probability of 0.99 and higher for all months and all QuikSCAT grid points. The correlations are higher at Q13 than Q2. Obviously the high correlation for the outer QuikSCAT grid points is due to the winds being more geostrophic with less coastal influences. The winds near the coast have lower correlations so ageostrophic winds are probably present.

3.5 CONCLUSIONS

The most significant finding from the climatology of the winds is that there is shear of the alongshore winds as one moves off-shore. The winds with the largest westward magnitude occur near to the coast and their magnitude decreases across the shelf. These westward winds generally have magnitudes of 3 to 4 m s^{-1} at the coast and they decrease by about 1 m s^{-1} in a distance of approximately 100 km. This shear of the alongshore winds is contrary to the winds in the California Current

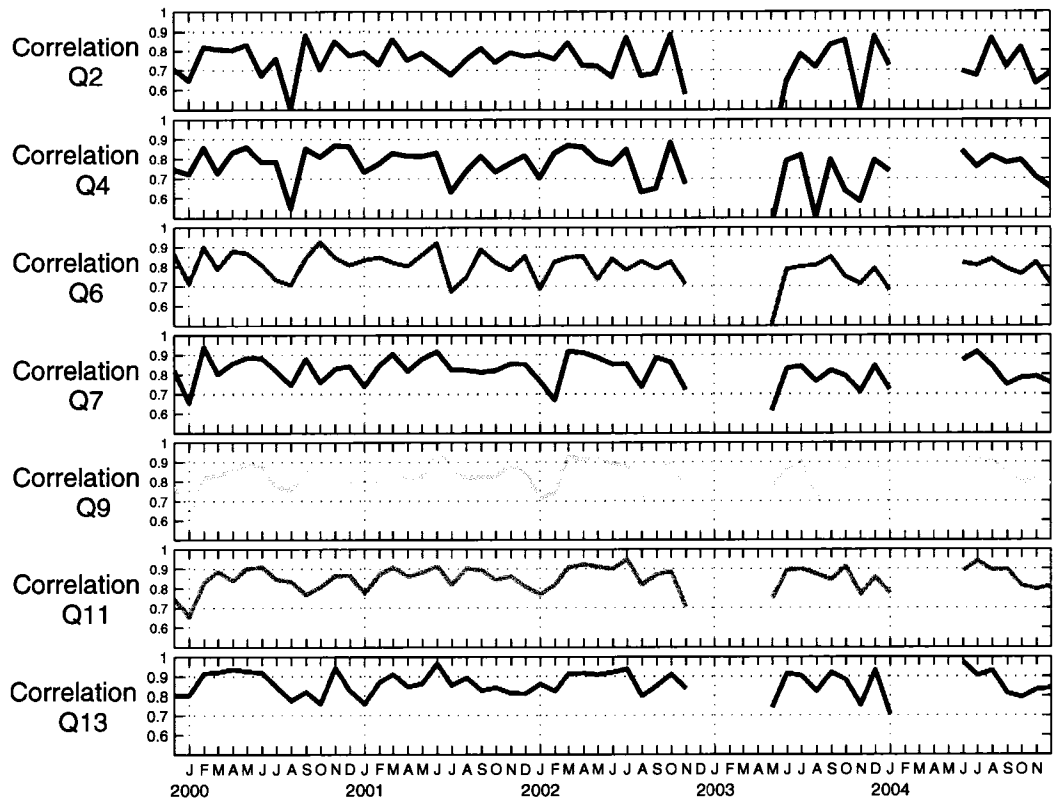

Figure 18. Spearman's Rank Correlation at lag 0 of the sea level pressure difference between buoys 46001 and PILA2 to the along-shore winds. The correlation is done at all 7 QuikSCAT grid points along the Seward Line. All correlations have significant correlations with probabilities of 0.99 and higher.

System (CCS) [*López-Mariscal and Clarke* 1993]. In the CCS the winds increase in magnitude offshore.

The duration of alongshore wind events across the Seward Line is around 3 $\pm u$ days. Long eastward (upwelling) events (more than 3 days) are common in October through December, while long westward events are common in any month. Large scale gradients in the SLP across the Gulf of Alaska tend to drive the alongshore wind events. Since the winds closer to shore are less correlated to changes in large scale SLP, it can be assumed that this region might experience ageostrophic winds such as barrier jets [*Winstead et al.* 2005, *Stabeno et al.* 2004].

CHAPTER 4

EKMAN TRANSPORT AND PUMPING

4.1 INTRODUCTION

A time series of QuikSCAT wind stress vectors is created to help elucidate hydrographic changes along the Seward Line. In multiple papers [*Royer* 2005, *Stabeno et al.* 2004, *Livingstone and Royer* 1980, *Weingartner et al.* 2005] the primary time series to study the effects of the wind are the alongshore components of the wind stress vector. Historically the only sources of wind data available were the calculated geostrophic winds and the wind vector measured at Middleton Island. While the alongshore wind stress vector promotes downwelling/upwelling by the process of Ekman transport, the curl of the wind over the shelf is now being recognized as important to shelf circulation. In recent studies [*Pickett and Paduan* 2003, *Croquette et al.* 2004] the curl of the wind stress has been considered to be an important time series. The curl of the wind stress vector produces upwelling/downwelling through the process of Ekman pumping.

4.2 METHODS

Ekman mass transport is calculated from *Pickett and Schwing* [2006]:

$$\boldsymbol{M} = \frac{1}{f\rho_w}\boldsymbol{\tau} \times \boldsymbol{k} \tag{7}$$

where k is the vertical unit vector, f is the Coriolis parameter, ρ_w is the average water density, and $\boldsymbol{\tau}$ is the wind stress vector. Ekman transport has units of $\mathrm{m}^2\ \mathrm{s}^{-1}$. Expanding 7 into along (M_x) and across-shelf (M_y) components results in:

$$M_x = \frac{\tau_y}{f\rho_w} \tag{8}$$

$$M_y = -\frac{\tau_x}{f\rho_w}\ . \tag{9}$$

Zonal winds (τ_x) will produce across-shelf mass transport (equation 9) and meridional winds (τ_y) will produce alongshore mass transport (equation 8) in the northern Gulf of Alaska. Specifically for the study area we are particularly interested in winds that blow from the east to west ($-u$) resulting in northward ($+M_y$) mass transport.

Ekman volume transport that is used to calculated the UI [*Bakun* 1973] is calculated by multiplying the across shelf component (equation 9) by a horizontal distance:

$$Q_y = XM_y \tag{10}$$

where X is the east/west distance and M_y is the north-south mass transport. If X is set to 1 meter then the units for Q_y is $m^3\ s^{-1}$ per 1 m of coast. For the UI, the alongshore distance X is set to 100 m and the resulting unit is $m^3\ s^{-1}$ per 100 m of coast. The UI has the opposite sign of Ekman transport to reflect that positive transport (transport that is onshore) will produce negative (downwelling) vertical transport and vice versa [*Schwing et al.* 1996]. Instead of dealing with the cumbersome units of $m^3\ s^{-1}$ per 100 m of coast, the units for Q_y will be given as $m^3\ s^{-1}$ with the understanding that it is per 100 m of coast.

The vertical water velocity, w, due to Ekman pumping was calculated following the method outlined in *Pickett and Paduan* [2003]. The Ekman pumping vertical velocity is calculated from:

$$\boldsymbol{w} = \frac{1}{f\rho_w}\boldsymbol{\nabla} \times \boldsymbol{\tau} = \frac{1}{f\rho_w}\left(\frac{\partial \tau_y}{\partial x} - \frac{\partial \tau_x}{\partial y}\right) \tag{11}$$

where the curl of the wind stress vector ($\boldsymbol{\tau}$) is for the daily QuikSCAT Liu algorithm wind stress, ρ_w is the average water density and f is the Coriolis parameter.

The curl of the wind stress was calculated at each of the seven QuikSCAT locations using center differencing. Figure 8 shows an example of the coordinates used for the calculation of the curl. Surrounding QuikSCAT station Q13 are four adjacent sites labeled 'a', 'b', 'c' and 'd'. Using equation 11, the upwelling velocity at QuikSCAT location Q13 can be written in center differencing terms as:

$$w_8 = \frac{1}{f\rho_w}\left(\frac{\tau_b^y - \tau_a^y}{\Delta x} - \frac{\tau_d^x - \tau_c^x}{\Delta y}\right) \tag{12}$$

where τ_a^y, τ_b^y, τ_c^x, and τ_d^x, are the wind stress at the respective locations, and Δx is the distance between points 'a' and 'b', and Δy is the distance between points 'c' and 'd'. The curl and distances in equation 12 were calculated using spherical coordinates with the routine 'uv2vr_cfd' from the NCAR Command Language (http://www.ncl.ucar.edu/).

For a given month the monthly climatological mean is calculated from all the daily data in that month for all the years. For example there are 31 days in December and

Table 6. The total number of days used in the calculation of the 3 different climatologies for Ekman transport and pumping.

Month	Total Number of Days for Q_y & w	Number of -Q_y Days	Number of +Q_y Days	Number of -w Days	Number of +w Days
1	155	95	59	65	89
2	142	100	42	57	85
3	155	86	69	62	93
4	150	89	61	49	101
5	155	84	70	58	93
6	150	95	55	57	91
7	168	77	87	52	112
8	186	85	98	61	122
9	180	86	93	49	131
10	186	93	93	45	141
11	180	102	74	46	129
12	186	93	91	73	111

6 total Decembers in the Q_y and w time series. Thus the December climatological mean is the average of 186 (31x6) daily values. Other variations of the monthly climatology is the average of only upwelling or downwelling daily data in the month for all the years. Table 6 lists the number of daily values used in the calculation of the three different climatologies for Ekman transport (Q_y) at Q4 and upwelling (w) due to Ekman pumping at Q7. The alongshore winds are a series of events that switch directions approximately every 3 days (Chapter 3.4). The implication is that the monthly climatological mean might be very small due to the cancellation of an equal amount of upwelling/downwelling events. This plays a more significant factor in the Ekman transport than the Ekman pumping. In about half of the months (Table 6) Ekman transport has approximately an equal amount of upwelling (+Q_y) and downwelling (-Q_y) days. Ekman pumping has more upwelling (+w) than downwelling (-w) days; i.e. for April through December, there are 1.5 to 3 times more upwelling days than downwelling days.

To estimate the effect of Ekman transport and pumping on the hydrographic data, correlation maps are constructed. Spearman's rank correlation method is used between hydrographic anomalies and Ekman transport and pumping anomalies. Ekman transport and pumping anomalies are constructed by taking the average of upwelling,

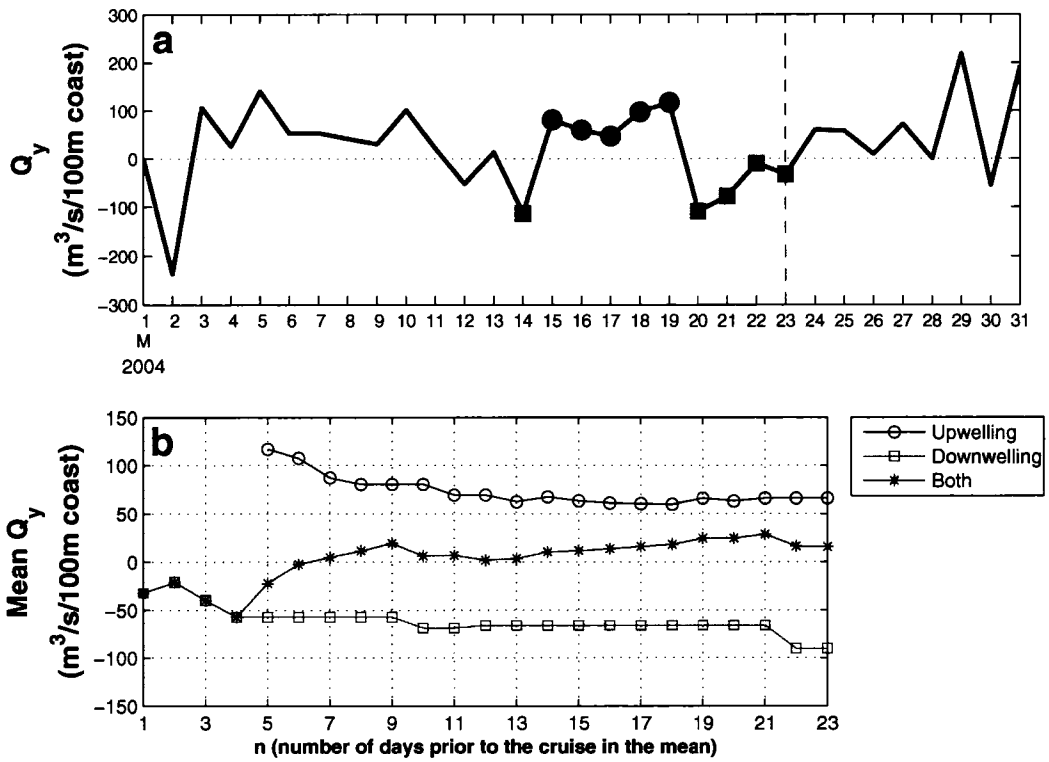

Figure 19. (a) March 2004 daily values of Q_y. The days marked with symbols are the 10 days before and including the starting date of the GLOBEC cruise. The circles are upwelling Q_y days and the squares are downwelling Q_y days. The vertical dotted line marks the first day of the March 2004 GLOBEC cruise (March 23). (b) Mean values of Q_y for 1 to 23 days in the calculation of the mean. Mean values are constructed by using only upwelling days, downwelling days or both (upwelling and downwelling days).

downwelling or upwelling and downwelling days ranging from 1 to n days in advance of the start date of the GLOBEC cruise. The reason that the 3 different means are considered can be addressed by referring to Figure 19. Figure 19a shows the daily Ekman transport (Q_y) values for March 2004; the 10 days with symbols (circles for upwelling and squares for downwelling) are the days preceding and including the first day of the GLOBEC cruise (marked by the vertical dotted line). The mean of all 10 days is 6.1 m^3 s^{-1}, which for this period of ten days is very weakly upwelling. But if just the upwelling and downwelling days are considered separately then the means are 80.6 m^3 s^{-1} and -68.5 m^3 s^{-1} respectively. So for the 10 days before the cruise there are periods of significant upwelling and downwelling. Different anomaly time series are constructed from means of Q_y and w for different number of days preceding

and including the first date of the cruise. Figure 19b shows the 3 different types of means (upwelling, downwelling, and both) for the March 2004 data (Figure 19a) as the number of days from the start of the cruise, used in the averaging, is increased from 1 to n days. In this example n is 23; there is nothing significant about the choice of 23 it just happens to be the number of days from the 1^{st} of March to the starting date of the cruise. The upwelling mean starts on the fifth day because the first four days preceding the cruise are downwelling days.

To distinguish the time series that will be used for correlations with the GLOBEC hydrographic data, Q_y and w are given new symbols. The new symbol for the Ekman transport time series is Q_n and the new symbol for Ekman pumping is W_n. Both Q_n and W_n are given one of two superscripts u (upwelling) and d (downwelling) and the subscript, n, is the number of days in the mean of the type denoted by the superscript. For example Q_6^u denotes that the Ekman transport time series uses only the upwelling days in the 6 days leading up to the cruise; if there are no upwelling days then the mean will be zero. If no superscript is given then the time integration is for both upwelling and downwelling days. When the mean has been calculated for one of the 7 QuikSCAT locations along the Seward Line the time series will be followed by the QuikSCAT station in parentheses, e.g. Q_6^u calculated at the QuikSCAT station Q7 will be denoted by Q_6^u(Q7). There were 35 GLOBEC cruises conducted from August 1999 to December 2004. Because the QuikSCAT data starts in July 1999 there are only 35 values in the Q_n and W_n time series.

4.3 RESULTS: EKMAN TRANSPORT SEASONAL CYCLE

Ekman transport is calculated (Equations 9 and 10) and then the sign is reversed to convert the Ekman transport units to the UI. A sample daily time series shows that the magnitude of the downwelling days (-Q_y) is larger than the upwelling days (+Q_y) (Figure 20). The majority of the upwelling days are in the months of March through September but there are periods where there are long periods of upwelling in the other months. For example, in November 2003 there is a period of 22 days of continuous upwelling. The long periods of upwelling, especially in the winter months, are not present in the UI at 60°N, 149°W (Figure 21). The average magnitudes of the upwelling and downwelling in the UI are not as large as in Q_y. The seasonal cycle appears to be the same, but there are no long periods of upwelling in the winter months. As mentioned before, Q_y in November 2003 has a period of 22 days

of persistent upwelling , but the UI during the same period has only nine days of upwelling with the longest period of persistent upwelling of three days.

The seasonal cycle of the percentage of the number of days with upwelling (Figure 22) has the number of days with upwelling in the QuikSCAT data between 30 to 60%, while the UI is between 10 to 70%. February and June are the months with the fewest upwelling days, between 30 and 40%, for the QuikSCAT data. While the months July through October have the greatest number of upwelling days, between 50 to 60%. The UI has the greatest number of upwelling days (greater than 40%) in the months of March through August, with the highest (70%) in July; while the remaining months experience between 10 to 30%. It is evident that the UI greatly underestimates the number of upwelling days in this region. This is especially evident in the months of January through March and October through December.

The climatology of Q_y (Figure 23) is calculated three different ways: using all daily values, both upwelling and downwelling; using only downwelling days; and using only upwelling days. The seasonal cycle, using both upwelling and downwelling days, (Figure 23a) of the transport is very similar to the alongshore winds (Figure 9). The largest magnitude downwelling occurs for Q2 and Q4 and the magnitude decreases across the shelf. January and February have the largest downwelling at Q2 with values approximately -75 $m^3\ s^{-1}$. The minimum value for the downwelling for Q2 is -5.9 $m^3\ s^{-1}$ in July. The climatology for the 3 inner locations (Q2, Q4 and Q5) have only downwelling (negative) values, while the other locations have upwelling values in some months, especially during July through December. QuikSCAT locations Q11 and Q13 have the largest magnitude of the upwelling for the months of September and October with values exceeding 19 $m^3\ s^{-1}$. The climatology of the UI has the largest magnitude of downwelling in January and December. In these months, the UI downwelling exceeds that at Q2 by 25 $m^3\ s^{-1}$. The June value of the UI exceeds the QuikSCAT locations by about 10 $m^3\ s^{-1}$. In all other months the UI falls within the range of values of the 7 QuikSCAT locations. For April through August the UI is closer to the values along the outer QuikSCAT locations, Q11 and Q13, and for September through March the UI values are closer to the inner QuikSCAT locations, Q2 and Q4.

The seasonal cycle of only the downwelling days (Figure 23b) ranges from a maximum in December and January, approximately -175 $m^3\ s^{-1}$, to a minimum in July, approximately -50 $m^3\ s^{-1}$. For the months with a wide spread of values between

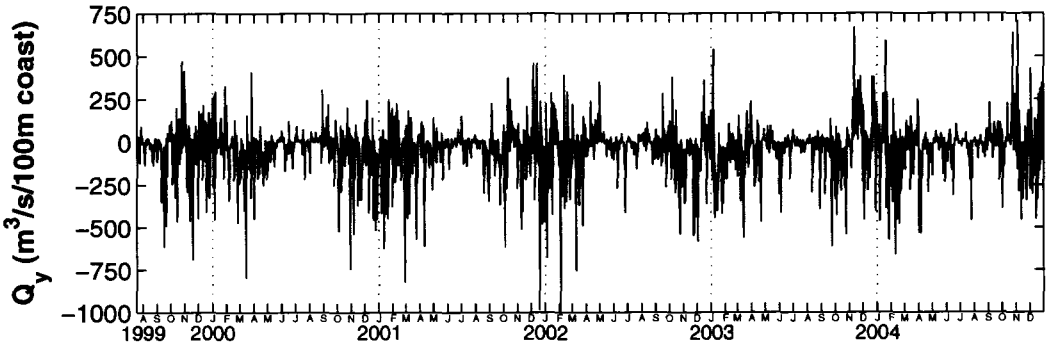

Figure 20. Time series of the daily Ekman transport at QuikSCAT location Q4. Positive values denote upwelling and negative values denote downwelling.

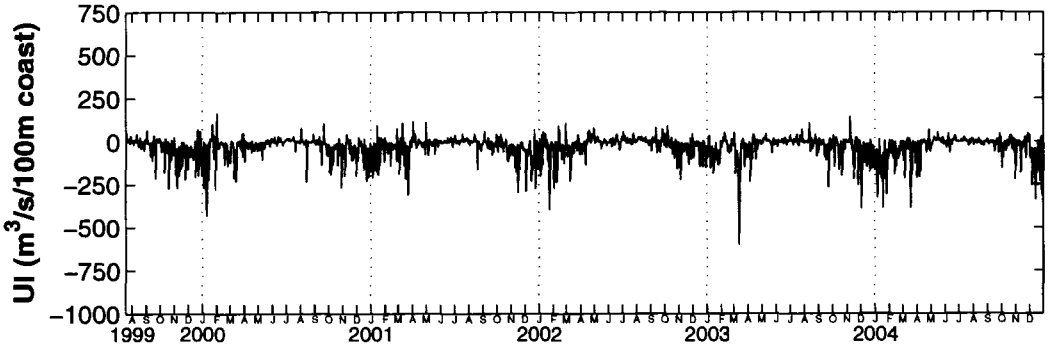

Figure 21. Time series of the daily UI at 60°N, 149°W. Positive values denote upwelling and negative values denote downwelling.

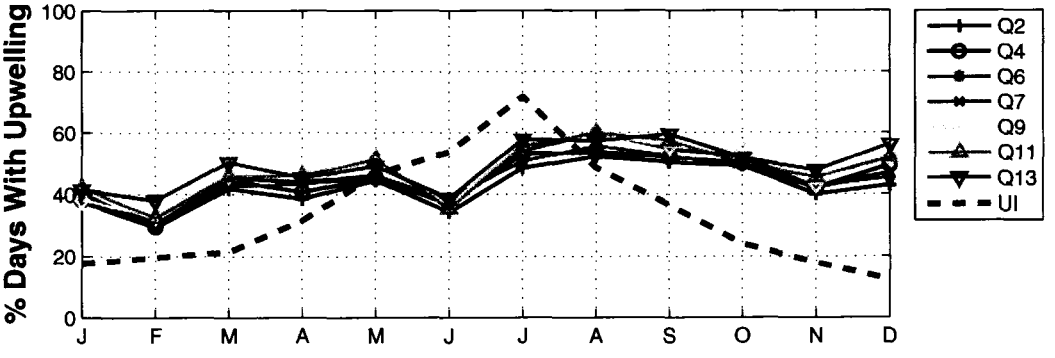

Figure 22. Seasonal cycle of the percentage of the number of days in a month that experience upwelling due to Ekman transport at the 7 QuikSCAT locations and for the upwelling index (UI).

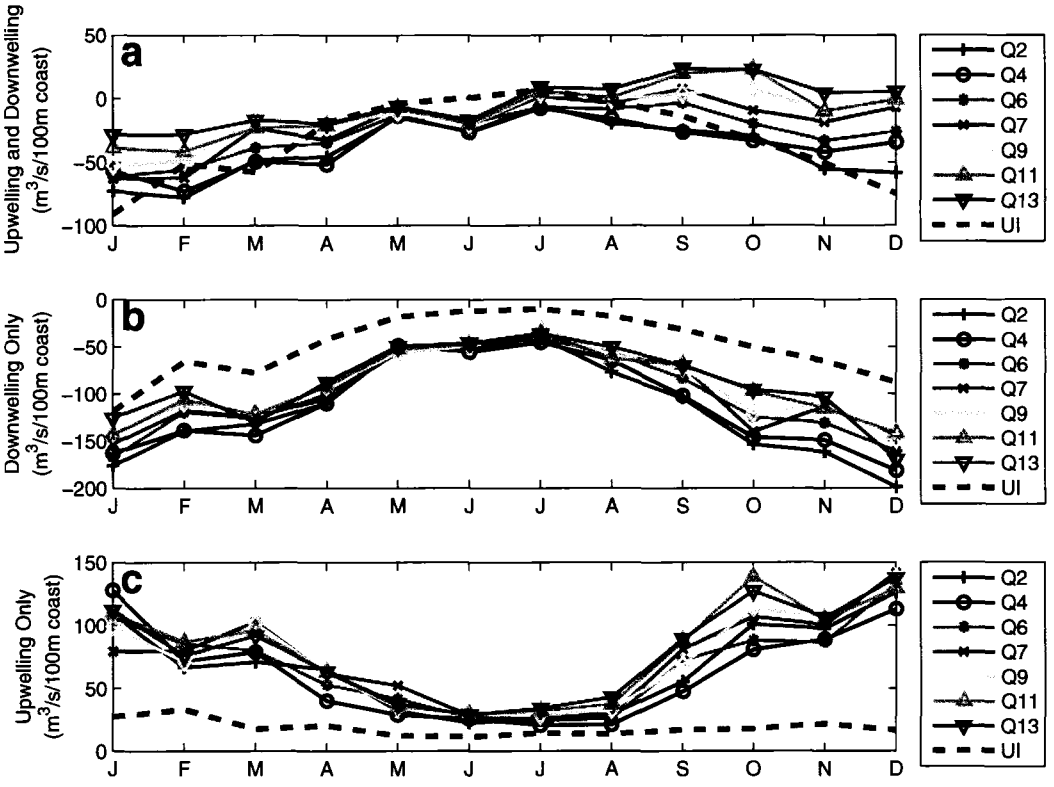

Figure 23. Seasonal cycle of Q_y at the 7 QuikSCAT locations and for the UI. The climatology is calculated three different ways: (a) using all available data (b) only using the downwelling days (-Q_y) (c) only using the upwelling days (+Q_y). (Note the three plots have different scales).

the QuikSCAT locations (January, February and October through December), it is the inner most locations, Q2 and Q4, which have the largest magnitudes and the outer locations, Q11 and Q13, which have the smallest magnitudes. The QuikSCAT climatology has larger magnitudes than the UI in all months, ranging from 6 to 53 $m^3\ s^{-1}$.

The seasonal cycle of only the upwelling days (Figure 23c) has maximum values from October through January with values ranging between 75 to 150 $m^3\ s^{-1}$. Minimum values of below 50 $m^3\ s^{-1}$ ooccur May through August. The inner QuikSCAT locations have smaller values of upwelling compared to the outer locations. QuikSCAT location Q4 has smaller values than Q2 for 8 of the 12 months; this is especially evident August through December. It is not certain whether this is a data error (quality of the QuikSCAT data diminishes towards the coast), but this has implications in the choice of the time series used in the correlations with the hydrographic data. The

UI has upwelling of approximately 20 m^3 s^{-1} for all twelve months; only the months of June through August are close to the QuikSCAT data.

4.4 RESULTS: EKMAN PUMPING SEASONAL CYCLE

The daily vertical velocity (w) time series at QuikSCAT location Q7 (Figure 24) has mostly upwelling ($+w$) days. The magnitude of the upwelling days are larger than those of downwelling ($-w$). From the time series a seasonal cycle can be deduced: small magnitude upwelling during the summer (May through August) and large magnitude upwelling during the rest of the year. Large magnitude downwelling days ($\geq$1.5 m day^{-1}) occur during the spring and winter, October through March.

The seasonal cycle of the percentage of days experiencing upwelling for the 7 QuikSCAT locations ranges between 40 to 75% (Figure 25). The seasonal cycles of Q2 and Q13 are very similar and on the whole have the lowest number of upwelling days in a month. These two locations have only the months of November through February with 50% or more upwelling days. The remaining QuikSCAT locations for all months have 50% or more upwelling days in a month. The fewest upwelling days occur in May and June, and the highest occur in September and November. QuikSCAT location Q7, of all the locations, has the highest percentage of upwelling days during September through November. There is considerable variation at the 7 QuikSCAT locations across the Seward Line and no clear pattern is evident.

As with the climatology of the daily Q_y time series the daily w time series climatology is calculated using three different methods: for both upwelling and downwelling day, for upwelling days only and downwelling days only. The first method used to calculate the climatology of w is to take the mean of all the days for a particular month no matter its value, i.e upwelling or downwelling (Figure 26a). The months May through August have the smallest values while the rest of the months are high. During the months of September through April the Q6 location has the highest (except for February) values for upwelling. QuikSCAT location Q2 has the most number of downwelling months.

The seasonal cycle of downwelling due to Ekman pumping (Figure 26b) has the same general cycle as that of upwelling: low during May through August and high during the remaining months. At QuikSCAT location Q2 the downwelling is much higher in magnitude than the other locations, especially for October through February, where the downwelling is from 0.2 to 1.0 m day^{-1} greater than the other

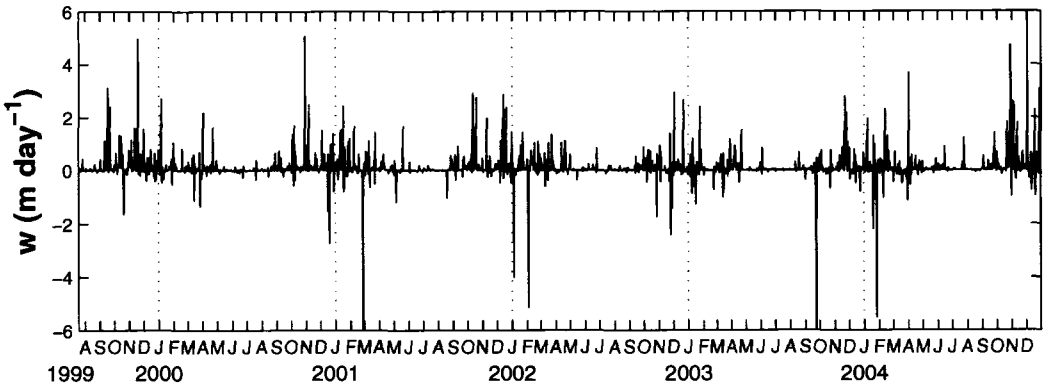

Figure 24. Time series of the daily vertical velocity, w, due to Ekman pumping at QuikSCAT location Q7. Positive values denote upwelling and negative values denote downwelling.

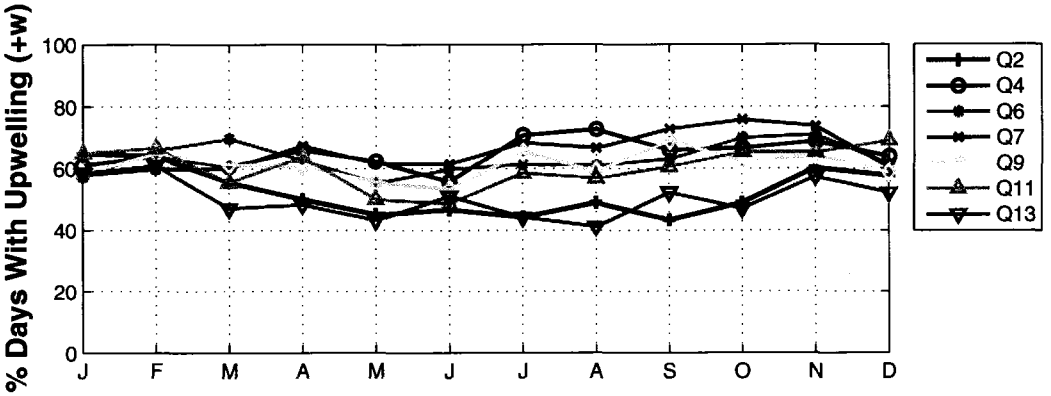

Figure 25. Seasonal cycle of the percentage of the number of days in a month that experience upwelling due to Ekman pumping at the 7 QuikSCAT locations.

QuikSCAT locations. The magnitude of the downwelling is mostly uniform for the remaining locations, except for the March value for Q6 which is much higher than the others.

The climatology using only the upwelling days for all 7 QuikSCAT locations is shown in Figure 26c. All seven locations have the same cycle: low during May through August and relatively high for the rest of the year. In general the magnitude of the cycle decreases offshore. For November through March, Q2 has the largest magnitude followed by Q6. Of note is the month of April for Q6 as the upwelling magnitude is approximately 0.2 m day^{-1} higher than all of the other locations.

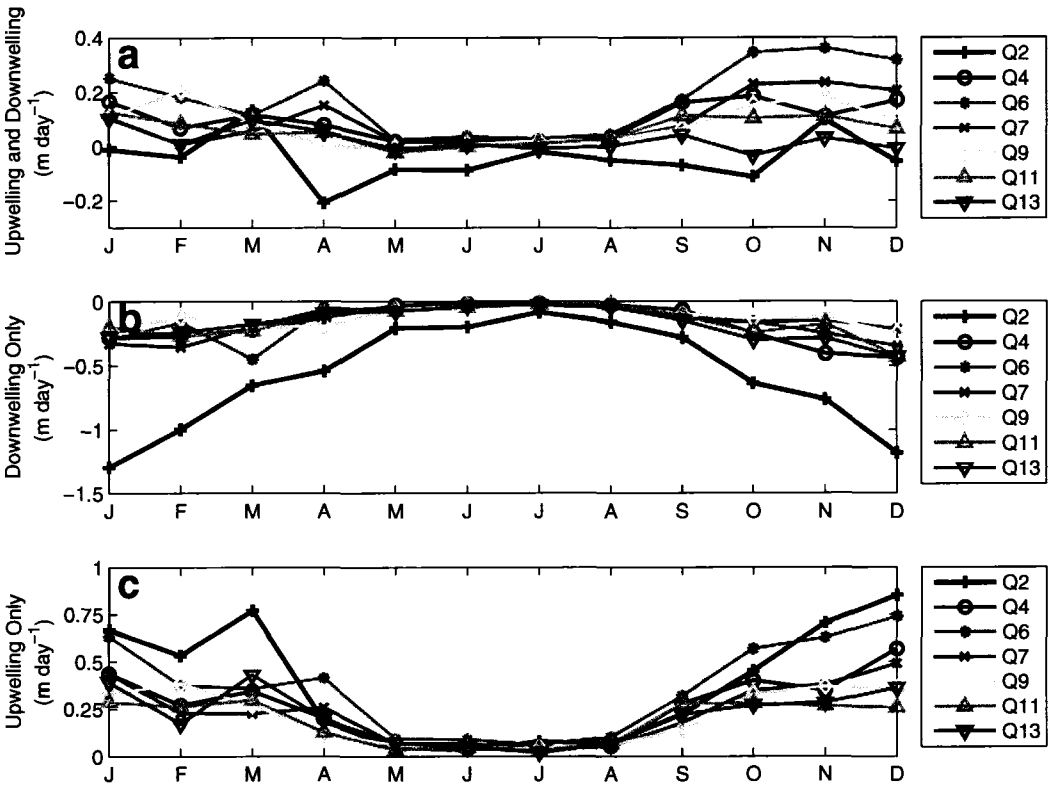

Figure 26. Seasonal cycle of the Ekman pumping (w) at the 7 QuikSCAT locations. The climatology was calculated three different ways: (a) using all available days (b) using only downwelling (-w) days (c) using only upwelling (+w) days. (Note the three plots have different scales).

Days with large magnitudes of positive upwelling are more likely to experience westward winds over the entire Seward Line. Across the Seward Line the 7 QuikSCAT locations have at least 200 or more days that have w velocities larger than 0.25 m day^{-1} (Table 7). The number of days range from 201 at Q13 to 350 at Q6. During these high upwelling days, the direction of the prevailing winds is westward. On the whole at least 60% to 77% of the high w days have westward winds.

4.5 RESULTS: EKMAN TRANSPORT AND HYDROGRAPHIC CORRELATION

It is expected that upwelling/downwelling due to Ekman transport should be present within the internal Rossby radius of deformation from the coast [*Pickett and Paduan* 2003]. Along the Seward Line the Rossby radius is variable throughout the

Table 7. Days that experience high rates of positive upwelling due to Ekman pumping also on average experience westward winds. The second column is the number of days (out of 1993) that have $w > 0.25$ m day^{-1}. The third column is the number of days out of the total listed in column 2 that experience westward winds. The fourth column is the percentage of the high upwelling days that experience westward winds, i.e. column 3 divided by column 2.

QuikSCAT Location	Number of days with w >0.25 m/day	Number of days with westward winds	% of days
Q2	297	201	67.7
Q4	298	184	61.7
Q6	350	236	67.4
Q7	281	173	61.6
Q9	226	135	59.7
Q11	213	131	61.5
Q13	201	156	77.6

year but is always confined to within 50 km of the shore. Only Q2 is usually within the Rossby radius and Q4 is just outside. Which QuikSCAT location should be used for the time series to correlate with the hdyrographic data? To best answer this question, GAK1 salinity anomalies between 2 to 275 meters were correlated with Q_n^d time series at the 7 QuikSCAT locations. The Q_n^d time series were constructed by taking the mean of only the downwelling days from 2 to 31 days before the cruise. The resulting contour plots show how the salinities at various depths correlate with downwelling over a variable number of days (Figure 27). QuikSCAT stations Q2 through Q6 have the most number of depths that are positively correlated at the 0.55 and 0.65 contour levels. These high correlations are for means between 4 to 12 days and depths between 50 to 200 meters. The remaining QuikSCAT stations have relatively low correlations for 1 to 12 days. All 7 QuikSCAT stations have the first 40 meters negatively correlated with the salinity; though, the negative correlations are very low, between -0.32 to 0. Of all 7 QuikSCAT stations the Q_{11}^d time series at Q4 has the highest correlations over the most depths. Because of this the Q_{11}^d(Q4) was used to best represent the Ekman transport over the Seward Line. The UI was also correlated with the GAK1 salinity anomalies and is shown in the last plot of Figure 27. The UI correlations have many more of the depths with negative correlations. For 2 to 10 days the negative correlations extend from 2 to 100 meters.

Also, there are no positive correlations of 0.55 or greater for the UI.

The time series of Q_{11}^{d}(Q4) (Figure 28a) has 35 values corresponding to the number of GLOBEC cruises from August 1999 to December 2004. The first thing to notice about the time series is that all the values are negative. This is important to keep in mind when the anomaly time series is constructed. Departures from the seasonal cycle that correspond to an increase in downwelling will have negative values not positive. The maximum downwelling is in winter and minimum downwelling is in summer. The upwelling index time series, UI_{11}^{d}, which was processed in the same way as Q_{11}^{d}(Q4), has the same general seasonal cycle but with smaller magnitudes. The anomaly time series (Figure 28b) shows which cruises experienced less than average downwelling (positive values) or more than average downwelling (negative values). The 11 days leading up to the October 2001 cruise is the period with the maximum downwelling of all the October cruises. The UI_{11}^{d} anomalies are very different from the Q_{11}^{d}(Q4) anomalies and only on a few occasions do they coincide with each other. There are only 7 months in the climatology of Q_{11}^{d}(Q4) (Figure 28c). The seasonal cycle has the lowest level of downwelling in July and the maximum level in December. The UI_{11}^{d} climatology has the same general shape as Q_{11}^{d}(Q4), with low values in May through August and high values in October through April, but the magnitude of the downwelling UI_{11}^{d} is smaller. This is especially evident in October and December.

Correlation maps of Ekman transport with the hydrographic data across the Seward Line are made between hydrographic data anomalies and Q_{11}^{d}(Q4) anomalies. Positive correlations occur when more (less) than average downwelling coincides with fresher (saltier) salinity anomalies. Negative correlations occur when more (less) downwelling coincides with saltier (fresher) salinity anomalies. The correlation between salinity and Q_{11}^{d}(Q4) (Figure 29) show that correlations of 0.5 to 0.6 are only present from GAK1 to GAK2. In this region near the shore the depth of 150 m has the greatest extent of significant positive correlations. The highest correlation is 0.69 at 104 m at the coast (GAK1). The positive correlations are attributed to downwelling winds pushing upper layer, fresher ACC water down into the water column. The largest positive correlations occur below the halocline – an area which should be sensitive to salinity changes due to downwelling. At GAK7 and GAK8 within the first 20 m of the surface there is a small region of significant negative correlations between -0.5 and -0.4. The negative correlations are in an area which is speculated to be a bifurcation of the ACC or shifting of the northern edge of the

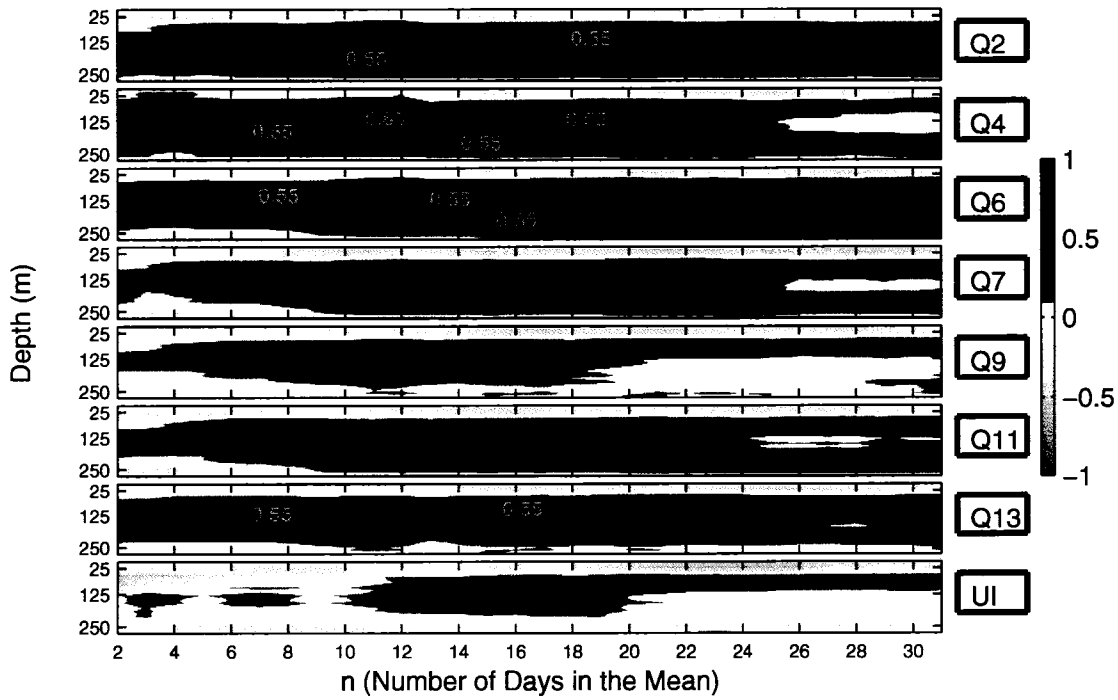

Figure 27. Correlation of salinity anomalies with Q_n^d at GAK1 for the 7 QuikSCAT stations. The salinity data are between 2 to 250 meters (y-axis) and the Q_n^d data are constructed for time integrations between 2 to 31 days (x-axis). Also shown is the correlation of salinity anomalies with UI_n^d. All labeled contours have a probability of 0.95 or higher.

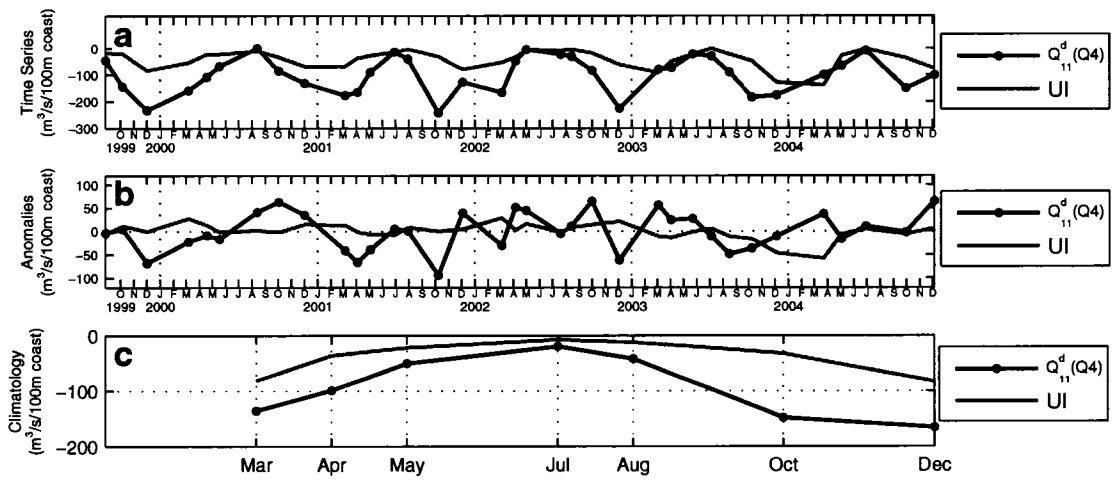

Figure 28. (a) Time series of Q_{11}^d(Q4). (b) Anomalies of Q_{11}^d(Q4). (c) Climatology of Q_{11}^d(Q4). Also in each plot is UI_{11}^d.

Alaskan Stream. Strong downwelling producing winds will transport saltier waters from offshore into this region in the Ekman layer resulting in the negative correlation. Conversely strong upwelling producing winds will transport fresher waters from the shore into this region which will also result in negative correlations. The significant correlations between temperature and Q^d_{11}(Q4) (Figure 30) are relatively small and have a probability of being significant at the 0.95 level. There are small areas of -0.4 correlations around GAK2 at 150 m and GAK3 at 50 m. Positive correlations of 0.4 are located offshore at GAK12 at depths between 250 and 300 m.

The correlation of the UI^d_{11} (the mean of only the downwelling data 11 days before the cruise) with the salinity have no significant positive correlations at zero lag (Figure 31). But the lag -1 correlation has positive correlations at the 0.99 probability level in a small region between 50 and 100 m near the coast (Figure 32). There is also a region of 0.4 positive correlations centered at 75 m around GAK8. A lag of -1 means that the salinity anomalies lead the UI anomalies by one cruise, e.g. the March 2000 salinity data is positively correlated with the April 2000 UI data. Since the UI is a large scale atmospheric index this suggests that the ocean is forcing the atmosphere. The lag -1 correlation of UI^d_{11} with temperature anomalies (Figure 33) has significant negative correlations starting around GAK6 and extending to the end of the Seward Line for depths around 100 m. Also at GAK2 from 50 to 150 m there is a band of significant negative correlations. The lag -1 temperature correlations suggest that warm surface temperatures will produce atmospheric conditions that will result in stronger winds (negative UI anomalies); conversely low surface temperatures are responsible for weaker winds (positive UI anomalies).

Royer [2005] suggests that a two layer system operates at GAK1. The two layer system is speculated to have offshore flows in the surface layer and onshore flows in the bottom layer. The offshore flow in the surface layer might be affected by relaxation of the downwelling winds, so a time series is needed to measure the relaxation of the downwelling winds. One time series is Q^u_n. This time series will measure the strength of the upwelling events before the start of a GLOBEC cruise. Another time series that should give an indication of the relaxation of the upwelling winds is derived from the mode 1 principal component (PC) of the EOF for the u wind stress upstream of the Seward Line (Chapter 3.3). The time series used is PC_n and positive values correspond to winds directed from the west to east (upwelling type) and vice versa. A figure similar to Figure 27 is constructed but with correlations between Q^u_n and

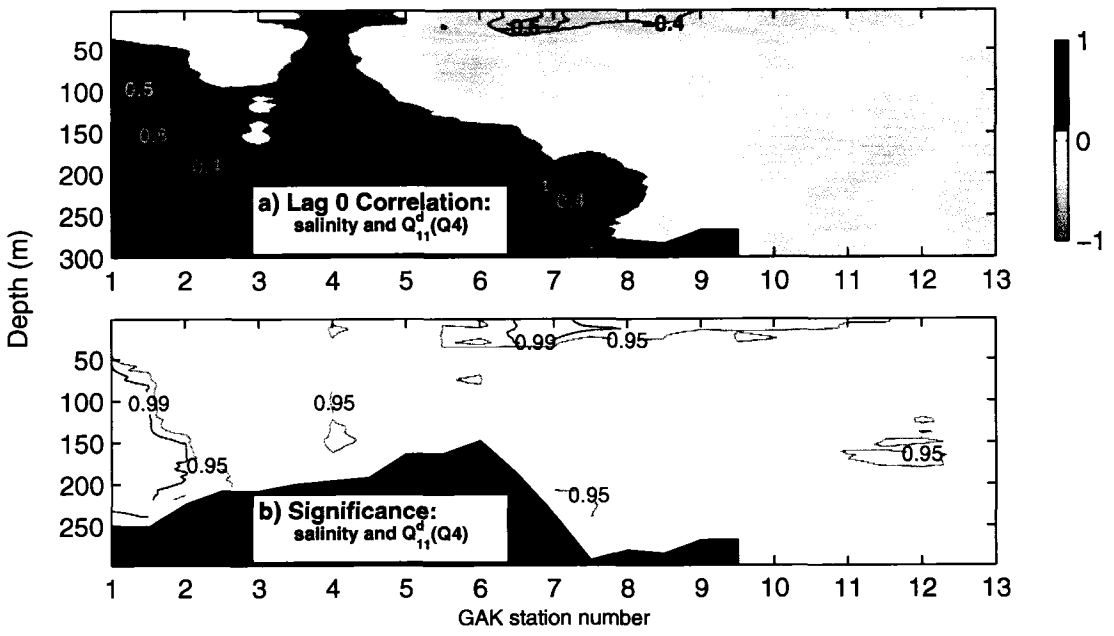

Figure 29. Correlation map of salinity anomalies and Q_{11}^d(Q4) anomalies across the Seward Line. (a) Spearman's rank correlations at zero lag. Only correlations with values lower/higher than -0.4/0.4 are labeled. (b) probability that the correlations are significant.

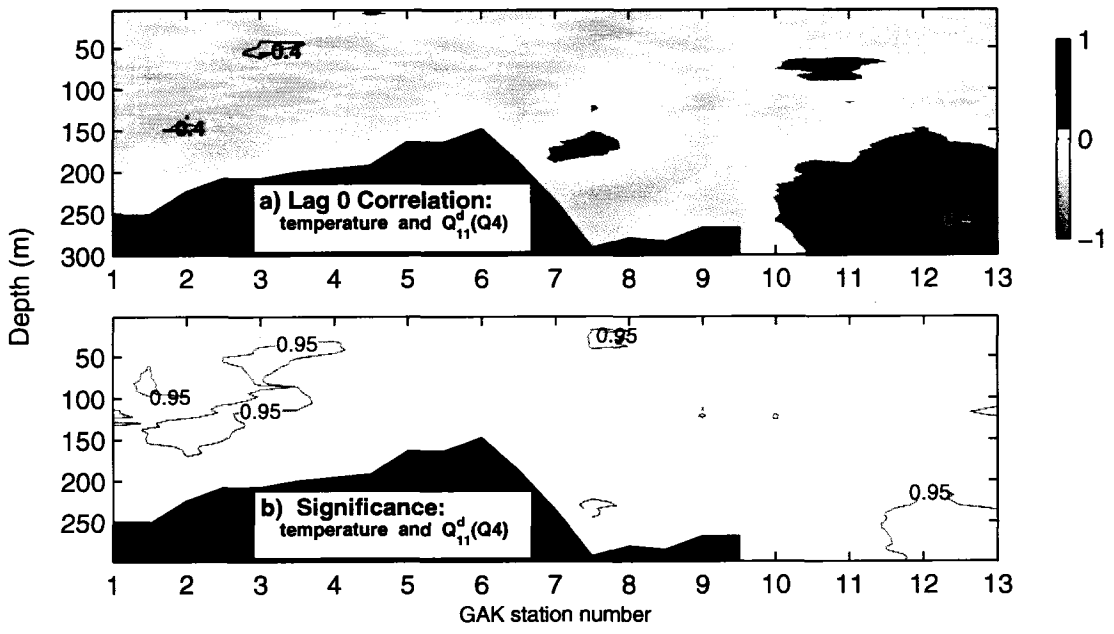

Figure 30. Correlation map of temperature anomalies and Q_{11}^d(Q4) anomalies across the Seward Line. Same as in Figure 29

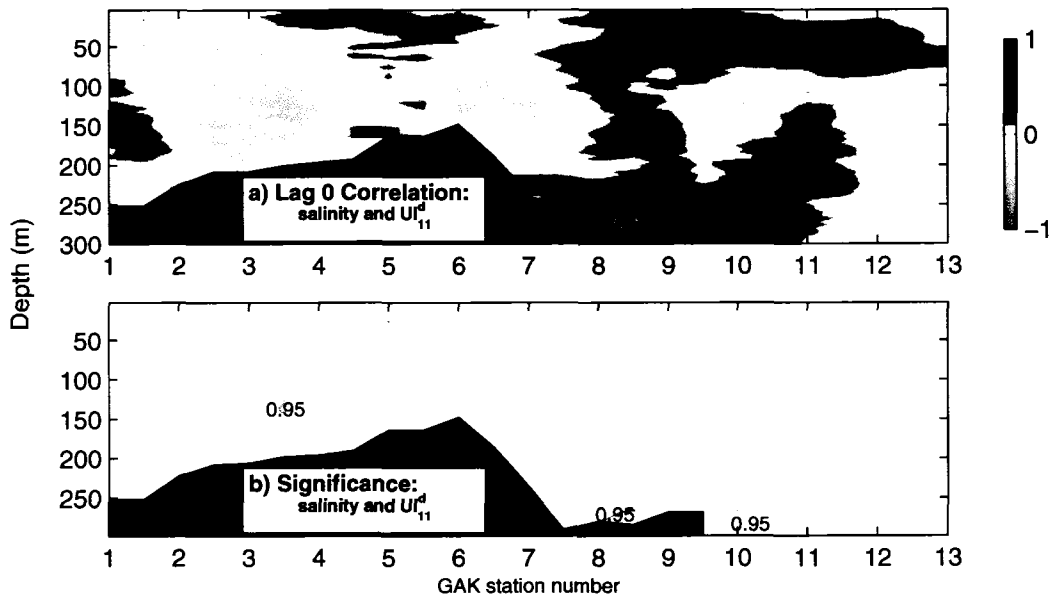

Figure 31. Correlation map of salinity anomalies and UI_{11}^{d} anomalies across the Seward Line. (a) Spearman's rank correlations at zero lag. Only correlations with values lower/higher than -0.4/0.4 are labeled. (b) probablility that the correlations are significant.

salinity anomalies at GAK4. The correlations are the highest for all the QuikSCAT locations between 11 to 16 days (Figure 34). The maximum correlation occurs for Q_{15}^{u}(Q13) at a depth of 198 m. The correlations for the Q_{n}^{u}(Q11) time series are peculiar; the correlations are lower than the correlations seen at Q9 and Q13. A possible reason is that the March climatological value of the alongshore winds at Q9 (Figure 9) is closer in magnitude to those at Q13; the Q9 March value has weaker downwelling winds than those at Q11 (Figure 9). Since this is an index measuring the relaxation of the downwelling winds an increase of the upwelling winds at Q11 for March will have smaller correlations. The PC_n correlations are smaller than those at the seven QuikSCAT locations. The maximum correlation is 0.55 at 198 m for PC_{12}. Thus Q_{15}^{u}(Q13) is a better time series to measure the relaxation of the downwelling winds than PC_{12}.

The time series of Q_{15}^{u}(Q13) (Figure 35a) also has 35 values corresponding to the number of GLOBEC cruises. The anomaly time series (Figure 28b) gives an estimate on the extent of the relaxation of the downwelling winds. Positive anomalies are periods when the downwelling winds are weaker than average (the downwelling winds are relaxed) and negative anomalies correspond to periods before the cruises which

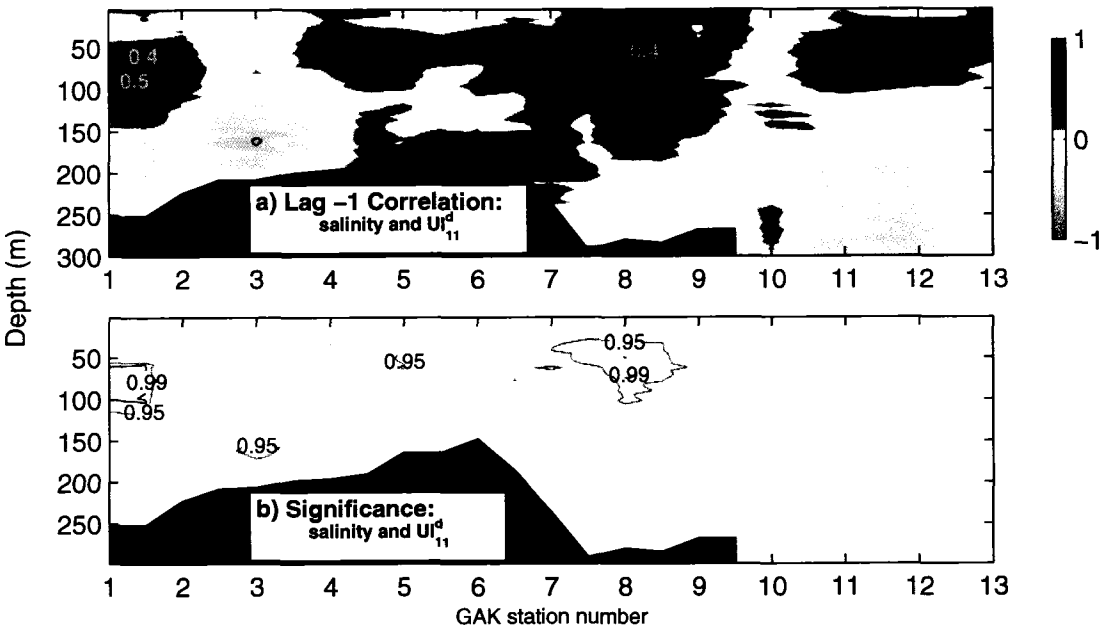

Figure 32. Lag -1 correlation map of salinity anomalies and UI^d_{11} anomalies across the Seward Line. (a) Spearman's rank correlations at lag -1. Lag -1 refers to the hydrographic data of the prior cruise. Only correlations with values lower/higher than -0.4/0.4 are labeled. (b) probability that the correlations are significant.

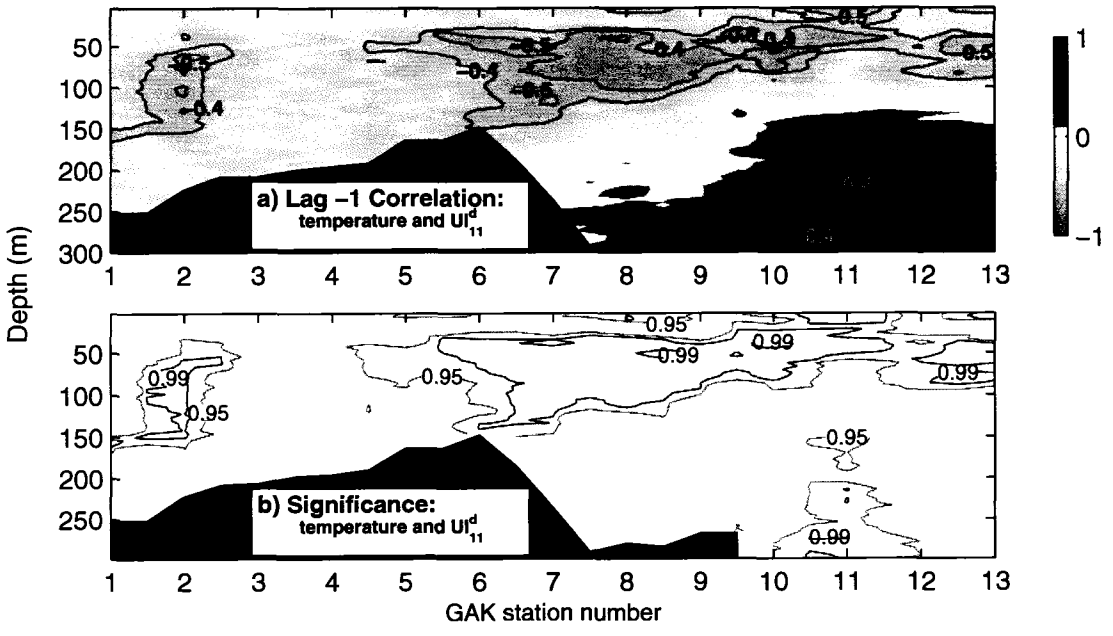

Figure 33. Lag -1 correlation map of temperature anomalies and UI^d_{11} anomalies across the Seward Line. Same as in Figure 32

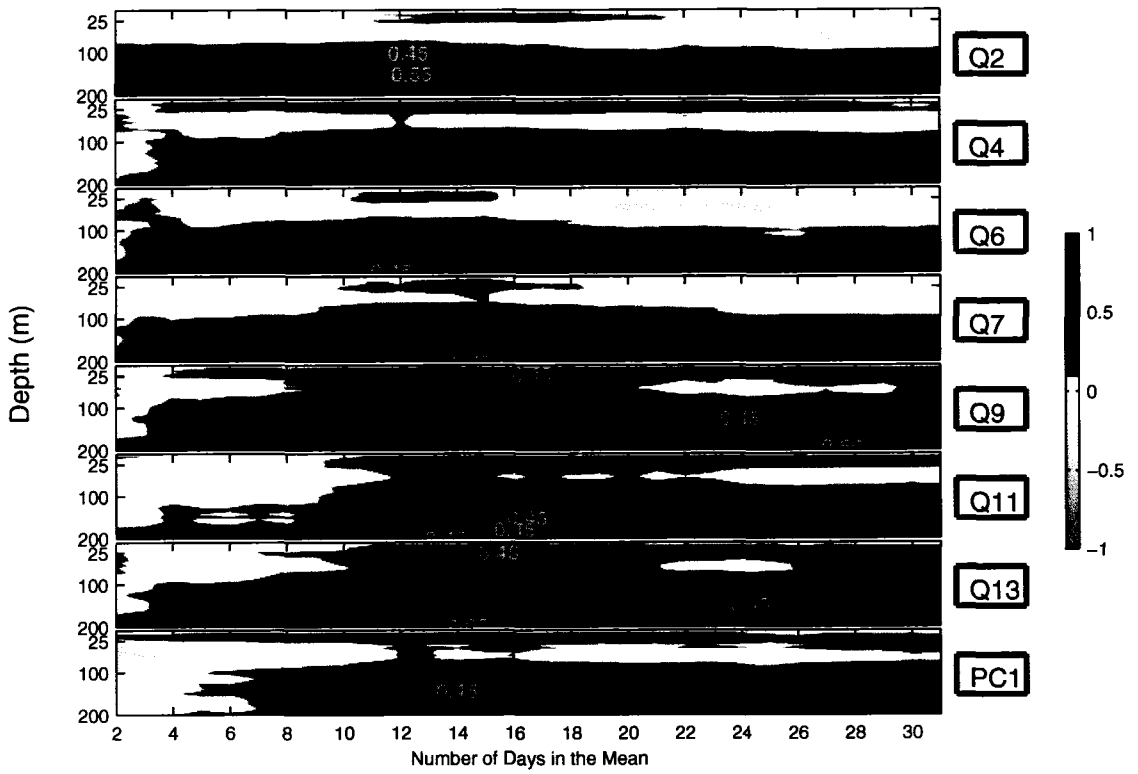

Figure 34. Correlation of salinity anomalies with Q_n^u at GAK4 for the 7 QuikSCAT stations. The salinity data are between 2 to 200 meters (y-axis) and the Q_n^u data are constructed for time integrations between 2 to 31 days (x-axis). Also shown is the correlation of salinity anomalies with PC_n. All labeled contours have a probability of 0.95 or higher.

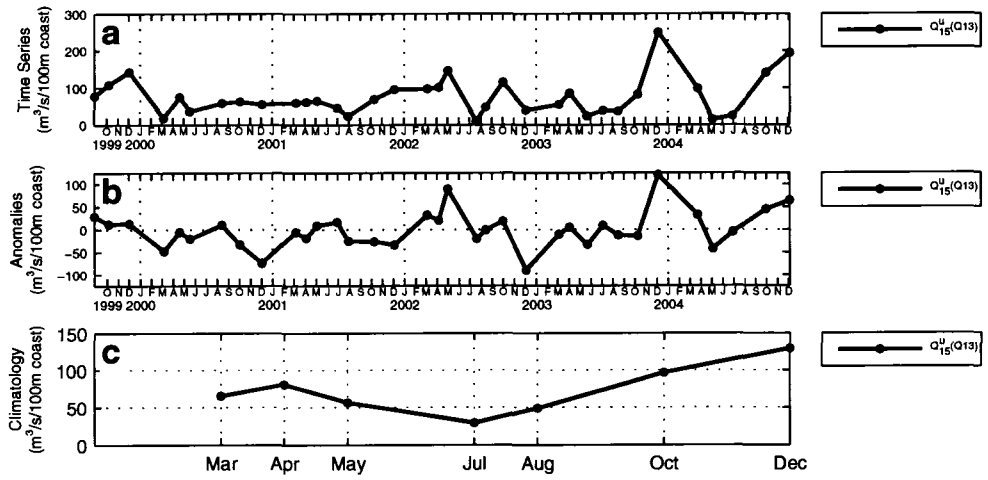

Figure 35. (a) Time series of $Q_{15}^u(Q13)$. (b) Anomalies of $Q_{15}^u(Q13)$. (c) Climatology of $Q_{15}^u(Q13)$.

are more downwelling (the downwelling winds are not relaxed). The 15 days leading up to the December 2003 cruise is the period with the most relaxed downwelling winds. The seasonal cycle (Figure 35c) has the maximum occurring in October and December and the minimum occurring in July.

The correlations between salinity and Q_{15}^{u}(Q13) anomalies have high correlations of 0.6 at GAK4 for depths between 150 and 200 m (Figure 36). Also, significant positive correlations (P>0.99) extend from GAK4 all the way to GAK9 all within 50 to 100 m from the bottom. These positive correlations are attributed to more (less) relaxed downwelling winds allowing for the intrusion of saltier (fresher) water in the bottom layer. Correlations between temperature and Q_{15}^{u}(Q13) of -0.6 are situated at 50 m for GAK5 (Figure 37). There are large areas of -0.4 and -0.5 correlations extending from GAK1 to GAK9 at depths from the surface down to 200 m. Most of the -0.5 correlations are located between GAK5 and GAK8. The negative correlations between temperature and Q_{15}^{u}(Q13) are the result of more (less) relaxed winds being correlated with colder (warmer) temperature anomalies. Both the salinity and temperature correlation maps have significant correlations between GAK1 and GAK2 for depths centered at 50 m. Significant correlations in this region are an indication of the strength of the ACC – when downwelling winds are less (more) relaxed salinities are fresher (saltier). For the temperature correlations the strong (weak) downwelling winds bring warmer (cooler) water down into this region.

4.6 RESULTS: EKMAN PUMPING AND HYDROGRAPHIC CORRELATION

The same dilemma faced in picking a Q_{n}^{u} time series is also present for the choice of the W_{n}^{u} time series. The same method used to find the best Q_{n}^{u} time series is also used for the W_{n}^{u} time series but correlations are made at GAK5 instead of GAK1. GAK5 is chosen because it is sufficiently away from the shore and is in a location of high upwelling due to Ekman pumping. QuikSCAT location Q7 is the only location of the seven to have high levels of positive correlations between W_{n}^{u} anomalies and salinity anomalies at GAK5 (Figure 38). From 23 days to 31 days in the mean there are correlations of 0.5 and higher for depths between 50 to 175 meters. The $W_{27}^{u}(Q7)$ time series has the most number of depths at the 0.6 correlation so this is the time series that will be used to represent Ekman pumping. Biological process studies were

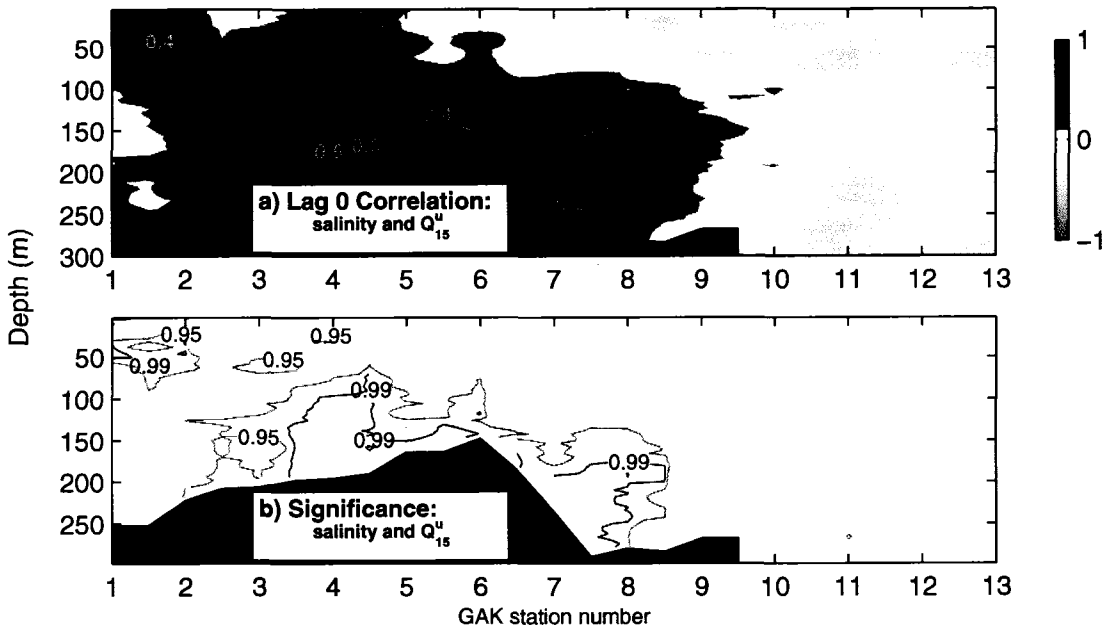

Figure 36. Correlation map of salinity anomalies and $Q^u_{15}(Q13)$ anomalies across the Seward Line. (a) Spearman's rank correlations at zero lag. Only correlations with values lower/higher than -0.4/0.4 are labeled. (b) probability that the correlations are significant.

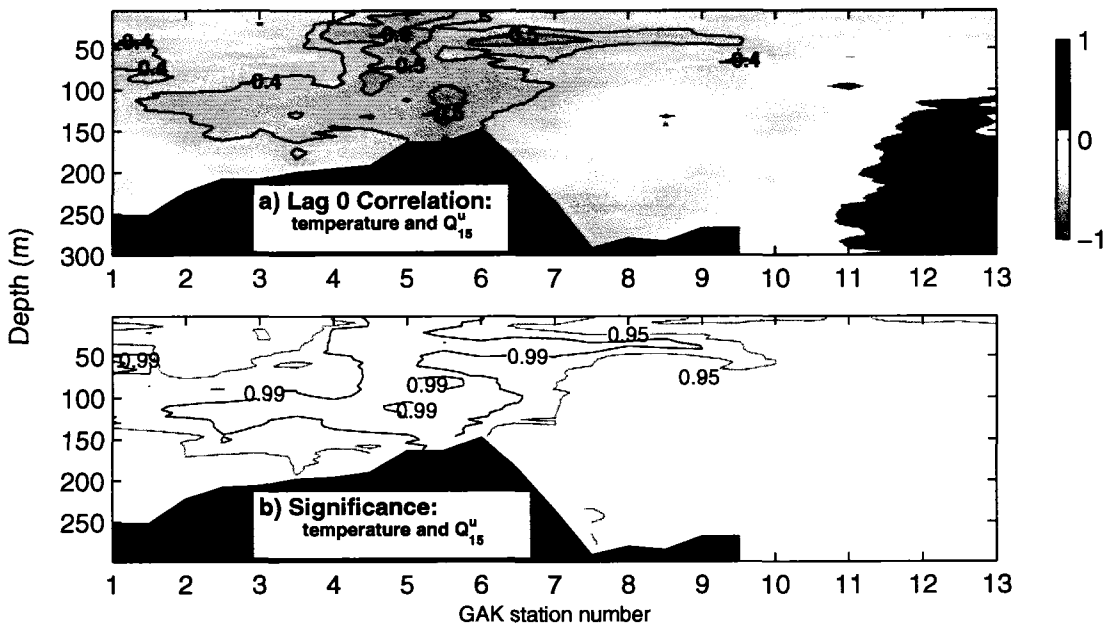

Figure 37. Correlation map of temperature anomalies and $Q^u_{15}(Q13)$ anomalies across the Seward Line. Same as in Figure 36

conducted at GAK4 and GAK6 on all cruises of the NEP GLOBEC program. The upwelling due to Ekman pumping could have implications on these process studies.

The time series of W_{27}^{u} at Q7 (Figure 39a) has 35 values corresponding to the number of GLOBEC cruises from October 1999 to December 2004. The maximum upwelling is in winter and minimum upwelling is in summer. The anomaly time series (Figure 39b) shows those cruises that experienced less than average seasonal upwelling (negative values) or more than average seasonal upwelling (positive values). The 27 days leading up to the October 1999 cruise is the period with the maximum upwelling of all the October cruises. There are only 7 months in the climatology of W_{27}^{u} (Figure 39c). The seasonal cycle has the lowest level of upwelling in August and the maximum level in December. October and December are months of highest upwelling due to Ekman pumping and they are also the months of highest downwelling due to Ekman transport (Chapter 4.3 and 4.5). Upwelling during these winter months could bring nutrients up the water column in advance of the spring bloom.

The correlations between salinity and W_{27}^{u}(Q7) anomalies have high correlations of 0.6 between GAK4 and GAK5 for depths between 100 and 200 m (Figure 40). Significant correlations of 0.4 and 0.5 (P>0.99) extend from GAK3 to GAK6 from 50 m to the bottom. Positive correlations between salinity and W_{27}^{u}(Q7) anomalies result when more (less) upwelling coincides with saltier (fresher) salinities. From the shore to GAK2, at a depth of 50 m, there is a region of significant correlations of 0.4. The Reason that the ACC is affected by the Ekman pumping is that positive anomalies of W_{27}^{u}(Q7) are also periods of strong westward winds (Table 7). The westward winds will push more saline water from outside the ACC towards the shore resulting in the positive correlations.

Correlations between temperature and W_{27}^{u}(Q7) of -0.4 are found in two locations: in the upper 50 meters from GAK1 to GAK4 and between 100 to 175 m for GAK2 to GAK4 (Figure 41). Large positive correlations of 0.6 are found beyond GAK12 at a depth of 150 m. The positive correlations are attributed to the onshore flow of warm water. Days of large positive w on average experience westward winds (Table 7). These westward winds will push water toward the coast. Thus GAK12 and GAK13 will be inundated by warmer offshore water from the central Gulf of Alaska. The same effect should be seen with correlations with Q_n^d and temperature, but with negative correlations instead of the positive. The reason that the correlations will

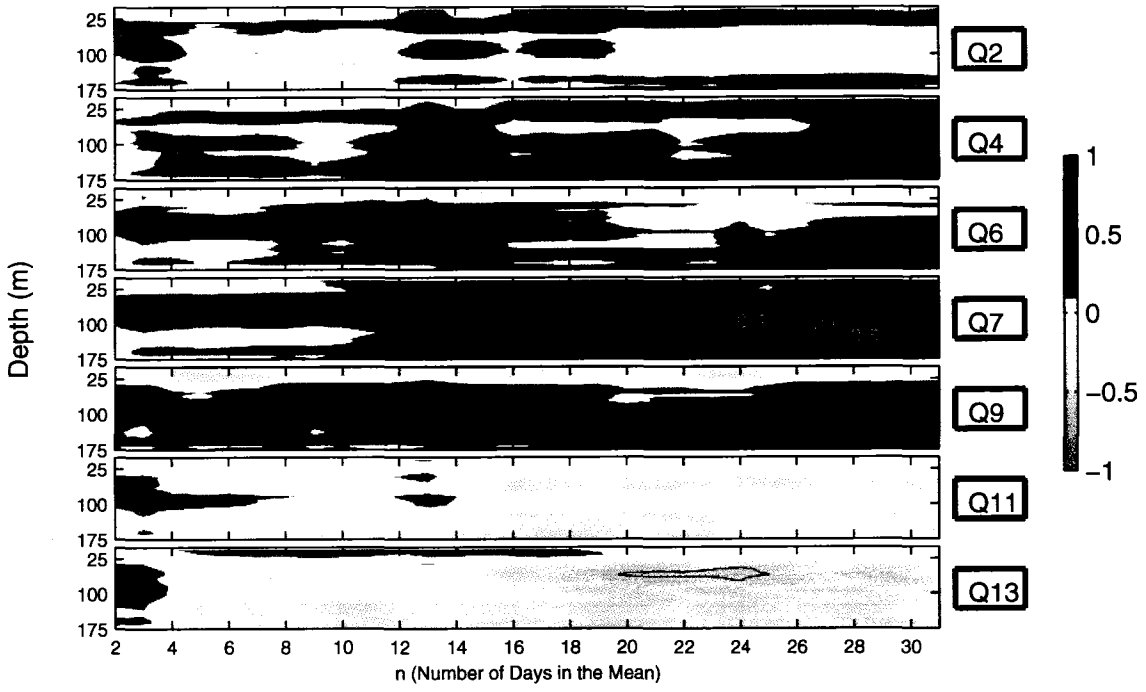

Figure 38. Correlation of salinity anomalies with W_n^u at GAK5 for the 7 QuikSCAT stations. The salinity data are between 2 to 175 meters (y-axis) and the Q_n^u data are constructed for time integrations between 2 to 31 days (x-axis). All labeled contours have a probability of 0.95 or higher.

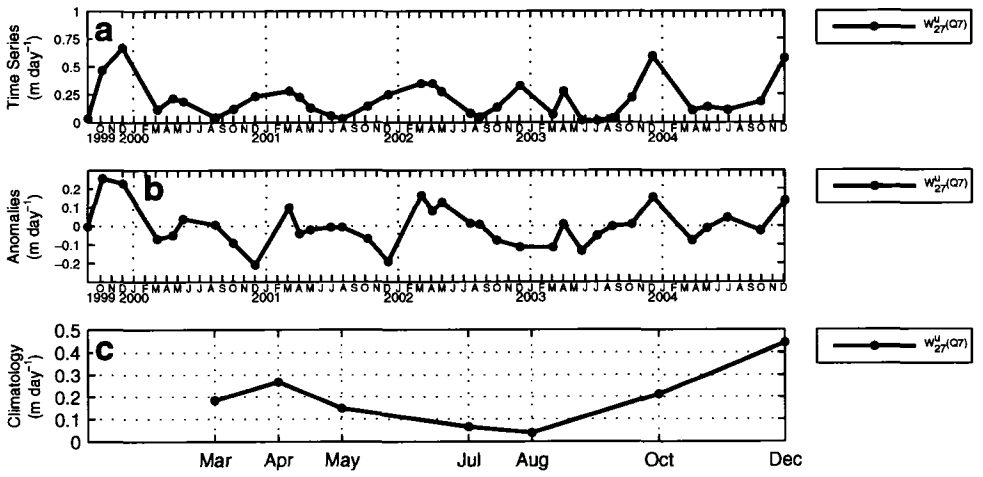

Figure 39. (a) Time series of $W_{27}^u(Q7)$. (b) Anomalies of $W_{27}^u(Q7)$. (c) Climatology of $W_{27}^u(Q7)$.

be negative is that large negative Q_n^d values represent strong westward wind events which will force warm water onto GAK12 and GAK13. Figure 42 shows QuikSCAT location Q2 and Q7 with the largest significant correlations; correlations of -0.6 are centered at a depth of 100 m for 26 to 30 days in the mean.

4.7 CONCLUSIONS

The upwelling and downwelling calculated from the the QuikSCAT winds differs considerably from that determined from the UI. The QuikSCAT winds show many more upwelling days than the UI and the magnitudes of the upwelling are much greater for the QuikSCAT winds. Also the QuikSCAT winds show a persistent positive wind stress curl which is evident throughout the course of a year. This positive wind stress curl will produce upwelling water velocities on the order of 1 to 2 m day^{-1}. These vertical velocities are fully capable of bringing nutrient rich water into the euphotic zone.

Ekman transport produced by the winds at location Q4 has the highest correlations with salinity anomalies in the region between GAk1 and GAK2 for depths below 50 m. The hydrography produced by these winds respond within 11 days before the cruise. The Ekman transport promotes downwelling along the shore and salinities are affected by the strength of the downwelling. Strong downwelling winds push fresher ACC water down into the water column and results in positive correlations between salinity and Q_{11}^d(Q4). In the same 11 day time period the UI is not correlated with the hydrographic data. However, the outer (GAK6 – GAK13) upper layer temperature and salinity appears to force the UI at a lag of over a month.

The mean of only the upwelling days 15 days prior to a cruise for the Q13 time series is a good indication of the relaxation of the upstream upwelling winds. The salinities at the bottom for GAK4 through GAK7 and temperatures across the whole shelf mostly for depths between 50 to 150 m are well correlated to the relaxation of the downwelling. The greater extent of the spatial locations of the salinity and temperature correlations suggest that the Q_{15}^u(Q13) time series influences some across shelf physical process.

Positive vertical water velocities produced by Ekman pumping at Q7 affect the hydrographic data at time scales on the order of one month (27 days). The salinity around GAK3 and GAK5 at the bottom are correlated with the upwelling, w, which results from Ekman pumping. The location of negative correlations of temperature

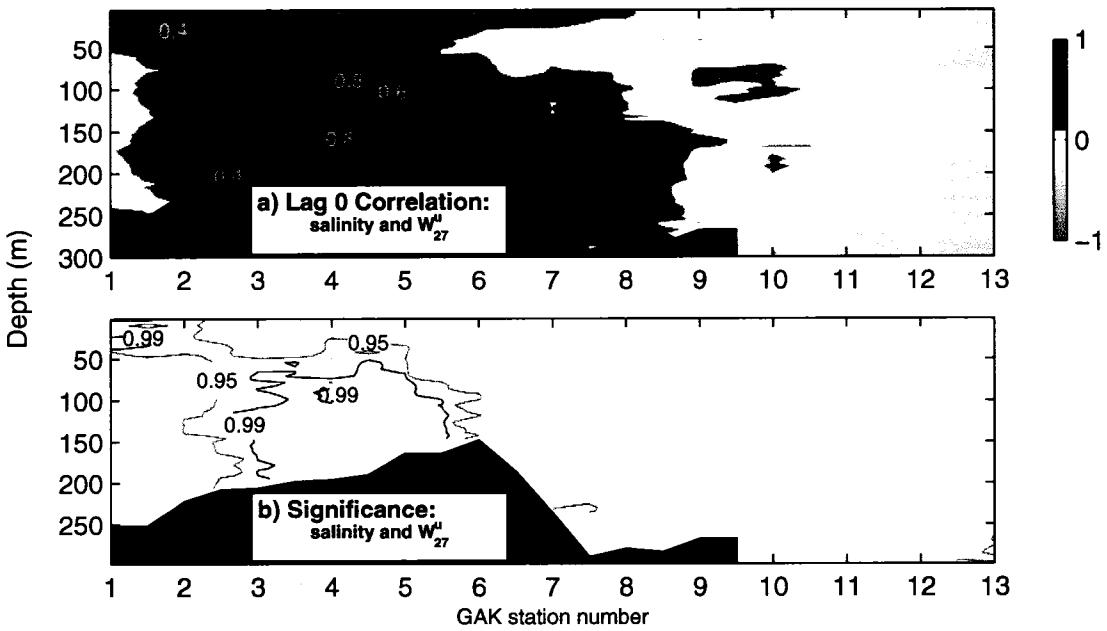

Figure 40. Correlation map of salinity anomalies and $W_{27}^{u}(Q7)$ anomalies across the Seward Line. (a) Spearman's rank correlations at zero lag. Only correlations with values lower/higher than -0.4/0.4 are labeled. (b) probability that the correlations are significant.

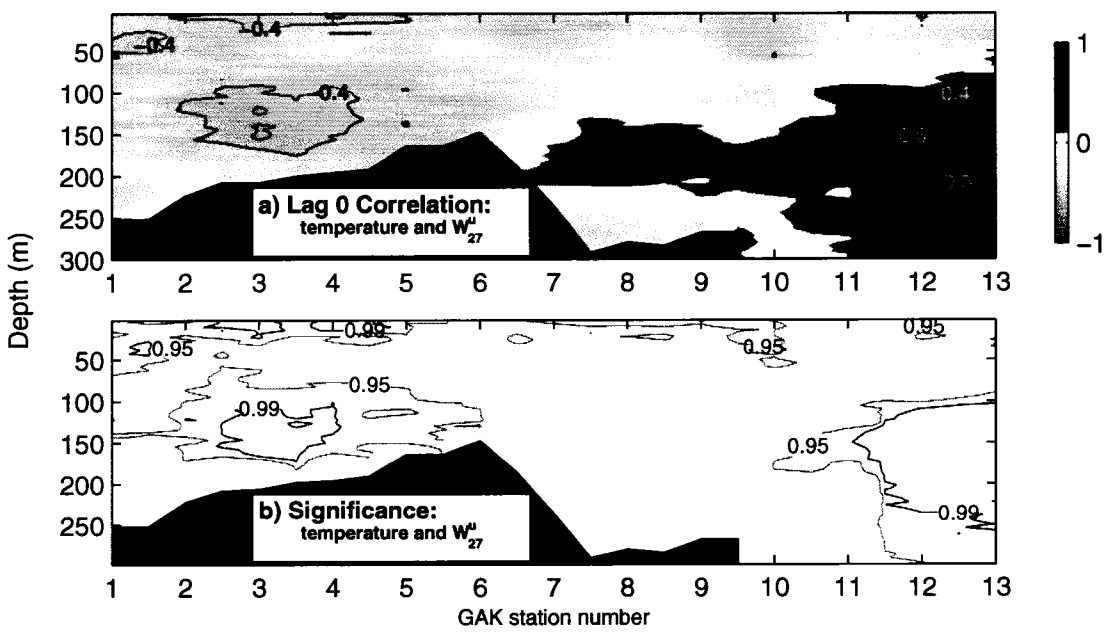

Figure 41. Correlation map of temperature anomalies and $W_{27}^{u}(Q7)$ anomalies across the Seward Line. Same as in Figure 40

with w is shifted shore ward, near GAK3, at a depth of 150 m. At the same depth but at GAK11 and GAK13 the temperature is positively correlated with w. The salinity and temperature correlations mid-shelf, GAK3 – GAK5, are expected if there is upwelling present. The positive temperature correlations located between GAK11 and GAK13 are hypothesized to be the result of westward winds, across the Seward Line, forcing warmer water from the central Gulf of Alaska into this region.

In summary, the hydrographic data along the Seward Line responds to different wind forcing at different time scales. To fully understand the interannual variability of temperature and salinity anomalies along the Seward Line three wind time series, as described above, are needed. A single time series such as the UI does not seem to exist that will be able to adequately describe the variability across the shelf.

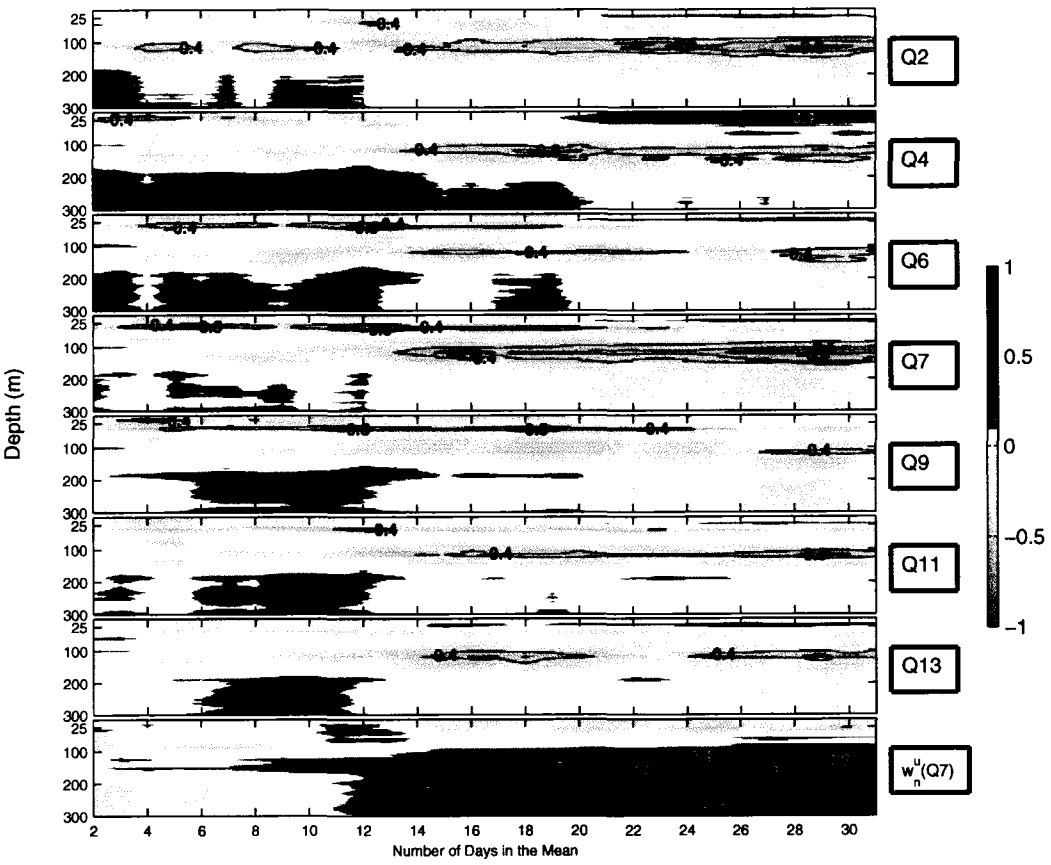

Figure 42. Correlation of temperature anomalies with Q_n^d at GAK13 for the 7 QuikSCAT locations. The temperature data is between 2 to 300 meters (y-axis) and the Q_n^d data is constructed for time integrations between 2 to 31 days (x-axis). Also shown is the correlation of temperature with $W_n^u(Q7)$. All labeled contours have a probability of 0.95 or higher.

CHAPTER 5

SVD BETWEEN TEMPERATURE AND SALINITY

5.1 INTRODUCTION

Royer [2005] proposed some possible scenarios to account for the seasonal changes in the salinity and temperature at GAK1. His analysis identified a two layer system with the interface between the layers at 100 m. He proposed a system that is affected by freshwater discharge, solar heat flux, relaxation of downwelling winds and strong downwelling winds. The effect of these different forces can be seen in how the phasing of the maximum/minimum salinity and temperature are different between the two layers. Royer first notes that the upper layer salinity has the same seasonal cycle as the freshwater discharge and the upper layer temperature has the same cycle as the solar heat flux. The lower layer temperature and salinity are affected by different types of wind forcing. For example, the relaxation in the downwelling winds is maximum during July and August and will allow an onshore flow of warm, high salinity waters from offshore. The result is that in the lower layer there is a maximum salinity and a warming in August. The lower layer salinity decreases from the August maximum until it reaches its minimum value in February; and the lower layer temperature increases to a maximum in November from the March minimum. Royer explains that both are due to an increase in downwelling winds which force warmer, fresher water from the upper layer into the lower layer. The maximum lower layer temperature is reached in November due to the fact that October upper layer waters are still warm, but the surface layer quickly cools from October to December causing the warm water to be replaced by cold surface waters. The time to reach the lower layer salinity minimum is longer because the surface layers are still fresh through December.

Another consequence of the high discharge in October is an across shore pressure gradient which might produce offshore ageostrophic flows [*Royer* 2005]. The high discharge could also result in an alongshore pressure gradient. The alongshore pressure gradient gets formed by an accumulation of freshwater as the ACC moves westward; thus, the free surface will be higher to the west, resulting in offshore geostrophic flows. This offshore flow, through entrainment, will cause an onshore lower layer flow bringing warmer and more saline water onto the shelf.

As described above, the seasonal cycle of temperature and salinity at GAK1 are coupled. So instead of performing an EOF analysis on the temperature and salinity alone, a Singular Value Decomposition (SVD) analysis is performed on the temperature and salinity. The SVD method will identify modes where temperature and salinity are strongly coupled. *Bretherton et al.* [1992] identified four statistical methods to identify relationships between couple fields. One of the methods is SVD and Bretherton states that it is parameterless, computationally efficient, and in some situations is superior to the other methods. The other methods are canonical correlation analysis, empirical orthogonal function (EOF) analysis on combined fields, and performing an EOF analysis on one field and then correlating the resulting principal components with the other field to obtain correlation maps. SVD analysis is desired when the individual spatial EOFs are dissimilar to the coupled signal.

5.2 METHODS

The Singular Value Decomposition method (SVD) of coupled fields is used to determine how the temperature and salinity covary across the Seward Line. The SVD method [*Venegas* 2001] is based on performing a singular value decomposition on the covariance matrix of two fields. Please note that the SVD method gets its name from the linear algebra problem called singular value decomposition. Singular value decomposition is a well known topic in linear algebra and is included in many numerical packages such as Matlab and IDL.

In the SVD method the matrix $\mathbf{C}$ is the correlation matrix between the temperature, $\mathbf{T}$, and salinity, $\mathbf{S}$, matrices. The matrices $\mathbf{T}$ and $\mathbf{S}$ are $n \times m$ with the rows corresponding to n time values and the columns corresponding to m spatial locations. All of the time series which make up the columns have been normalized by subtracting out the temporal mean and dividing by the standard deviation. Once $\mathbf{T}$ and $\mathbf{S}$ have been constructed, matrix $\mathbf{C}$ is found by multiplying the transpose of the temperature matrix by the salinity matrix:

$$\mathbf{C} = \mathbf{T}^t * \mathbf{S} \tag{13}$$

the result is a $m \times m$ matrix.

A singular value decomposition is now performed on the matrix $\mathbf{C}$ such that

$$\mathbf{C} = \mathbf{U}\mathbf{D}\mathbf{V}^t . \tag{14}$$

The matrices **U**, **V** and **D** are all $m \times m$. The columns of **U** are orthogonal to each other and are the singular vectors of the salinity. The rows of $\mathbf{V}^t$ are orthogonal to each other and are the singular vectors of the temperature. The matrix **D** is a diagonal matrix in which the elements of the main diagonal are called the singular values, λ_i. A singular value, λ_i, is used to explain the amount of squared covariance between the i^{th} mode of the salinity and temperature singular vectors. This quantity is called the squared covariance fraction (SCF) and is calculated from

$$SCF_i = \frac{\lambda_i^2}{\sum_{i=1}^{m} \lambda_i^2} . \tag{15}$$

Time series that describe how the singular vectors change over time are called expansion coefficients. The expansion coefficient for salinity, $\mathbf{S}_{ec}$, is calculated by projecting the salinity data matrix **S** onto the **V** matrix:

$$\mathbf{S}_{ec} = \mathbf{SV} \tag{16}$$

and the expansion coefficient for temperature, $\mathbf{T}_{ec}$, is calculated by projecting the temperature data matrix **S** onto the **U** matrix:

$$\mathbf{T}_{ec} = \mathbf{TU} . \tag{17}$$

The columns of the matrices $\mathbf{S}_{ec}$ and $\mathbf{T}_{ec}$ correspond to individual modes.

The results are displayed as homogeneous correlation maps; that is the i^{th} mode expansion coefficient of salinity (temperature) are correlated with the salinity (temperature) time series at each spatial location. These time series have t_k values where k is between 1 to n. For a particular spatial location the correlations are done using Pearson's correlation:

$$S_{sp} = \sum_{k=1}^{n} S_{ec}(t_k) S(t_k) \tag{18}$$

for salinity. Similarly, for temperature,

$$T_{sp} = \sum_{k=1}^{n} T_{ec}(t_k) T(t_k) . \tag{19}$$

To form a homogeneous correlation map a total of m Pearson's correlations, corresponding to the number of spatial locations, are calculated. The expansion coefficients, S_{ec} and T_{ec}, are for the i^{th} mode. Homogeneous correlation maps will be constructed for the first 2 modes (i=1,2).

Table 8. The square covariance fraction (SCF), the Pearson correlation between the salinity and temperature expansion coefficients and the significance level of the correlation for the first 3 modes of the SVD.

Mode	SCF (%)	r	Significance Level (%)
1	50.5	0.85	0.99
2	30.1	0.78	0.99
3	14	0.55	0.99

5.3 RESULTS: SPATIAL PATTERNS AND EXPANSION COEFFICIENT DESCRIPTIONS

The first three modes of the SVD analysis account for 94.7% of the total square covariance. Table 8 summarizes the square covariance fraction, the correlation between the temperature and salinity expansion coefficients, and the correlation significance levels for the first three modes. The correlation in the table is the Pearson correlation and is used to mark the strength of the correlation. All three correlations for the modes have a correlation with 99% significance levels, and the r value suggests that mode 1 has the greatest coupling between the temperature and salinity. The r value for mode 3 for the correlation between the expansion coefficients is only 0.55 suggesting a weak coupling. Mode 3 accounts for only 14% of the total square variance and is not included in the following discussion.

The mode 1 salinity spatial pattern (S_{sp}) has regions of maximum positive homogeneous correlation (equations 18 and 19) in the region between GAK1 and GAK2 at 200 m; and regions of minimum negative correlations around GAK12 at 10 m (Figure 43a). A positive correlation of 0.6 and higher is confined to depths of 100 m and below, from GAK1 to GAK6. This region will have the highest r^2 values and thus have the greatest amount of the variance explained. The temperature spatial pattern (T_{sp}) has maximum homogeneous correlations of 0.8 and higher across the whole Seward Line in the top 50 m; the minimum correlations are approximately -0.6 and are centered around GAK8 at a depth of 250 m (Figure 43b).

Of the first 3 modes, the expansion coefficients (S_{ec} and T_{ec}) for mode 1 have the greatest coupling (r=0.85) and the two have a clear seasonal signal (Figure 44a). On the whole there are positive values in July through October and negative values in March through May for both salinity and temperature. Sometimes the coupling

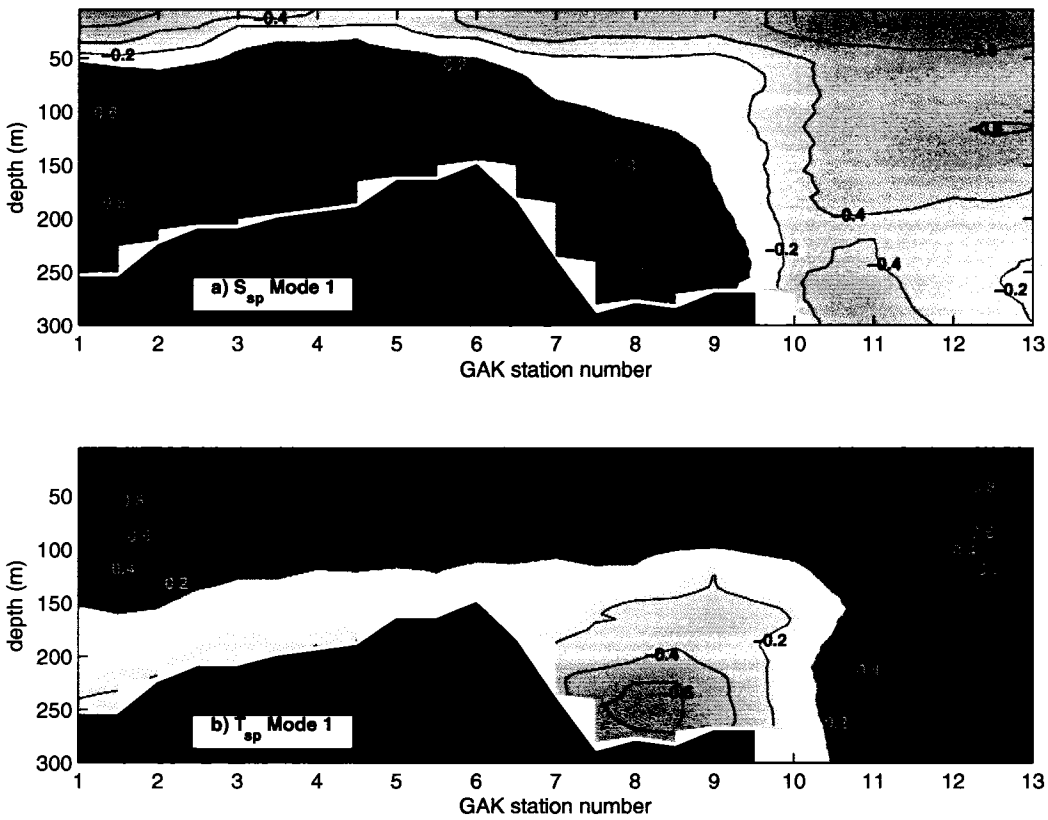

Figure 43. Mode 1 spatial patterns for (a) salinity (S_{sp}) and (b) temperature (T_{sp}). The spatial patterns are constructed from homogeneous correlations.

between the two decreases, e.g. April and May 2003. The seasonal cycle for mode 1 T_{ec} and S_{ec} (Figure 44a,b) has positive values for July through October and negative values for the remaining months. The April S_{ec} standard deviation is the largest while August has the minimum standard deviation. The temperature standard deviations are less than salinity with April, May and December having roughly the same maximum standard deviation while the minimum is in August.

The mode 2 salinity spatial pattern (S_{sp}) has maximum positive homogeneous correlation of 0.6 in the region around GAK1 at 50 m (Figure 45a). In the upper 50 m, regions of positive correlations of approximately 0.4 extend across the shelf until GAK8, except between GAK4 and GAK6 where the correlations drop to 0.2. This region between GAK4 and GAK6 is affected by Ekman pumping upwelling which might cause the correlations to lessen. Regions of minimum negative correlations of -0.6 are centered around 200 m offshore, at GAK11 and GAK13. Small negative values of -0.2 are located at the bottom between GAK1 and GAK4.

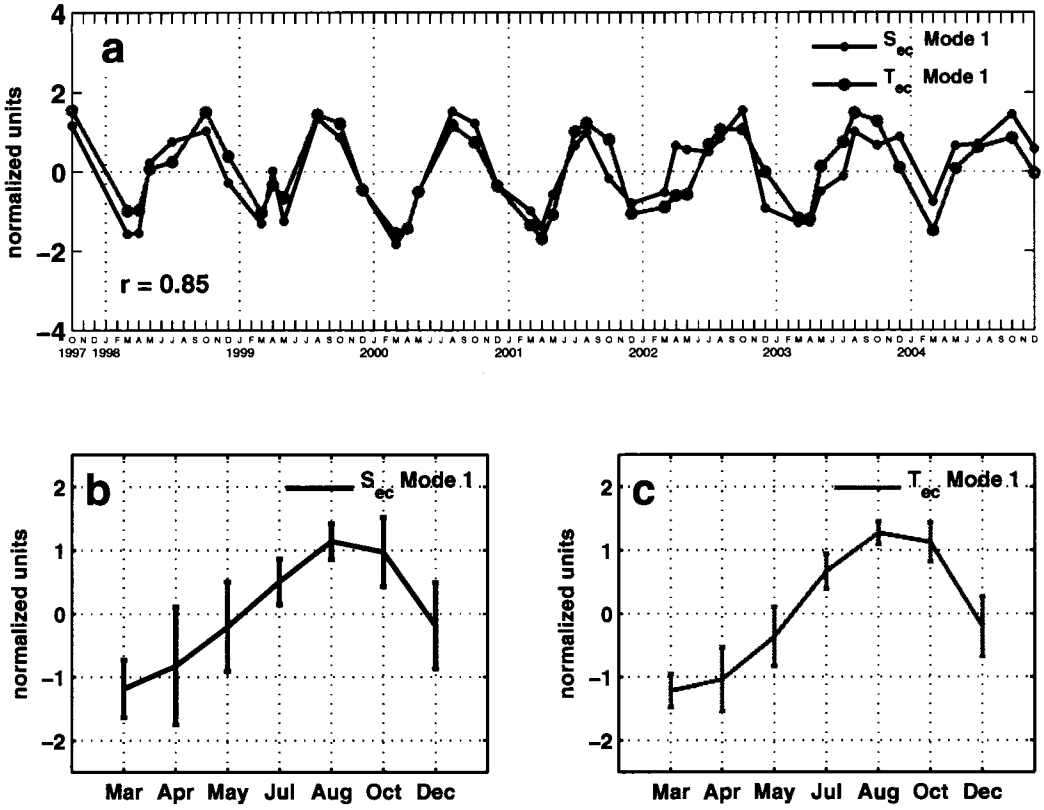

Figure 44. (a) Mode 1 monthly expansion coefficients for salinity (S_{ec}) and temperature (T_{ec}). The correlation between S_{ec} and T_{ec} is 0.855. (b) Mode 1 seasonal cycle of S_{ec}. (c) Mode 1 seasonal cycle of T_{ec}. The error bars are the standard deviation of all expansion coefficients for a particular month.

The mode 2 temperature spatial pattern (T_{sp}) has a large region of negative (-0.8) correlations extending from GAK1 to GAK9 at depths of 75 to 200 m (Figure 45b). Maximum positive correlations are found offshore at GAK12 to GAK13 at depths between 250 to 300 m.

The mode 2 expansion coefficients for salinity and temperature are highly coupled with a Pearson correlation coefficient, r, of 0.78 (Figure 46a). The coupling between the two agrees for the entire record, except for a few noticeable periods, e.g. April through October of 2002 and all months in 2004 except July. The seasonal cycle of the two are similar (Figure 46b,c) with positive values in March through July and negative values in October and December. The error bars are the standard deviation and these are quite large, especially in April and July for the salinity and in March and April for temperature.

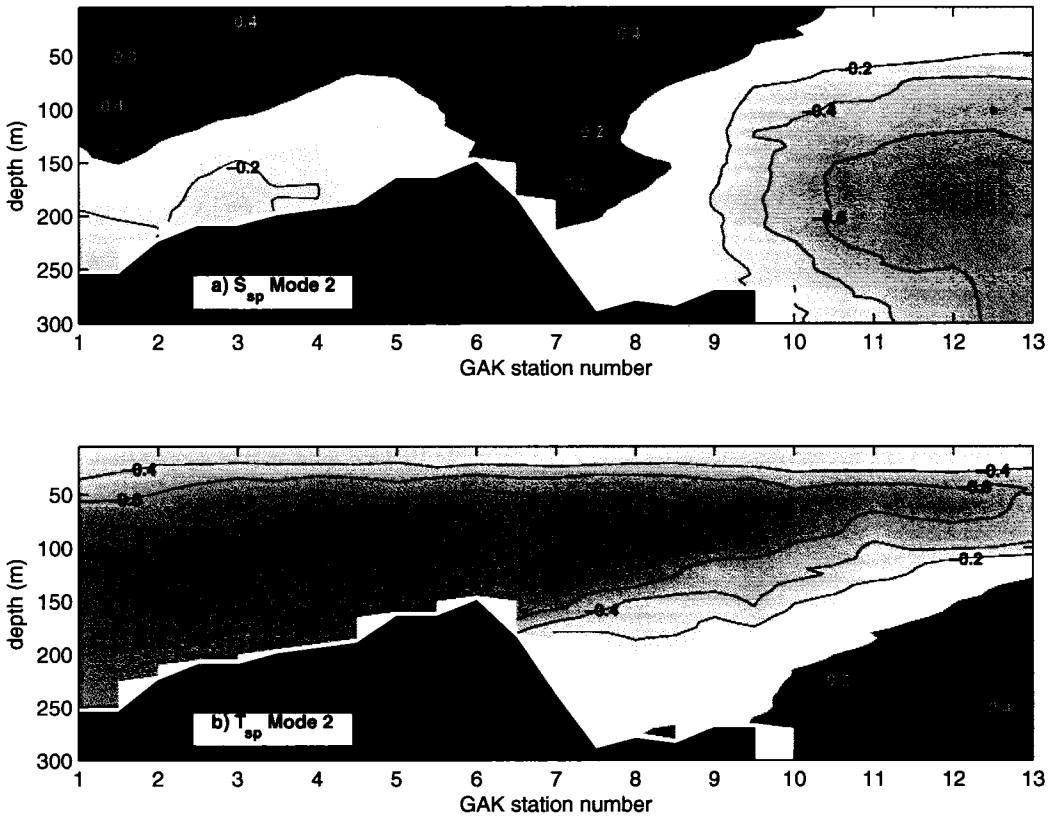

Figure 45. Mode 2 spatial patterns for (a) salinity (S_{sp}) and (b) temperature (T_{sp}). The spatial patterns are constructed from homogeneous correlations.

5.4 RESULTS: CORRELATIONS WITH FORCING

In the context of the two layer system discussed by *Royer* [2005], the first two modes of the SVD will be explained. The spatial patterns and the seasonal cycle of the expansion coefficients are comparable to the two-layer system at GAK1. The mode 1 homogeneous correlation for salinity (S_{sp}) shows strong correlations at the surface from GAK1 to GAK2 and at depth between GAK1 to GAK6 (Figure 43). This is a two layer system with the upper and lower layers out of phase with each other, e.g. when the upper layer is fresher the lower layer will be saltier.

The mode 1 correlation field for temperature (T_{sp}) shows large positive correlations across the entire Seward Line in the upper 100 m and large negative correlations around GAK8 at 250 m. There are very small negative correlations of -0.2 and less for the lower layers from GAK1 to GAK5.

The two layer system for both temperature and salinity are only seen on the shelf.

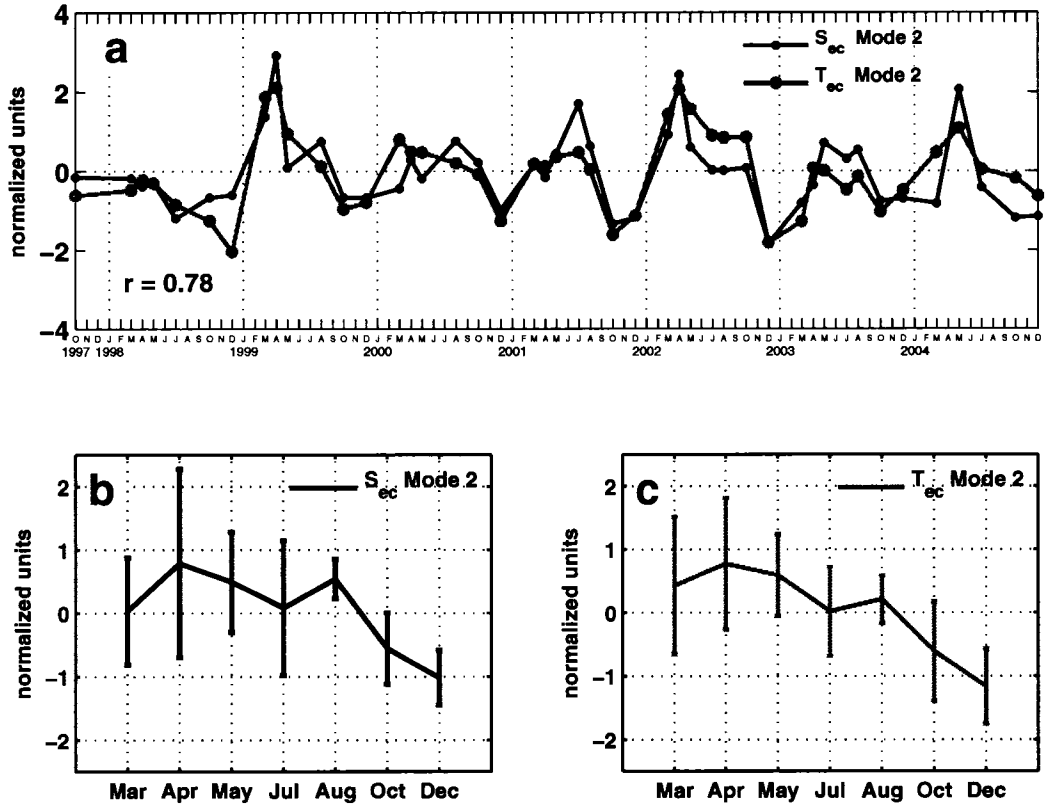

Figure 46. (a) Mode 2 monthly expansion coefficients for salinity (S_{ec}) and temperature (T_{ec}). The correlation between S_{ec} and T_{ec} is 0.855. (b) Mode 2 seasonal cycle of S_{ec}. (c) Mode 2 seasonal cycle of T_{ec}. The error bars are the standard deviation of all expansion coefficients for a particular month.

At GAK10 the S_{sp} correlations are negative for the whole 300 m with the correlations decreasing with depth. For T_{sp} the transition is at GAK10, where the correlations decrease from 0.8 at the surface to less than 0.4 at 300 m.

The seasonal cycle of S_{ec} is very similar to the seasonal cycle noted by *Royer* [2005] for the lower layer (the lower layer for GAK1 has a maximum salinity in August). The lower layer has a seasonal cycle which suggests that it is forced by the relaxation of the downwelling. The seasonal cycle of the u winds (Figure 9) shows that the upwelling producing winds are prevalent for the months of July through September. The upwelling/relaxation of downwelling winds in these months will allow for an incursion of warmer higher salinity water in the lower layer. The S_{ec} seasonal cycle (Figure 44b) has a maximum positive value in August coinciding with the maximum relaxation of downwelling winds. The seasonal cycle of the alongshore winds, u, (Figure 9) has the strongest downwelling producing winds in February. As

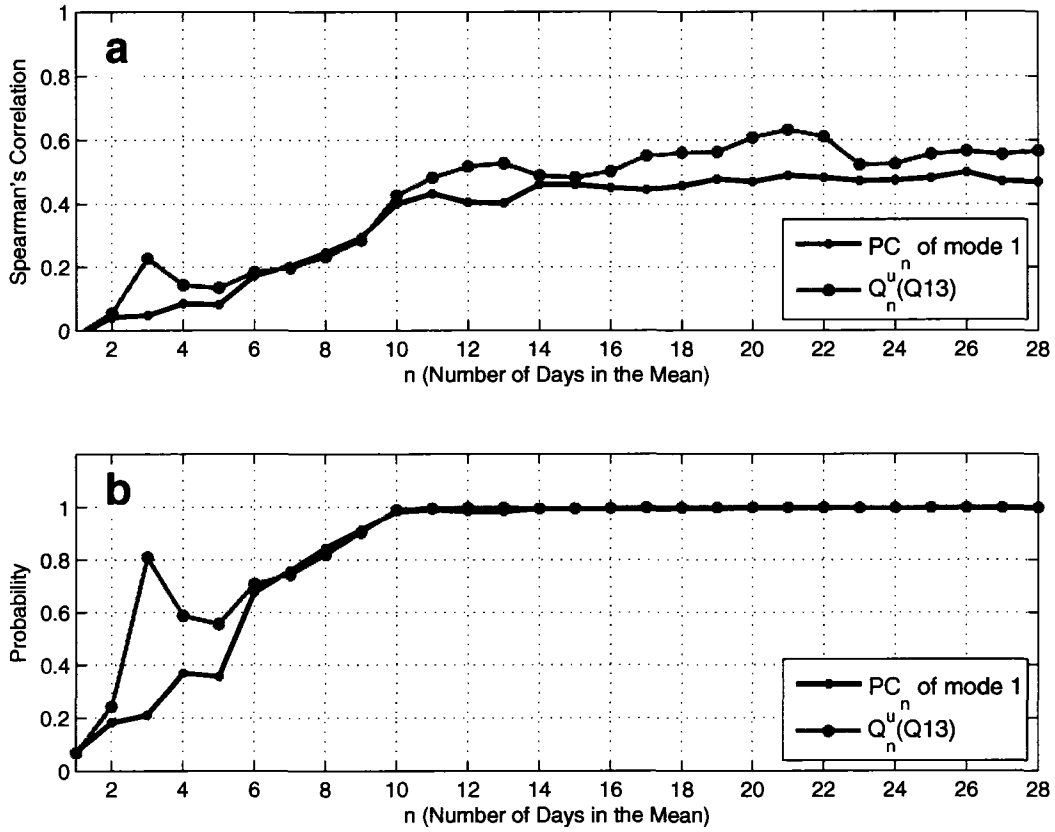

Figure 47. Spearman's Rank Correlation between S_{ec} anomalies and two different time series which should give an indication of the relaxation of the upstream downwelling winds. The two time series are Q_n^u and PC_n.

mentioned above, downwelling will bring fresher upper layer water to the lower layers there and as a result the freshest lower layer water occurring in February. For the S_{ec} seasonal cycle (Figure 44b) the minimum is in March.

To explore the relationship between the winds and the mode 1 S_{ec}, the correlation between S_{ec} anomalies and two different time series is calculated, which should "measure" the upstream relaxation of downwelling winds. The two time series are Q_n^u(Q13) and PC_n (the first principal component of the EOF for the region upstream of the Seward Line (Figure 15)). The results of the correlations are plotted versus the number of days in the mean of Q_n^u(Q13) and PC_n (Figure 47a). The two have very similar correlations up to 10 days in the mean, but with more than 10 days in the mean, the correlations of Q_n^u(Q13) become larger than PC_n. The maximum correlation for the two is for Q_n^u at 21 days. The maximum correlation for PC_n is also at 21 days, though it is approximately 0.1 less than Q_n^u(Q13). The correlations for the

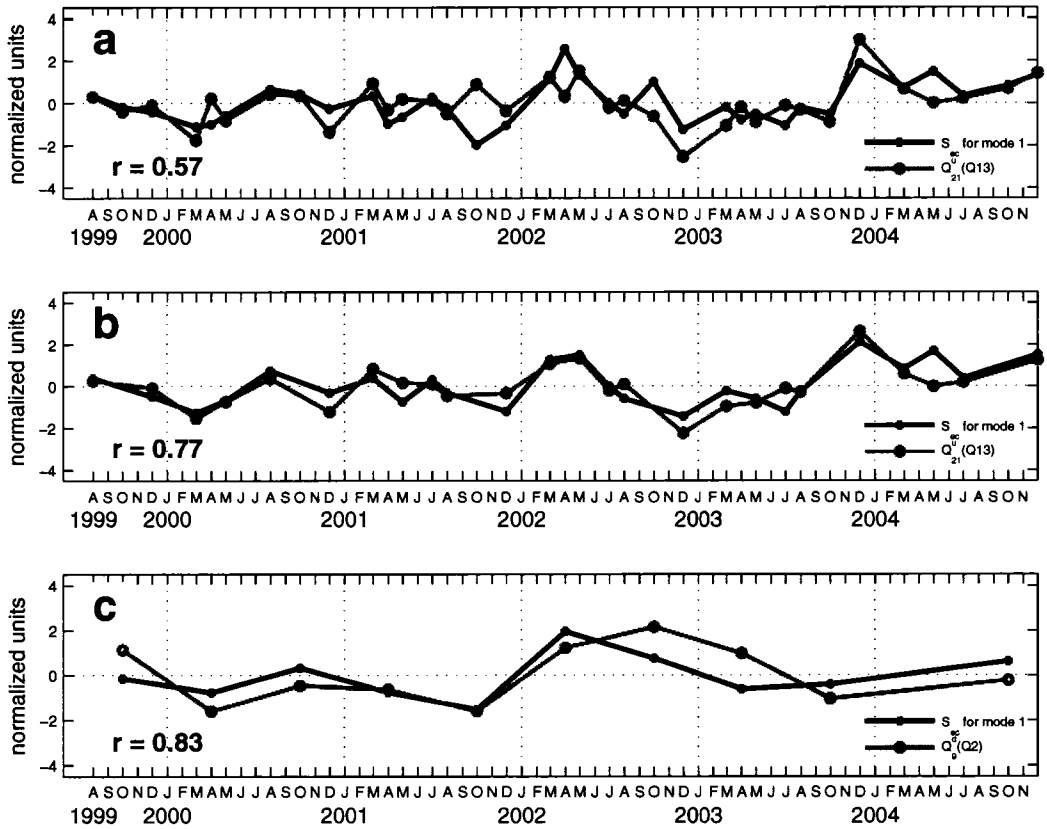

Figure 48. (a) The S_{ec} anomalies and Q^u_{21}(Q13) anomalies all GLOBEC dates since August 1999. (b) The S_{ec} anomalies and Q^u_{21}(Q13) anomalies excluding the 10 April and October values. (c) The S_{ec} anomalies and Q^d_9(Q2) anomalies for all April and October dates. For all three plots the r value in the lower left is the Spearman's rank correlation. All three have probabilities of 0.99 of being significant.

two have probabilities of being significant only for 10 days and greater (Figure 47b).

Since Q^u_{21}(Q13) has the maximum correlation it is helpful to see the two time series that create this maximum value (Figure 48a). The correlation between the two is 0.57 with a probability of 0.99 of being significant. Though the probability is high it appears that a significant number of the April and October Q^u_{21}(Q13) values are not correlated with the S_{ec} anomalies. If the ten months of April and October are removed from the time series then the resulting time series is seen in Figure 48b. Now the correlation improves to an r value of 0.77 with a probability of 0.99 of being significant. So it appears that for all months except April and October, mode 1 is responding to relaxation of downwelling winds. But what is happening in April and October? Instead of the relaxation of the upstream downwelling it might be a local

effect. To determine the effect of the local winds on the April and October values of S_{ec}, anomalies are plotted along with Q_9^d(Q2). The correlation between the two time series is 0.83 (P > 0.99).

Mode 1 T_{ec} anomalies are not correlated with the winds, either regionally or locally. For both the regional and local winds the correlations are below 0.2 and the probabilities are much lower than 0.95 (not shown). The T_{ec} anomalies are correlated to the mean SLP (buoy 46001), where the SLP mean is constructed from the SLP three days before the starting date of a particular cruise. This correlation between the mean SLP and T_{ec} anomalies is only 0.4 but it has a significant probability level of 0.99 (not shown). The T_{ec} anomalies are probably correlated with some other forcing function, but it does not appear to be greatly affected by the winds or mixing.

Mode 2 is speculated to be picking up the strength of any offshore flows that might get established in the upper layer. One such process, suggested by *Royer* [2005], is offshore flows caused by an alongshore pressure gradient. In mode 2 this offshore flow of fresher water will be seen as negative values of S_{ec} and would be expected to be prevalent in months of high discharge. Negative S_{ec} values will correspond to fresher water across the shelf from GAK1 to GAK8 at the surface; also more saline water will be present offshore and at depth across the inner shelf. This modes looks like the offshore surface flow is causing an onshore flow in the lower layer. *Royer* [2005] speculates that an "estuarine-type" system could be established by the upper layer offshore flow causing a lower layer onshore flow. This lower layer onshore flow will bring warm, more saline water onto the shelf. T_{sp} and T_{ec} for mode 2 also agrees with an onshore flow of warm water in the lower layers. When T_{ec} is positive then the temperature across the shelf from 100 to 200 m is cooler, and when T_{ec} is negative the temperature in this region is warmer.

There is no correlation between time series of T_{ec} and S_{ec} with discharge anomalies (not shown). The discharge anomaly time series is the monthly value previous of the GLOBEC cruise unless the start of a cruise occurred on the 20^{th} or later. The discharge time series is constructed in this fashion because a majority of the GLOBEC cruises were conducted in the first week of the month. However, there is a correlation between the March and April values of T_{ec} and S_{ec} and discharge anomalies (Figure 49). The correlation is greater for T_{ec} than S_{ec}, though both have probabilities of being significant above 0.97. In the other months the influence of winds and freshwater discharge together might influence the strength of "estuarine-type"

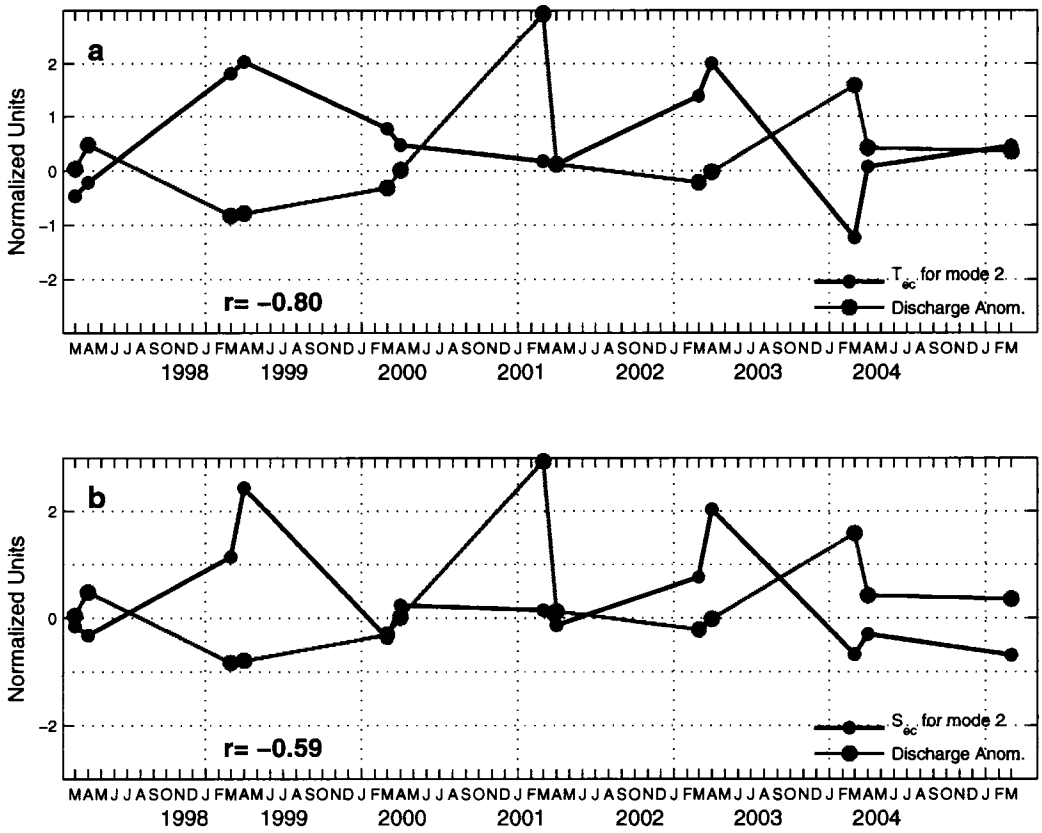

Figure 49. Correlation between the discharge anomaly time series and March and April values of (a) T_{ec} and (b) S_{ec}.

system.

To determine the effect of discharge and winds on the strength of mode 2, interannual variability of T_{ec} and S_{ec} is analyzed for the month of March. March is analyzed because it is a well mixed system and the preceding month of February is historically low in freshwater discharge. This should make March particularly sensitive to discharge effects. Figure 50 has the March values of T_{ec} and S_{ec}, discharge anomalies, Ekman transport (Q_y) at Q4 and Q13. The Ekman transport is integrated over 2 to 30 days before the start of the March GLOBEC cruises. The following is an interannual assessment on how the discharge and winds affect the March expansion coefficients:

1998 The discharge is low; it is comparable to the March 2002 discharge value. So the small negative values of T_{ec} and S_{ec} are surprising. The small negative T_{ec} and S_{ec} values would suggest that the winds leading up to the start of the

GLOBEC cruise were strongly upwelling producing. Eastward winds would drive an offshore surface flow.

1999 The discharge is very low so the expansion coefficients are expected to be positive. There are no wind data, but it would have to be strongly upwelling to get any Ekman transport offshore. The large positive T_{ec} and S_{ec} values agree with the small discharge value.

2000 The discharge is second lowest of all the March values. The T_{ec} and S_{ec} values are expected to be positive. The winds at Q4 and Q13 are strongly downwelling producing during the 30 days leading up to the cruise. The wind forcing should counter the offshore flow produced by the discharge. The large positive value of T_{ec} is consistent with the low discharge and downwelling. The negative value of S_{ec} is not consistent with the discharge and wind forcing. Some other physical mechanism might be occurring to explain the disparity in the sign and magnitude between T_{ec} and S_{ec}.

2001 The freshwater discharge is the highest of all the March values. Negative T_{ec} and S_{ec} values are expected for the large discharge value, but instead they are very near zero. The winds at Q4 and Q13 are very strongly downwelling producing for the five days before the start of the March 2001 cruise. The strong downwelling will repress any surface offshore flow, resulting in the nearly zero values for T_{ec} and S_{ec}.

2002 The discharge is very low; it is the third lowest of the seven March discharge values. The T_{ec} and S_{ec} values are positive, which is expected from the low discharge value. The winds range from slightly upwelling to slightly downwelling over the 30 days before the March 20002 cruise. The winds should not effect the T_{ec} and S_{ec} values. The low discharge alone is sufficient to explain the expansion coefficients.

2003 The discharge is very high. The T_{ec} and S_{ec} values are negative, which is expected from the large discharge. The winds have about the same magnitude and direction as in 2002, so they are not expected to affect the expansion coefficients. The high discharge value explains why T_{ec} and S_{ec} have negative values.

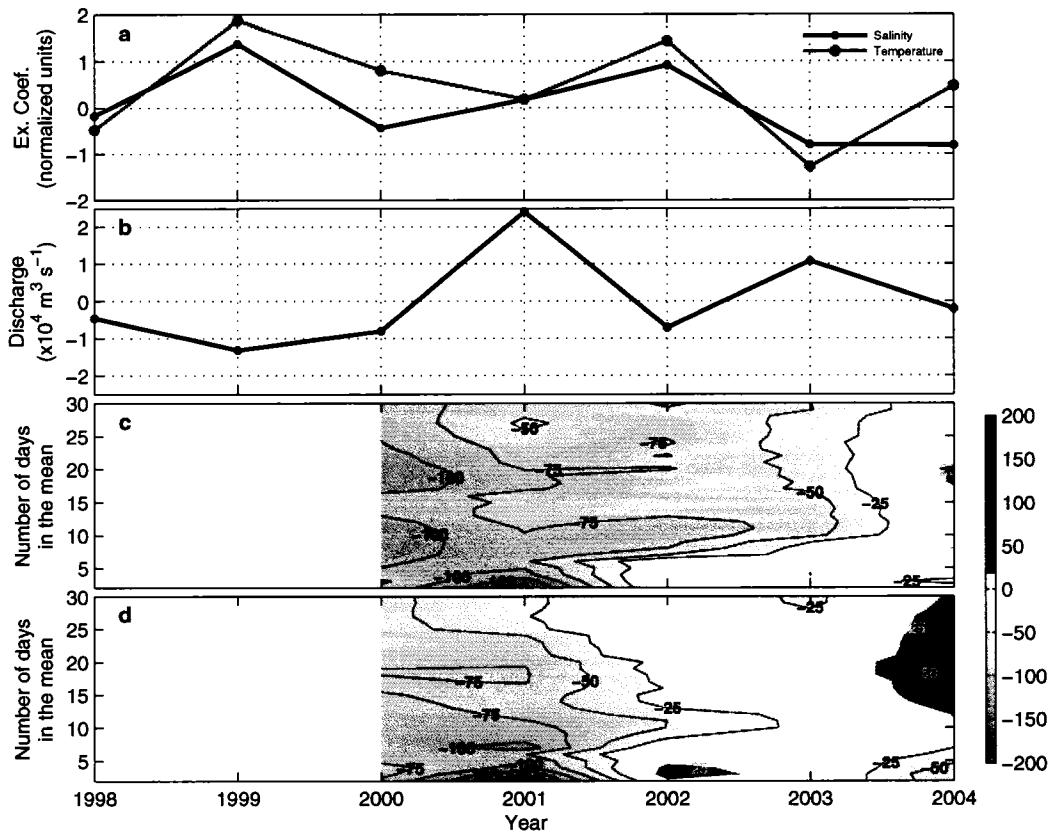

Figure 50. The March values of (a) T_{ec} and S_{ec} (b) the discharge anomalies (c) the mean Ekman transport (Q_y) at Q4 (d) the mean Ekman transport (Q_y) at Q13. The mean Q_y for both Q4 and Q13 are integrated over periods of 2 to 30 days before the start of the March GLOBEC cruise. The units for Q_y is $m^3\ s^{-1}$.

2004 The discharge is the third highest. The negative S_{ec} value is consistent with the high discharge. The T_{ec} value is positive which is expected in low discharge years. The winds are upwelling producing, especially at Q13, for 10 to 30 days before the start of the March 2004 cruise. The upwelling producing winds should drive an offshore surface layer flow. Possibly the disparity in the sign of T_{ec} and S_{ec} is an indication that the "estuarine-type" system is not operating in this month. Though, the high discharge value explains the negative S_{ec} value.

5.5 CONCLUSIONS

A two layer system has been identified for GAK stations across the shelf. This two layer system is especially noticeable between GAK1 and GAK6. This two layer

system is very similar to the one suggested by *Royer* [2005]. The first mode of the SVD for salinity picks up the largest correlations at depth. The seasonal cycle of the salinity mode is very similar the GAK1 lower layer seasonal cycle. The anomalies of salinity are very highly correlated to the relaxation of the regional winds, especially for the months March, May, July, August and December. For April and October the salinity anomalies are highly correlated to the local downwelling winds. The first mode of the SVD for temperature picks up the largest correlations at the surface. The seasonal cycle is similar to the solar heat flux. The temperature anomalies are not correlated to the local or regional winds. They are slightly correlated to the mean SLP at buoy 46001.

The second mode for salinity has correlations that are the highest at the surface between GAK1 and GAK8. This is attributed to the effect of an offshore flow. Below the surface offshore flow is an onshore flow in the lower layer. The surface offshore flow is fresher, while the lower layer is more saline waters.

The temperature second mode has large correlations over much of the lower layer from 100 to 200 m between GAK1 and GAK9. When the salinity is fresher in the upper layer, the temperature is warmer in the lower layer (due to the incursion of warm/salty offshore waters). Below 200 m for GAK10 to GAK13 the correlations are opposite to those on the shelf. This is expected for the same reason given above for salinity.

The March and April salinity and temperature expansion coefficients for mode 2 are correlated to discharge anomalies. The fact that the remaining months are not correlated with the discharge anomalies might be due to the influence of local/regional winds on the discharge. On its own large discharge should induce offshore surface flows. Also upwelling winds should induce offshore surface flows. When the discharge and upwelling winds are strong then the estuary type flow is present. But when the winds are strongly downwelling, they can inhibit the offshore surface flow. So when downwelling winds are strong, the estuary type flow is not present even if the discharge is high.

CHAPTER 6

CONCLUSIONS

One of the ongoing debates in the NEP GLOBEC community is why the shelf in the northern Gulf of Alaska is such a biologically productive area. The confusion is mostly attributed to the region being a coastal downwelling shelf. All the wind measurements (upwelling index, Middleton Island winds, NCEP/NCAR Reanalysis, NDBC buoys and QuikSCAT) show that the seasonal cycle of the winds in the Gulf are either always downwelling producing throughout the whole year or slightly upwelling producing only in some of the summer months [*Royer* 2005, *Stabeno et al.* 2004, *Livingstone and Royer* 1980]. The waters of the central Gulf of Alaska are high in nutrients. Several mechanism have been proposed that will bring these high nutrient waters onto the shelf. *Stabeno et al.* [2004] proposed nutrients, especially nitrate, can be brought onto the shelf from the central gulf through the simple process of Ekman transport across the shelf from the central gulf driven by the downwelling winds. A numerical study showed that onshelf movement of floats (at 5 m depth) south and upstream of Prince William Sound, however there was no onshore flow in the vicinity of the Alaska Stream. Another process is outlined in *Weingartner et al.* [2005] and says that onshore transport of high nutrient water in the bottom boundary layer is due to the weakening of alongshore geostrophic transport. As the alongshore wind stress relaxes in strength in the summer months the alongshore transport decreases, allowing for the renewal of saline water near the coast. Another mechanism proposed by *Royer* [2005] has already been outlined in Chapter 5. A final mechanism is the onshore flux of deep waters from canyons. *Childers et al.* [2005] notes increased nutrients and salinities measured in Hinchinbrook Canyon and Resurrection Canyon. Only the onshore flux in the Ekman layer directly brings the nutrients to the euphotic zone. The other three mechanisms replete the lower layer with nutrients but how are these nutrients brought to the surface? Coastal upwelling, upwelling due to Ekman pumping and mixing due to storm events are all processes that can bring the nutrients to the surface [*Childers et al.* 2005, *Stabeno et al.* 2004, *Sarkar et al.* 2005].

In this dissertation the SVD between salinity and temperature gives strong evidence of the onshore flow of nutrient rich water brought on by the offshore flow of the Alaska Coastal Current and entrainment as proposed by *Royer* [2005]. The first and

second modes of the SVD show annual and interannual increases of onshore flow of high saline water at depth responding to the winds and discharge. These high saline waters will be high in nutrients [*Stabeno et al.* 2004, *Mordy et al.* 2005].

All other wind products, especially the Upwelling Index, show that coastal upwelling events are rare, but the QuikSCAT data are punctuated by upwelling events throughout the year. Some upwelling events with time spans of 9 days have been recorded, by QuikSCAT, in the months of October and December for QuikSCAT location Q2. Also the QuikSCAT data is the only source of observational data that is able to detect wind shears across the shelf.

Coastal upwelling and upwelling due to Ekman pumping are shown to play an important role in causing interannual variability at different locations across the shelf. The hydrographic data between GAK1 and GAK2 respond to the downwelling winds on integrated time scales of 11 days before the start of a cruise. The upwelling due to Ekman pumping is most evident between GAK3 and GAK6. Here the salinity anomalies are positively correlated to w anomalies on integrated time scales of 27 days before the start of a cruise. Thus coastal upwelling and upwelling due to Ekman pumping are seen to have different locations of influence across the shelf and have different response times.

Future work is needed to observe if upwelling due to Ekman pumping is actually taking place. The upwelling velocities are very small and would be very direct to measured. Altimetry data is tidally contaminated on the shelf in the area around the Seward Line [*Okkonen et al.* 2003] and cannot be used to located seasurface depressions. Results from numerical models forced with high resolution winds are needed to study the upwelling. The wind forcing used needs to be of higher spatial resolution than the NCEP/NCAR reanalysis winds. Other future work is to correlate nutrient/productivity across the shelf with the SVD results, especially those of mode 2.

REFERENCES

Bakun, A. (1973), Coastal upwelling indices, west coast of North America, 1946-71, *Tech. Rep. NMFS SSRF-671*, NOAA.

Bretherton, C. S., C. Smith, and J. M. Wallace (1992), An intercomparison of methods for finding coupled patterns in climate data, *J. Climate*, *5*, 541–560.

Chelton, D. B., M. G. Schlax, M. H. Freilich, and R. F. Milliff (2004), Satellite measurements reveal persistent small-scale features in ocean winds, *Science*, *303*, 978–983.

Childers, A. R., T. E. Whitledge, and D. A. Stockwell (2005), Seasonal and interannual variability in the distribution of nutrients and chlorophyll *a* across the Gulf of Alaska shelf: 1998-2000, *Deep-Sea Res. II*, *52*, 193–216, doi:10.1016/j.dsr2.2004.09.018.

Cooney, R., J. Allen, M. Bishop, D. Eslinger, T. Kline, B. Norcross, C. Mcroy, J. Milton, J. Olsen, V. Patrick, A. Paul, D. Salmon, D. Scheel, G. Thomas, S. Vaughan, and T. Willette (2001), Ecosystem controls of juvenile pink salmon (*Onchorynchus gorbuscha*) and Pacific herring (*Clupea pallasi*) populations in Prince William Sound, Alaska, *Fish. Oceanogr. (Suppl. 1)*, *10*, 1–13.

Croquette, M., G. Eldin, and V. Echevin (2004), On the contributions of Ekman transport and pumping to the dynamics of coastal upwelling in the South-East Pacific, *Gayana (Concepción)*, *68*, 136–141.

Ebuchi, N., H. C. Graber, and M. J. Caruso (2002), Evaluation of wind vectors observed by QuikSCAT/sea winds using ocean buoy data, *J. Atmos. Oceanic Technol.*, *19*, 2049–2062.

Ekman, V. W. (1905), On the influence of the earth's rotation on ocean currents, *Ark. Mat. Astron. Fys.*, *2*, 1–53.

Kendall, M., and J. D. Gibbons (1990), *Rank Correlation Methods*, Edward Arnold, New York, USA.

Kundu, P. K. (1976), Ekman veering observed near the ocean bottom, *J. Phys. Oceanogr.*, *6*, 238–242.

Ladd, C., and N. A. Bond (2002), Evaluation of the NCEP/NCAR reanalysis in the NE Pacific and the Bering Sea, *J. Geophys. Res.*, *107*, 3158–3166.

Large, W., and S. Pond (1981), Open ocean momentum flux measurements in moderate to strong winds, *J. Phys. Oceanogr.*, *11*, 324–336.

Livingstone, D. M., and T. C. Royer (1980), Observed surface winds at Middleton Island, Gulf of Alaska and their influence on the ocean circulation, *J. Phys. Oceanogr.*, *10*, 753–764.

López-Mariscal, M., and A. J. Clarke (1993), On the influence of wind-stress curl on low-frequency shelf water flow, *J. Phys. Oceanogr.*, *23*, 2717–2727.

Mordy, C. W., P. J. Stabeno, C. Ladd, S. Zeeman, D. P. Wisegarver, S. A. Salo, and J. George L. Hunt (2005), Nutrients and primary production along the eastern Aleutian Island Archipelago, *Fish. Oceanogr.*, *14*, 55–76.

Murphree, T., P. Green-Jessen, F. Schwing, and S. Bogra (2003), The seasonal cycle of wind stress curl and its relationship to subsurface ocean temperature in the northeast Pacific, *Geophys. Res. Lett.*, *30*, 1469–1472.

Narváez, D. A., S. A. Navarrete, J. Largier, and C. A. Vargas (2006), Onshore advection of warm water, larval invertebrate settlement, and relaxation of upwelling off central Chile, *Mar. Ecol. Prog. Ser.*, *309*, 159–173.

Niebauer, H. J., J. Roberts, and T. C. Royer (1981), Shelf break circulation in the northern Gulf of Alaska, *J. Geophys. Res.*, *86*, 13,041–13,047.

Okkonen, S. R., T. J. Weingartner, S. L. Danielson, D. L. Musgrave, and G. M. Schmidt (2003), Satellite and hydrographic observations of eddy-induced shelf-slope exchange in the northwestern Gulf of Alaska, *J. Geophys. Res.*, *108*, 3033, doi:10.1029/2002JC001342.

Pickard, G. L., and W. J. Emery (1990), *Descriptive Physical Oceanography, An Introduction*, 5^{th} (SI) Enlarged ed., Butterworth-Heinemann Ltd., Jordan Hill, Oxford, England.

Pickett, M. H., and J. D. Paduan (2003), Ekman transport and pumping in the California Current based on the U.S. Navy's high-resolution atmospheric model (COAMPS), *J. Geophys. Res.*, *108*, 25–1.

Pickett, M. H., and F. B. Schwing (2006), Evaluating upwelling estimates off the west coasts of North and South America, *Fish. Oceanogr.*, *15*, 256–269.

Pond, S., and G. L. Pickard (1995), *Introductory Dynamical Oceanography*, 2^{nd} ed., Butterworth-Heinemann Ltd., Jordan Hill, Oxford, England.

Royer, T. C. (1981), Baroclinic transport in the Gulf of Alaska, II, A fresh water driven coastal current, *J. Mar. Res.*, *39*, 251–266.

Royer, T. C. (1982), Coastal freshwater discharge in the northeast Pacific, *J. Geophys. Res.*, *87*, 2017–2021.

Royer, T. C. (2005), Hydrographic responses at a coastal site in the northern Gulf of Alaska to seasonal and interannual forcing, *Deep-Sea Res. II*, *52*, 267–288, doi:10.1016/j.dsr2.2004.09.022.

Royer, T. C., C. E. Grosch, and L. A. Mysak (2001), Interdecadal variability of northeast Pacific coastal freshwater and its implications on biological productivity, *Prog. Oceanogr.*, *49*, 95–111.

Sarkar, N., T. C. Royer, and C. E. Grosch (2005), Hydrographic and mixed layer depth variability on the shelf in the northern Gulf of Alaska, 1974-1998, *Cont. Shelf Res.*, *25*, 2147–2162.

Schwing, F. B., M. O'Farrell, J. Steger, and K. Baltz (1996), Coastal upwelling indices, west coast of North America, 1946-1995, *Tech. Rep. NOAA-TM-NMFS-SWFSC-231*, NOAA.

Stabeno, P. J., N. A. Bond, A. J. Hermann, N. B. Kachel, C. W. Mordy, and J. E. Overland (2004), Meteorology and oceanography of the northern Gulf of Alaska, *Cont. Shelf Res.*, *60*, 859–897, doi:10.1016/j.csr.2004.02.007.

Tang, W., W. Liu, and B. Stiles (2004), Evaluation of high-resolution ocean surface vector winds measured by QuikSCAT scatterometer in coastal regions, *IEEE Transactions on Geoscience and Remote Sensing*, *42*, 1762–1769, doi:10.1109/TGRS.2004.831685.

Venegas, S. A. (2001), Statistical methods for signal detection in climate, *Tech. Rep. 2*, Danish Center for Earth System Science, Copenhagen, Denmark.

Weingartner, T. J., S. L. Danielson, and T. C. Royer (2005), Freshwater variability and predictability in the Alaska Coastal Current, *Deep-Sea Res. II*, *52*, 169–191.

Wilks, D. S. (1995), *Statistical Methods in the Atmospheric Sciences - An Introduction*, vol. 59 of *International Geophysics Series*, Academic Press.

Wilson, J. G., and J. E. Overland (1986), Meteorology, in *The Gulf of Alaska physical environment and biological resources*, edited by D. W. Hood and S. T. Zimmerman, OCS Study MMS86-0095, pp. 31–54, Minerals Management Service, Springfield, VA.

Winstead, N. S., B. A. Colle, J. B. Olson, G. S. Young, and K. Loescher (2005), Meteorology, in *Improving the forecasting of barrier jets using remote sensing, modeling and a SARJET field study*, Preprints: 21st Conference on Weather Analysis and Forecasting, August 1-6 Washington D.C.

APPENDIX A

LIST OF SYMBOLS

GOA	Gulf of Alaska
NEP	Northeast Pacific
GLOBEC	GLOBal ocean ECosystems dynamics
NDBC	National Data Buoy Center
ACC	Alaska Coastal Current
UI	Bakun Upwelling Index
u	Zonal component of wind velocity ($+u$ are headed eastward and $-u$ headed westward)
v	Meridional component of wind velocity ($+v$ are headed northward and $-v$ headed southward)
Q#	QuikSCAT time series location (# is a either 2, 4, 6, 7, 9, 11, 13)
GAK	Gulf of Alaska hydrographic station
EOF	Emperical Orthogonal Function
PC	Principal Component
Q_y	Across shelf component of Ekman volume transport
w	Vertical water velocity produced by Ekman pumping
Q_n	Ekman transport time series constructed by integrating the n days before and including the start of a GLOBEC cruise
Q_n^u	Ekman transport time series constructed by integrating only the upwelling days in the n days
Q_n^d	The same as Q_n^u but integrating the downwelling days
Q_n(Q#)	The times series Q_n calculated for QuikSCAT time series location Q# (# is a either 2, 4, 6, 7, 9, 11, 13)
W_n	Ekman pumping time series constructed by integrating the n days before and including the start of a GLOBEC cruise
W_n^u	Ekman pumping time series constructed by integrating only the upwelling days in the n days
W_n^d	The same as W_n^u but integrating the downwelling days
W_n(Q#)	The times series W_n calculated for QuikSCAT time series location Q# (# is a either 2, 4, 6, 7, 9, 11, 13)

UI_n^u	Upwelling Index time series constructed by integrating only the upwelling days in the n days before and including the start of a GLOBEC cruise
PC_n	Mode 1 PC time series constructed by integrating the n days before and including the start of a GLOBEC cruise
SVD	Singular Value Decomposition
SCF	Squared covariance fraction
S_{sp}	SVD homogeneous correlation map for salinity
T_{sp}	SVD homogeneous correlation map for temperature
S_{ec}	SVD expansion coefficient for salinity
T_{ec}	SVD expansion coefficient for temperature

VITA

Isaac Schroeder
Department of Oceanography
Old Dominion University
Norfolk, VA 23529

EDUCATION

B.S. Physics, December 1992, Murray State University, Murray, KY

M.S. Physics, August 1996, Department of Physics, University of Missouri, Columbia, MO

Ph.D. Oceanography, August 2007, Center for Coastal Physical Oceanography, Department of Ocean, Earth and Atmospheric Sciences, Old Dominion University, Norfolk, VA 23529

MANUSCRIPTS IN PREPARATION

Schroeder, Isaac, C. E. Grosch and T. C. Royer. NCEP-NCAR Reanalysis: Comparison with Observations from the Coast of Alaska and the Gulf of Alaska, submitted to Journal of Climate.

Typeset using LaTeX.